SYNTHESIS OF RARE-EARTH DOPED LITHIUM TRIBORATE

A THESIS SUBMITTED TO
THE GRADUATE SCHOOL OF NATURAL AND APPLIED SCIENCES
OF
MIDDLE EAST TECHNICAL UNIVERSITY

BY

BURCU ARDIÇOĞLU

IN PARTIAL FULFILLMENT OF THE REQUIREMENTS
FOR
THE DEGREE OF MASTER OF SCIENCE
IN
MINING ENGINEERING

JULY 2005

Approval of the Graduate School of Natural and Applied Sciences

Prof. Dr. Canan Özgen
Director

I certify that this thesis satisfies all the requirements as a thesis for the degree of Master of Science.

Prof. Dr. Ümit Atalay
Head of Department

This is to certify that we have read this thesis and that in our opinion it is fully adequate, in scope and quality, as a thesis for the degree of Master of Science.

Assist. Prof. Dr. Ayşen Yılmaz	Prof. Dr. Gülhan Özbayoğlu
Co-Supervisor	Supervisor

Examining Committee Members

Prof. Dr. Ümit Atalay	(METU, MINE)	
Prof. Dr. Gülhan Özbayoğlu	(METU, MINE)	
Assist. Prof. Dr. Ayşen Yılmaz	(METU, CHEM)	
Prof. Dr. Ali İhsan Arol	(METU, MINE)	
Prof. Dr. Tayfur Öztürk	(METU, METE)	

I hereby declare that all information in this document has been obtained and presented in accordance with academic rules and ethical conduct. I also declare that, as required by these rules and conduct, I have fully cited and referenced all material and results that are not original to this work.

Burcu Ardıçoğlu

ABSTRACT

SYNTHESIS OF RARE-EARTH DOPED LITHIUM TRIBORATE

Ardıçoğlu, Burcu
M. Sc., Department of Mining Engineering
Supervisor: Prof. Dr. Gülhan Özbayoğlu
Co-Supervisor: Assist. Prof. Dr. Ayşen Yılmaz

July 2005, 126 Pages

Research in the field of non-linear optical (NLO) devices lead to an increasing interest in new borate compounds, capable of expanding the frequency range provided by common laser sources. Lithium triborate (LBO) is a newly developed ideal non-linear optical crystal used in laser weapon, welder, radar, tracker, surgery, communication, etc. Borates containing rare-earth elements are of great interest since they are found to be superior in non-linear optical applications. In this study, synthesis and identification of rare-earth doped lithium triborate was carried out.

Lithium triborate was produced from the solid-state reaction. LBO was then doped with some rare-earth elements (Gd, La, Y) in several different concentrations.

Appropriate quantities of Li_2CO_3 and H_3BO_3, weighted separately, were mixed and finely powdered. Then, the mixture was heated at 750 ºC for 14 hrs. The expected reaction is given below.

$$Li_2CO_3 + 6H_3BO_3 \rightarrow 2LiB_3O_5 + CO_2 + 9H_2O$$

Prepared LiB_3O_5 and Gd_2O_3, La_2O_3 and Y_2O_3 samples were weighed separately at different concentrations and ground together. The mixture was then heated at 750 ºC for 7 hrs.

Characterization of the new products was done by X-Ray Diffraction (XRD) and Infrared (IR) analysis. Differential Thermal Analysis (DTA) was used for examination of the thermal properties of the compounds, morphology of new compounds was observed by Scanning Electron Microscopy (SEM). The compounds are then subjected to thermoluminescence (TL) studies.

From the XRD studies, no change in the LBO phase related to the addition of rare-earth elements was observed. However, peaks of those elements were also become apparent. IR analysis showed that there is no change related to B-O link with the addition of rare earth elements. DTA studies showed that the melting point of LBO decreases with the addition of rare earth elements. In the SEM images, two phases belonging to particles of rare earth elements and lithium triborate were observed clearly. With the TL analysis, it was considered that the samples show dose response but also it was realized that they are affected by fading.

Keywords: Lithium triborate; Rare earth elements; Non-linear optics; Solid-state synthesis; Luminescence

ÖZ

NADİR TOPRAK ELEMENTLERİ İLE KATKILANMIŞ LİTYUM TRİBORAT SENTEZİ

Ardıçoğlu, Burcu
Yüksek Lisans, Maden Mühendisliği Bölümü
Tez Yöneticisi: Prof. Dr. Gülhan Özbayoğlu
Ortak Tez Yöneticisi: Yrd. Doç. Dr. Ayşen Yılmaz

Temmuz 2005, 126 Sayfa

Son zamanlarda, borat bileşikleri, lazer kaynaklarında frekans aralığı arttırabilme özellikleri nedeniyle, non-linear optik cihazlar üzerine yapılan araştırmaların odağı haline gelmiştir. Yeni keşfedilen non-lineer optik bir malzeme olan lityum triborat, lazer, kaynak, radar yapımı, cerrahi ve haberleşme alanlarda kullanılmaktadır. Bu çalışma, nadir toprak elementleri içeren lityum triborat bileşiğinin üretimi ve karakterizasyonunu içermektedir.

Lityum triborat, lityum karbonat ve borik asit'in katı hal senteziyle elde edilmiştir. Elde edilen bileşik nadir toprak elementleriyle (Gd, La, Y) ile katkılanmıştır.

Başlangıç malzemeleri olan Li_2CO_3 ve H_3BO_3 uygun miktarlarda karıştırılarak homojen hale getirilmiştir. Karışım daha sonra porselen krozelerde 750°C'de 14 saat süreyle ısıtılmıştır. Beklenen reaksiyon aşağıdaki gibidir.

$$Li_2CO_3 + 6H_3BO_3 \rightarrow 2LiB_3O_5 + CO_2 + 9H_2O$$

Bu reaksiyonlar sonucunda elde edilen LiB_3O_5, çeşitli konsantrasyonlarda hazırlanan Gd_2O_3, La_2O_3 ve Y_2O_3 ile 750°C'de 7 saat süreyle katkılanmıştır.

Ürünlerin karakterizasyonu X-Işını Difraksiyonu (XRD) ile yapılmıştır. Yapısı Kızılötesi (IR) Analizi, termal özellikleri Diferansiyel Termal Analiz (DTA) kullanılarak incelenmiştir. Bileşiklerin yapısının incelenmesinde Taramalı Elektron Mikroskobu (SEM) kullanılmıştır. Daha sonra Termoluminesans (TL) okuyucu kullanılarak bileşiklerin dozimetrik özellikleri incelenmiştir.

Bu analizlere göre, lityum triborat'ın X-Işını deseninde farklılık gözlenmemiştir. Nadir toprak elementleri sistemde oksit bileşikleri halinde, fakat az miktarda bulunmaktadır. Kızılötesi Analizine göre, nadir toprak elementlerinin bor atomuna bağlanmadığı gözlenmiştir. Diferansiyel Termal Analiz, nadir toprak elementlerinin eklenmesiyle, lityum triborat'ın ergime sıcaklığının düştüğünü göstermiştir. Taramalı Elektron Mikroskobu resimlerinde lityum triborat taneciklerinin üzerine yapışmış olan nadir toprak elementleri açıkca görülmektedir. Termoluminesans sonuçlarına göre bileşiğin dozimetrik özelliği olduğu görülmüştür.

Anahtar Kelimeler: Lityum triborat, Nadir toprak elementi, Non-linear optik, Katı hal sentezi, Luminesans

To My Family

ACKNOWLEDGEMENTS

I would like to express my gratitude to Prof. Dr. Gülhan Özbayoğlu and Assist. Prof. Dr. Ayşen Yılmaz for their guidance, encouragement and patience at every stage of this thesis.

I am grateful to my beloved family for their support by all means, my mother K. Nalan Ardıçoğlu, my father Kemalettin Ardıçoğlu and my dear sister N. Yasemin Ardıçoğlu; for they never grudge their love, guidance, and encouragement.

I offer sincere thanks to Zeynep Özdemir for her suggestions and helpful discussions.

I wish to extend my sincere thanks to my dear E. Tuğcan Tuzcu for his continuous help, encouragement and spiritual aid.

I would like to thank to my dear friends Gizem E. Dülgergil, Çiğdem Çırpar, Filiz Toprak and Asli Aksoy for never leaving me alone.

I am ever so greatful to Semih Seyyidoğlu, F. Mustafa Genişel and Selcan Tuncel from the Chemistry Department for their friendly help and to Assoc. Prof. Dr. A. Necmettin Yazıcı from Gaziantep University for his immediate support.

Finally, I offer sincere thanks to all my colleagues from the Mining Engineering Department for their guidance, assistance, technical and non-technical support during this research.

TABLE OF CONTENTS

PALIGIARISM iii
ABSTRACT iv
ÖZ vi
DEDICATION viii
ACKNOWLEDGEMENTS ix
TABLE OF CONTENTS x
LIST OF TABLES xii
LIST OF FIGURES xiii
CHAPTER
1. INTRODUCTION 1
1.1. General Remarks 1
1.2. Statement of the Problem 2
1.3. Objectives of the Thesis 3
1.4. Methodology of the Thesis 3
1.5. Thesis Outline 3
2. LITERATURE SURVEY 5
2.1. General Features of Boron 5
2.2. Borates 7
2.2.1. Borate Deposits 7
2.2.2. Uses of Borates 9
2.3. Lithium Triborate 11
2.3.1. Rare-earth Doped Borates 17
2.3.2. Rare-earth Doped Lithium Triborate 18
2.4. Borates in Nonlinear Optics 19
2.5. Borates in Radiation Protection 20

3. MATERIALS AND METHODS 23
3.1. Materials 23
3.2. Instrumentation 23
3.2.1. Powder X-Ray Diffractometer 23
3.2.2. Infrared Spectrometer 24
3.2.3. Differential Thermal Analyser 24
3.2.4. Scanning Electron Microscope 25
3.2.5. Thermoluminescence Reader 25
3.2.6. Furnace 25
3.3. Experimental Procedure 26
3.3.1. Synthesis of Lithium Triborate 26
3.3.2. Synthesis of Rare-earth Doped Lithium Triborate 26
4. RESULTS AND DISCUSSION 28
4.1. Synthesis of Rare-earth Doped Lithium Triborate 28
4.1.1. Powder X-Ray Diffraction 28
4.1.2. Infrared Spectra 33
4.1.3. Differential Thermal Analysis 37
4.1.4. Scanning Electron Microscopy 41
4.1.5. Thermoluminescence 47
5. CONCLUSIONS AND RECOMMENDATIONS 51
REFERENCES 53
APPENDICES
A. XRD PATTERNS OF THE PRODUCED MATERIALS 56
B. IR SPECTRA OF THE PRODUCED MATERIALS 82
C. DTA CURVES OF THE PRODUCED MATERIALS 108
D. TL CURVES OF THE PRODUCED MATERIALS 116

LIST OF TABLES

TABLES

2.1 World's Borate Reserves 8

2.2 LiB_3O_5 X-ray diffraction data 12

2.3 Frequencies of the vibrational modes for the LiB_3O_5 phase 16

3.1 Concentrations of rare earth elements in LiB_3O_5 27

LIST OF FIGURES

FIGURES

2.1 X-ray powder diffraction patterns of LBO material synthesized by solid-state sintering method 13

2.2 Powder X-ray diffraction patterns recorded for the polycrystalline LBO materials synthesized by solid-state sintering at: (a) 650°C for 24 h and (b) 700°C for 120 h 14

2.3 Infrared spectra of: $Li^{11}B_3O_5$, $Li_{nat}B_3O_5$, and $Li^{10}B_3O_5$ 15

4.1 Powder x-ray diffraction pattern of LiB_3O_5 and LiB_3O_5 doped with Gd_2O_3 30

4.2 Powder x-ray diffraction pattern of LiB_3O_5 and LiB_3O_5 doped with La_2O_3 31

4.3 Powder x-ray diffraction pattern of LiB_3O_5 and LiB_3O_5 doped with Y_2O_3 32

4.4 IR spectra of LiB_3O_5 and LiB_3O_5 doped with Gd_2O_3 34

4.5 IR spectra of LiB_3O_5 and LiB_3O_5 doped with La_2O_3 35

4.6 IR spectra of LiB_3O_5 and LiB_3O_5 doped with Y_2O_3 36

4.7 DTA curves of LiB_3O_5 and LiB_3O_5 doped with Gd_2O_3 38

4.8 DTA curves of LiB_3O_5 and LiB_3O_5 doped with La_2O_3 39

4.9 DTA curves of LiB_3O_5 and LiB_3O_5 doped with Y_2O_3 40

4.10 SEM of LiB_3O_5 obtained from the solid-state reaction of Li_2CO_3 and H_3BO_3 at 750°C for 14 hours 42

4.11 SEM of LiB_3O_5 doped with 11% wt. Gd_2O_3 at 750°C for 7 hours 42

4.12 SEM of LiB_3O_5 doped with 11% wt. Gd_2O_3 at 750°C for 7 hours 43

4.13 SEM of LiB_3O_5 doped with 11% wt. Gd_2O_3 at 750°C for 7 hours 43

4.14 SEM of LiB_3O_5 doped with 11% wt. La_2O_3 at 750°C for 7 hours 44

4.15 SEM of LiB_3O_5 doped with 11% wt. La_2O_3 at 750°C for 7 hour 44

4.16 SEM of LiB_3O_5 doped with 11% wt. La_2O_3 at 750°C for 7 hour 45

4.17 SEM of LiB_3O_5 doped with 11% wt. Y_2O_3 at 750°C for 7 hours 45

4.18 SEM of LiB_3O_5 doped with 11% wt. Y_2O_3 at 750°C for 7 hours 46
4.19 SEM of LiB_3O_5 doped with 11% wt. Y_2O_3 at 750°C for 7 hours 46
4.20 The glow curve of LiB_3O_5 and LiB_3O_5 samples doped with Gd_2O_3 48
4.21 The glow curve of LiB_3O_5 and LiB_3O_5 samples doped with La_2O_3 49
4.22 The glow curve of LiB_3O_5 and LiB_3O_5 samples doped with Y_2O_3 50
A.1 Powder x-ray diffraction pattern of LiB_3O_5 57
A.2 Powder x-ray diffraction pattern of LiB_3O_5 doped with 3% wt. Gd_2O_3 58
A.3 Powder x-ray diffraction pattern of LiB_3O_5 doped with 5% wt. Gd_2O_3 59
A.4 Powder x-ray diffraction pattern of LiB_3O_5 doped with 7% wt. Gd_2O_3 60
A.5 Powder x-ray diffraction pattern of LiB_3O_5 doped with 9% wt. Gd_2O_3 61
A.6 Powder x-ray diffraction pattern of LiB_3O_5 doped with 11% wt. Gd_2O_3 62
A.7 Powder x-ray diffraction pattern of LiB_3O_5 doped with 15% wt. Gd_2O_3 63
A.8 Powder x-ray diffraction pattern of LiB_3O_5 doped with 20% wt. Gd_2O_3 64
A.9 Powder x-ray diffraction pattern of LiB_3O_5 doped with 25% wt. Gd_2O_3 65
A.10 Powder x-ray diffraction pattern of LiB_3O_5 doped with 3% wt. La_2O_3 66
A.11 Powder x-ray diffraction pattern of LiB_3O_5 doped with 5% wt. La_2O_3 67
A.12 Powder x-ray diffraction pattern of LiB_3O_5 doped with 7% wt. La_2O_3 68
A.13 Powder x-ray diffraction pattern of LiB_3O_5 doped with 9% wt. La_2O_3 69
A.14 Powder x-ray diffraction pattern of LiB_3O_5 doped with 11% wt. La_2O_3 70
A.15 Powder x-ray diffraction pattern of LiB_3O_5 doped with 15% wt. La_2O_3 71
A.16 Powder x-ray diffraction pattern of LiB_3O_5 doped with 20% wt. La_2O_3 72
A.17 Powder x-ray diffraction pattern of LiB_3O_5 doped with 25% wt. La_2O_3 73
A.18 Powder x-ray diffraction pattern of LiB_3O_5 doped with 3% wt. Y_2O_3 74
A.19 Powder x-ray diffraction pattern of LiB_3O_5 doped with 5% wt. Y_2O_3 75
A.20 Powder x-ray diffraction pattern of LiB_3O_5 doped with 7% wt. Y_2O_3 76
A.21 Powder x-ray diffraction pattern of LiB_3O_5 doped with 9% wt. Y_2O_3 77
A.22 Powder x-ray diffraction pattern of LiB_3O_5 doped with 11% wt. Y_2O_3 78
A.23 Powder x-ray diffraction pattern of LiB_3O_5 doped with 15% wt. Y_2O_3 79
A.24 Powder x-ray diffraction pattern of LiB_3O_5 doped with 20% wt. Y_2O_3 80
A.25 Powder x-ray diffraction pattern of LiB_3O_5 doped with 25% wt. Y_2O_3 81

B.1 IR spectrum of LiB_3O_5 obtained from the solid-state reaction of Li_2CO_3 and H_3BO_3 at 750°C for 14 hours 83
B.2 IR spectrum of LiB_3O_5 doped with 3% wt. Gd_2O_3 at 750°C for 7 hours..... 84
B.3 IR spectrum of LiB_3O_5 doped with 5% wt. Gd_2O_3 at 750°C for 7 hours..... 85
B.4 IR spectrum of LiB_3O_5 doped with 7% wt. Gd_2O_3 at 750°C for 7 hours..... 86
B.5 IR spectrum of LiB_3O_5 doped with 9% wt. Gd_2O_3 at 750°C for 7 hours..... 87
B.6 IR spectrum of LiB_3O_5 doped with 11% wt. Gd_2O_3 at 750°C for 7 hours..... 88
B.7 IR spectrum of LiB_3O_5 doped with 15% wt. Gd_2O_3 at 750°C for 7 hours..... 89
B.8 IR spectrum of LiB_3O_5 doped with 20% wt. Gd_2O_3 at 750°C for 7 hours..... 90
B.9 IR spectrum of LiB_3O_5 doped with 25% wt. Gd_2O_3 at 750°C for 7 hours..... 91
B.10 IR spectrum of LiB_3O_5 doped with 3% wt. La_2O_3 at 750°C for 7 hours 92
B.11 IR spectrum of LiB_3O_5 doped with 5% wt. La_2O_3 at 750°C for 7 hours 93
B.12 IR spectrum of LiB_3O_5 doped with 7% wt. La_2O_3 at 750°C for 7 hours 94
B.13 IR spectrum of LiB_3O_5 doped with 9% wt. La_2O_3 at 750°C for 7 hours 95
B.14 IR spectrum of LiB_3O_5 doped with 11% wt. La_2O_3 at 750°C for 7 hours 96
B.15 IR spectrum of LiB_3O_5 doped with 15% wt. La_2O_3 at 750°C for 7 hours 97
B.16 IR spectrum of LiB_3O_5 doped with 20% wt. La_2O_3 at 750°C for 7 hours 98
B.17 IR spectrum of LiB_3O_5 doped with 25% wt. La_2O_3 at 750°C for 7 hours 99
B.18 IR spectrum of LiB_3O_5 doped with 3% wt. Y_2O_3 at 750°C for 7 hours..... 100
B.19 IR spectrum of LiB_3O_5 doped with 5% wt. Y_2O_3 at 750°C for 7 hours..... 101
B.20 IR spectrum of LiB_3O_5 doped with 7% wt. Y_2O_3 at 750°C for 7 hours..... 102
B.21 IR spectrum of LiB_3O_5 doped with 9% wt. Y_2O_3 at 750°C for 7 hours..... 103
B.22 IR spectrum of LiB_3O_5 doped with 11% wt. Y_2O_3 at 750°C for 7 hours..... 104
B.23 IR spectrum of LiB_3O_5 doped with 15% wt. Y_2O_3 at 750°C for 7 hours..... 105
B.24 IR spectrum of LiB_3O_5 doped with 20% wt. Y_2O_3 at 750°C for 7 hours..... 106
B.25 IR spectrum of LiB_3O_5 doped with 25% wt. Y_2O_3 at 750°C for 7 hours..... 107
C.1 DTA curves of LiB_3O_5 obtained from the solid-state reaction of Li_2CO_3 and H_3BO_3 at 750°C for 14 hours 109
C.2 DTA curves of LiB_3O_5 doped with 5% wt. Gd_2O_3 at 750°C for 7 hours..... 110

C.3 DTA curves of LiB_3O_5 doped with 11% wt. Gd_2O_3 at 750°C for 7 hours..... 111
C.4 DTA curves of LiB_3O_5 doped with 5% wt. La_2O_3 at 750°C for 7 hours 112
C.5 DTA curves of LiB_3O_5 doped with 11% wt. La_2O_3 at 750°C for 7 hours 113
C.6 DTA curves of LiB_3O_5 doped with 5% wt. Y_2O_3 at 750°C for 7 hours..... 114
C.7 DTA curves of LiB_3O_5 doped with 11% wt. Y_2O_3 at 750°C for 7 hours..... 115
D.1 The glow curve of LiB_3O_5 from the solid-state reaction of Li_2CO_3 and H_3BO_3 at 750°C for 14 hours 117
D.2 The glow curve of LiB_3O_5 doped with 5% wt. Gd_2O_3 at 750°C for 7 hours ... 118
D.3 The glow curve of LiB_3O_5 doped with 7% wt. Gd_2O_3 at 750°C for 7 hours ... 119
D.4 The glow curve of LiB_3O_5 doped with 11% wt. Gd_2O_3 at 750°C for 7 hours . 120
D.5 The glow curve of LiB_3O_5 doped with 5% wt. La_2O_3 at 750°C for 7 hours.... 121
D.6 The glow curve of LiB_3O_5 doped with 7% wt. La_2O_3 at 750°C for 7 hours.... 122
D.7 The glow curve of LiB_3O_5 doped with 11% wt. La_2O_3 at 750°C for 7 hours.. 123
D.8 The glow curve of LiB_3O_5 doped with 5% wt. Y_2O_3 at 750°C for 7 hours 124
D.9 The glow curve of LiB_3O_5 doped with 7% wt. Y_2O_3 at 750°C for 7 hours 125
D.10 The glow curve of LiB_3O_5 doped with 11% wt. Y_2O_3 at 750°C for 7 hours ... 126

CHAPTER I

INTRODUCTION

1.1. General Remarks

Borates are one of the most interesting industrial minerals, having been known and used since the earliest recorded history, first for precious metal working and later in ceramics. Boron and its compounds have unusually large applications from glass to fibres, flame-retardants to nuclear applications, leading us to the idea that many new applications will be found in the future.

Turkey has by far the world's largest borate reserves. Priceite deposits began to be operated in the late 1800s, and continued as the country's only borate producers until 1950-1970 when the large colemanite, ulexite, and borax deposits were discovered and slowly commercialised. Initially only crude priceite, colemanite and ulexite were shipped, but in ever increasing tonnage. After nationalization, washing facilities were installed to upgrade the products, and finally large scale purified borax, sodium perborate, and boric acid facilities were built. Nowadays, despite the increase in competition, Turkey is trying to increase its market share in world's boron production. In order to achieve these goals, special attention is paid on meeting the requirements in producing high technology borate compounds.

Research in the field of non-linear optical (NLO) devices lead to an increasing interest in new borate compounds, capable of expanding the frequency range provided by common laser sources.

Intense research on NLO borate materials began with the advent of low-temperature beta barium borate and lithium triborate, which are up to now still by far the most frequently used NLO borate materials. Presently, lithium triborate (LBO) is cited as a versatile modem optical material enjoying various applications: among them are the second harmonic generators, optical parametric oscillators, optical wave-guides and some of the other optical units.

In addition to those, due to the developments in the field of radiation protection dosimetry, nowadays, attention was directed toward new thermoluminescent (TL) materials such as borates. The borates are relatively stable chemical compounds and respond without serious problems to attempts to dope them with TL sensitisers such as the rare earths, copper and manganese ions. The resultant materials show high sensitivity, linearity and good storage properties.

1.2. Statement of the Problem

A subsequent search for new borate compounds led to the continued discovery of new borate compounds with improved NLO properties. Nowadays, rare-earth doped borate compounds are of great interest since they are found to be superior in NLO applications. Due to the high cost of the most popular thermoluminescence dosimeters, special attention have been paid on the applications of newly developed dosimeters. Very few thermoluminescent materials are tissue equivalent. Lithium borate based TL dosimeters appeared to be the most attractive. In this direction, in order to identify new optical devices, devices for specific utility, or devices with enhanced performance, sensitive and cheap devices for radiation protection, active work should be carried out on the research of appropriate new hosts doped with rare earth elements.

1.3. Objectives of the Thesis

The objective of this research is to synthesize rare-earth doped lithium triborate by solid-state reaction. In this thesis, the aim is to investigate the nature and mechanisms of the reactions occurred in the structure of lithium triborate when doped with rare-earth ions at high temperatures, and to characterize the new products, and examine any modifications in structural, morphological and thermal properties of lithium triborate doped with rare-earth elements.

1.4. Methodology of the Thesis

Lithium triborate was prepared by solid-state synthesis at high temperatures. LBO is then doped with rare-earth ions in several different concentrations. And LBO and the new products were characterized by X-Ray Diffraction (XRD) and Infrared (IR) analysis. Differential Thermal Analysis (DTA) was used for examination of the thermal properties of the compounds and the morphology of new compounds was observed by using Scanning Electron Microscopy (SEM). Dosimetric properties of the compounds were investigated by Thermoluminescence (TL) technique. Modifications in the properties of lithium triborate with the addition of rare-earth ions were examined by comparing the results obtained from the XRD, IR, DTA, SEM and TL studies carried out both for the synthesized lithium triborate and rare-earth doped lithium triborate.

1.5. Thesis Outline

Following the introduction in Chapter I, a literature survey covering very broad concepts about borates, synthesis of borates and rare-earth doped borates, their uses in non-linear optics and radiation protection is carried out in Chapter II.

Chapter III covers materials and methods employed for the synthesis of rare-earth containing borates. Materials and instrumentation used, and the experimental procedure is described.

Experimental results are stated in Chapter IV. Brief analyses of the results are given in this section. Modifications in the structural, thermal, morphological, etc. properties of lithium triborate with the addition of rare-earth elements were examined by comparing the results obtained from the XRD, IR, DTA, SEM, and TL studies.

Finally, Chapter V provides conclusions and recommendations pertinent to this study. Additional information associated with the thesis is given in the Appendices.

CHAPTER II

LITERATURE SURVEY

2.1. General Features of Boron

Boron compounds have been known for thousands of years, but the element was not isolated until 1808 by Sir Humphry Davy, and independently by Joseph-Louis Gay-Lussac and Baron Louis Jaques Thénard. This was accomplished through the reaction of boric acid with potassium.

The element is not found free in nature, but occurs as orthoboric acid usually in certain volcanic spring waters and as borates in borax and colemanite. Ulexite, another boron mineral, is interesting as it is nature's own version of "fibre optics." Important sources of boron are the ores rasorite (kernite) and tincal (borax ore). Extensive borax deposits are found in Turkey.

Boron exists naturally as 19.9% ^{10}B isotope and 80.1% ^{11}B isotope. Ten other isotopes of boron are known. High-purity crystalline boron may be prepared by the vapour phase reduction of boron trichloride or tribromide with hydrogen on electrically heated filaments. The impure, or amorphous, boron, a brownish-black powder, can be obtained by heating the trioxide with magnesium powder. Boron of 99.9999% purity has been produced and is available commercially. It has interesting optical characteristics, transmitting portions of the infrared, and is a poor conductor of electricity at room temperature, but a good conductor at high temperature [1].

Amorphous boron is used in pyrotechnic flares to provide a distinctive green colour, and in rockets as igniters. By far the most commercially important boron compound is $Na_2B_4O_7 \cdot 5H_2O$. This pentahydrate is used in very large quantities in the manufacture of insulation fibreglass and sodium perborate bleach. Boric acid is also an important boron compound with major markets in textile fibreglass and in cellulose insulation as a flame retardant. Next in order of importance is borax ($Na_2B_4O_7 \cdot 10H_2O$), which is used principally in laundry products. Use of borax as a mild antiseptic is minor. Boron compounds are also extensively used in the manufacture of borosilicate glasses. The isotope boron-10 is used as a control for nuclear reactors, as a shield for nuclear radiation, and in instruments used for detecting neutrons. Boron nitride has remarkable properties and can be used to make a material as hard as diamond. The nitride also behaves like an electrical insulator but conducts heat like a metal. It also has lubricating properties similar to graphite. The hydrides are easily oxidized with considerable energy liberation, and have been used as rocket fuels. Demand is increasing for boron filaments, a high strength, and lightweight material chiefly employed for advanced aerospace structures. Boron is similar to carbon in that it has a capacity to form stable covalently bonded molecular networks. Carboranes, phosphacarboranes, metalloboranes, and other families comprise thousands of compounds [1].

Elemental boron and the borates are not considered to be toxic, and they do not require special care in handling. However, some of the more exotic boron hydrogen compounds are definitely toxic and do require care.

Boron's chemistry and reactivity are fascinating because they form a wide variety of oxygen compounds (the borates) that occur in unending variety of simple to exceedingly complex molecules.

2.2. Borates

Among industrial minerals, borates are one of the most interesting ones. They are an unusually large grouping of minerals, but the number of commercially important borates is limited, and their chemistry and crystal structure are both unusual and complex. About 230 naturally occurring borate minerals were identified, and the increasing sophistication of analytical instruments, computer assistance, and crystallographic identification ensures that many new ones will be found in the future. The number of nonmineral borates produced in the laboratory is also very large. The reason for this abundance is boron's ability to form boron-oxygen compounds in many molecular and polymer forms. However, despite these long lists, only a few of the borates are important in commercial deposits. This includes the hydrogen borate: sassolite (H_3BO_3), the two sodium borates: borax ($Na_2B_4O_7.10H_2O$) and kernite ($Na_2B_4O_7.4H_2$), the calcium borates: colemanite ($Ca_2B_6O_{11}.5H_2O$), inyoite ($Ca_2B_6O_{11}.13H_2O$), priceite ($Ca_4B_{10}O_{19}.7H_2O$), the sodium-calcium borates: ulexite ($NaCaB_5O_9.8H_2O$), and probertite ($NaCaB_5O_9.5H_2O$), the magnesium borates: szaibelyite (ascharite) ($Mg_2B_2O_5.H_2O$), inderite or kurnakovite ($Mg_2B_6O_{11}.15H_2O$), and pinnoite ($MgB_2O_4.3H_2O$), the magnesium-calcium borate: hydroboracite ($CaMgB_6O_{11}.6H_2O$), the borosilicates: datolite ($Ca_2B_2Si_2O_9.H_2O$) and ludwigite (Mg_2FeBO_5), and magnesium chloride double salt boracite ($Mg_3B_7O_{13}Cl$). Each of these minerals is being, or has been, mined and processed on a commercial scale [2].

2.2.1. Borate Deposits

World's borate reserves are shown in *Table 2.1*. Turkey has by far the world's largest borate reserves followed by USA, Russia, Chile, China, Peru, Bolivia, Kazakhstan and Argentina.

Table 2.1 *World's Borate Reserves* [3]

Countries	**Reserve (Million tones B_2O_3)**	**Reserve (% B_2O_3)**
Turkey	563	64
Russia	100	11
USA	80	9
Chile	41	4
China	36	4
Peru	22	3
Bolivia	15	2
Kazakhstan	15	2
Argentina	9	1
Total	885	100

By far the world's largest reserves of borates occur in a 300 km east-west, 150 km north-south, L-shaped area in western Turkey. It is south of Marmara Sea in western Anatolia and 70-100 km east of the Aegean Sea and the city of İzmir. There are four main borate districts, each having different mineralization, but of a similar age, with sediments deposited from inland lakes during active volcanic periods [2].

In northwestern corner of this borate district (Bursa province), the Sultançayırı deposit contained predominantly priceite in a gypsum-clay matrix, whereas nearby, Kestelek has colemanite in more normal clay-marl strata. Bigadiç (Balıkesir province), in the district's southwestern corner, has both colemanite and ulexite, while Emet (Kütahya province), in the south-central district, is similar to Kestelek. Finally, Kırka (Eskişehir province) in the southeastern corner contains primarily borax.

Kırka, the world's largest borax deposit, is located in western Anatolia 240 km west of Ankara, and in the southern corner of the borate district. Colemanite outcrops were first discovered at Kırka in 1960 on its western and southern edges. Advanced exploration of the area showed that the ore deposit was consisted mostly of borax, with minor amount of colemanite and ulexite. The estimated reserve is 500 million metric tons containing 25% B_2O_3.

2.2.2. Uses of Borates

Boron and its compounds have unusually large applications from glass, abrasives and refractories, cleaning compounds and bleaches, fibres and composites to flame retardants, fuels, glazes, frits and enamels, etc. They also find application in agriculture, medicine, metallurgy and nuclear applications. [2].

In general, boron considerably reduces the thermal expansion of glass, provides good resistance to vibration, high temperatures and thermal shock, and improves its toughness, strength, chemical resistance and durability. It also greatly reduces the viscosity of the glass melt as its being made. These features, and others, allow it to form superior glass for many industrial and specialty applications.

The boride compounds are very hard and are used as abrasives and refractories. Boron nitride (BN), and boron carbide (B_4C) are the most important compounds that have application in these fields.

Boron is essential to plant growth, being one of the basic plant nutrients. Another important function of boron is in cell growth and structure. A deficiency changes the cell walls, making most of them thinner.

The mild alkalinity of borax allows it to emulsify oil and greases, and to reduce the surface tension of water, which aids in loosening dirt particles. This combination

gives borax a strong but gentle cleansing action for personal use, and on many types of fabrics, surfaces and contaminants.

Composites of boron and boride fibres in a matrix of plastics, ceramics or metals have great strength and a high modulus of elasticity. The initial applications for these advanced composites were the military, primarily in the air or spacecraft. Other applications include sports equipment such as golf club shafts, tennis rackets, etc.

Boric acid, borax and pentahydride have been used to make inexpensive cellulose insulation material. If the cellulose is treated with a borate solution it becomes reasonably fire resistant, toxic to bacteria, and unpalatable for rats, mice, and insects.

Boron and its hydrides have the highest heat of combustion per unit weight of all the elements, causing it to be considered as a fuel for aircraft or space.

One of the earliest uses of borates, and one that is still important even though it does not consume much borax, is the production of glazes and frits to impart colour and texture, as well a heat, chemical, or wear resistance to appliances, ceramics, and tile. Borax assists in the production of smooth, hard, resistant, blemishless, and craze-free ceramic surfaces.

Boric acid and sodium borate are mild antiseptics that inhibit gram-negative bacteria, and boric acid has long been used as eyewash. Some heterocyclic boron compounds inhibit tumour growth, while borax and some of its ores are highly effective in killing parasites. In other medical applications, some boron compounds reduce serum cholesterol and other harmful proteins.

The addition of 0.001% to 0.003% boron to steel reduces the amount of nickel, chromium, or molybdenum required in many alloys. Boron strengthens high-performance, low-alloy steels by precipitating certain carbides, and by its effect on

crystal structure. Many electroplating-bath compositions include boron chemicals as buffers, cleansers, and agents to reduce the deposit's pitting and porosity.

In nuclear reactors the fission of radioactive material produces heat and a variety of alpha and beta particles, gamma rays and neutrons. The most effective materials for shielding the neutrons are boron (especially ^{11}B), hydrogen, lithium, polyethylene and water. Most of the shielding materials produce secondary gamma rays, which then require heat removal and further shielding. Boron is unique in its ability to absorb thermal neutrons and produce only a soft gamma ray and an easily absorbed alpha particle.

2.3. Lithium Triborate

Lithium triborate, LiB_3O_5 (LBO) is a new non-linear optical (NLO) crystal. Mazzetti and Carli [4] proved the existence of the LiB_3O_5 compound in 1926, followed by Rollet and Bouaziz [5]. In 1958, a binary phase diagram $Li_2O–B_2O_3$ was elaborated by Sastry and Hummel [6]. In this diagram, the presence of the $Li_2O·3B_2O_3$ compound, melting incongruently at about 834 °C was established. The structure of LBO was described by, König and Hoppe [7] 20 years later. Chen [8] discovered the possible application of LBO crystals in non-linear optics.

According to König and Hoppe, lithium triborate crystallizes in the orthorhombic system with the space group $Pna2_1–C_{2v}$. The unit cell parameters are: a = 8.446 Å, b = 5.13 Å, c = 7.38 Å.

In 1997, Bétourné and Touboul [9] have refined the LiB_3O_5 cell parameters from those known using X-ray powder diagram: a = 8.456 Å, b = 7.376 Å, c = 5.133 Å, the space group $Pna2_1$. The indexed X-ray powder diagram of LiB_3O_5 is given in the following table.

Table 2.2 *LiB_3O_5 X-ray diffraction data (Bétourné and Touboul, 1997)*

hkl	$2\theta_{obs}$ (°)	$2\theta_{calc}$ (°)	$\Delta 2\theta$ (°)	d_{obs} (Å)	I_{obs}
110	15.900	15.932	0.032	5.569	100
200	21.026	20.995	– 0.031	4.222	4
111	23.541	23.576	0.035	3.786	92
210	24.232	24.245	0.013	3.670	36
120	26.362	26.345	– 0.017	3.378	39
201	27.302	27.307	0.005	3.264	94
211	29.907	29.918	0.011	2.985	99
121	31.683	31.670	– 0.013	2.822	72
220	32.179	32.184	0.005	2.779	87
002	34.923	34.937	0.014	2.567	4
221	36.747	36.746	– 0.001	2.4438	71
130	38.073	38.089	0.016	2.3616	68
311	38.426	38.394	– 0.032	2.3407	53
320	40.245	40.239	– 0.006	2.2390	30
031	40.666	40.659	– 0.007	2.2168	26
202	41.115	41.115	0.000	2.1937	11
131	42.110	42.098	– 0.012	2.1441	62
400	42.645	42.739	0.094	2.1184	66
022	42.920	42.902	– 0.018	2.1055	21
122	44.188	44.281	0.093	2.0480	24
401	46.429	46.418	– 0.011	1.9542	50
411	48.111	48.120	0.009	1.8897	14
330	49.121	49.135	0.014	1.8532	6
140	50.559	50.629	0.070	1.8038	8

In 2003, Sabharwal et al. [10] have recorded the powder diffraction pattern for LBO material synthesized by solid-state sintering. The starting Li_2CO_3 and B_2O_3 powders taken in stoichiometric ratio was ball milled and sintered at 700°C for 48h to form the phase. All the measurements were performed using Cu Kα source. The powder diffraction pattern shown in the following figure is found to match very well with the powder diffraction data reported in LBO phase [11].

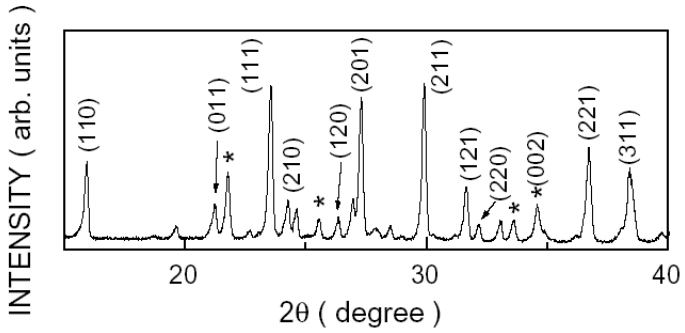

Figure 2.1 *X-ray powder diffraction patterns of LBO material synthesized by solid-state sintering method. The reflections marked by (*) have been identified with $Li_2B_4O_7$ (Sabharwal et al., 2003)*

In 2004, again Sabharwal et al. [12] have recorded the powder XRD patterns for materials prepared by solid-state sintering at 650°C and 700°C using Cu Kα source. In the former case, while the predominant phase formed is LiB_3O_5 [11], the presence of impurity phases, namely $Li_2B_4O_7$ [13] and $Li_2B_8O_{13}$ [14], is also revealed by plot (a) in *Figure 2.2*. The presence of impurity phases was also seen in materials sintered at 700°C for 24 h. However, on increasing the sintering period to 120 h, the impurity phase concentration was significantly reduced, as can be seen from *Figure 2.2* (b).

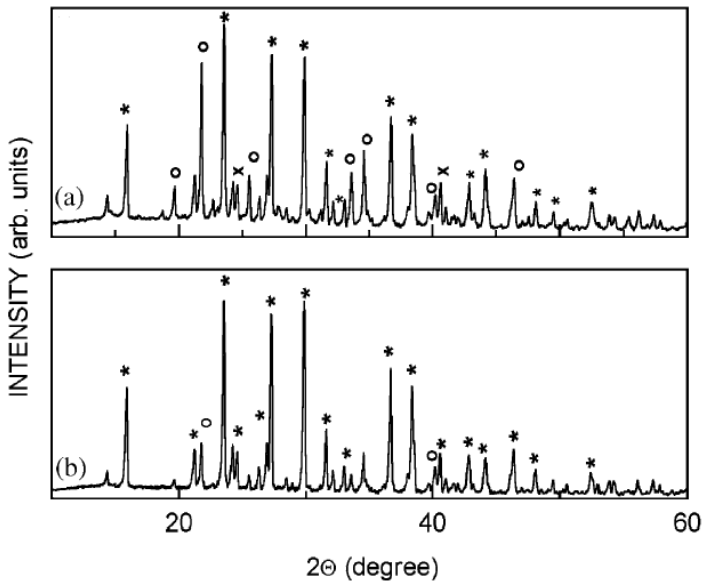

Figure 2.2 *Powder X-ray diffraction patterns recorded for the polycrystalline LBO materials synthesized by solid-state sintering at: (a) 650℃ for 24 h and (b) 700℃ for 120 h. The reflections marked by (*) have been identified with LiB_3O_5, (o) with $Li_2B_4O_7$ and (×) with $Li_2B_8O_{13}$ (Sabharwal et al., 2003)*

Moryc and Ptak [15] in 1999, studied the infrared spectra of LBO. The LBO samples were made from lithium carbonate, natural boric acid, boric acid containing isotope ^{10}B (94.4%) and ^{11}B (98.4%) and hydrated lithium hydroxide with ^{6}Li isotope.

Homogenized mixtures were heated in a platinum crucible at 750°C for 6 h. The synthesized samples were investigated in the IR regions. The obtained spectra are presented in *Figure 2.3*. The observed frequencies for various isotopic composition and their assignments to the respective vibrations are given in *Table 2.3*.

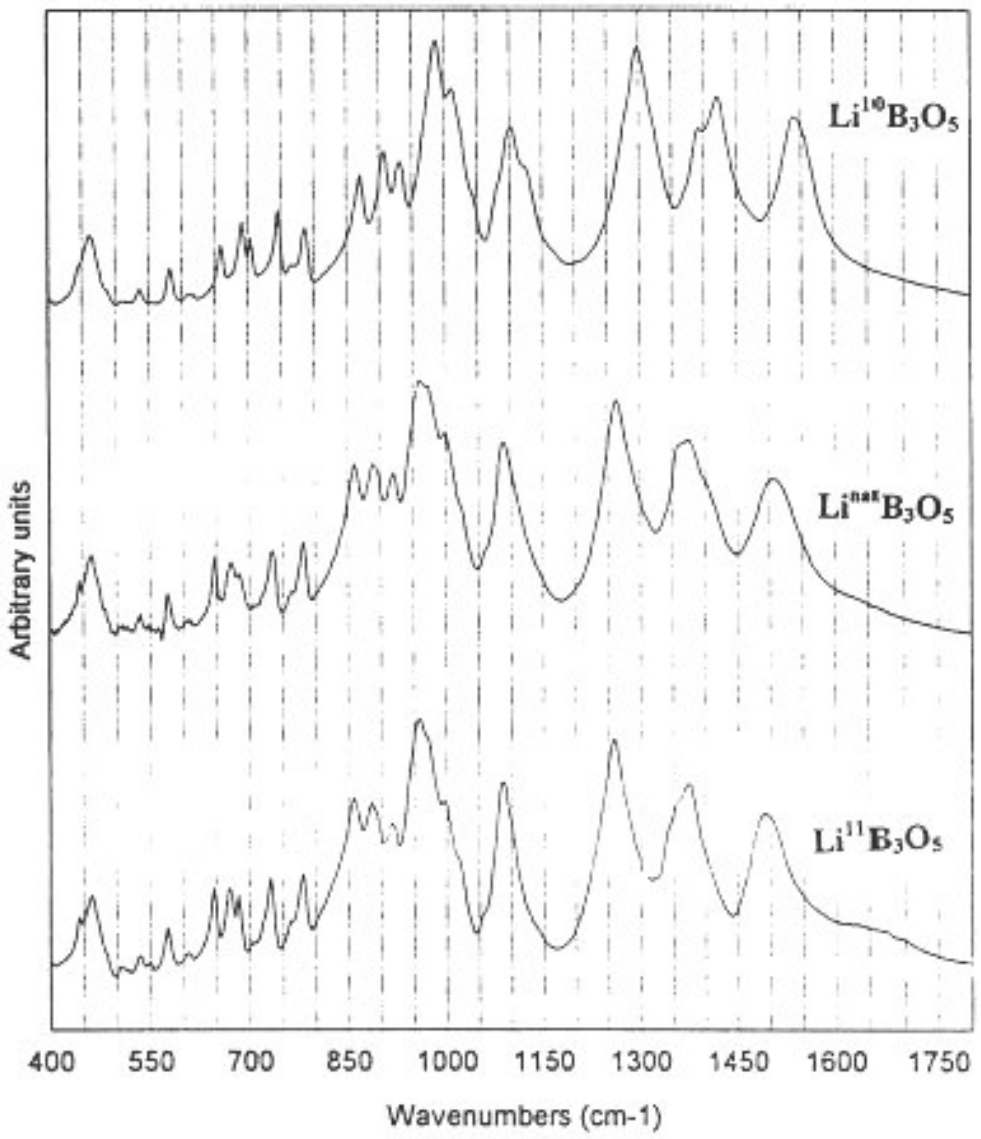

Figure 2.3 *Infrared spectra of: $Li^{11}B_3O_5$, $Li_{nat}B_3O_5$, and $Li^{10}B_3O_5$ (Moryc and Ptak, 1999)*

Table 2.3 *Frequencies of the vibrational modes for the LiB_3O_5 phase (Moryc and Ptak, 1999)*

$Li^{10}B_3O_5$	$Li_{nat}B_3O_5$	$Li^{11}B_3O_5$
1540 vs	1506 vs	1491 vs
1422 vs	1372 vs	1374 vs
1391 vs		
1298 vs	1263 vs	1260 vs
1102 vs	1089 vs	1088 vs
1011 vs	1000 vs	997 vs
	973 vs	970 vs
988 vs	961 vs	960 vs
932 s	920 s	918 s
909 s	889 s	885 s
872 s	860 s	858 s
787 m	782 m	781 m
766 w	765 w	
747 m	736 m	731 m
	713 vw	708 vw
706 m	686 m	683 m
693 m	673 m	669 m
660 m	648 m	646 m
617 vw	601 vvw	608 vw
610 vw	578 m	577 m
583 m	563 w	
554 vvw	550 w	548 w
536 w	535 w	534 w
511 vvw	508 vvw	505 w
463 m	482 w	461 m
	463 m	
446 m	444 m	444 m

2.3.1. Rare-earth Doped Borates

Rare earth elements have a long history in optical and magnetic applications. Among these, luminescent devices using single crystals, powders, and glasses have been particularly important. Rare earths have important characteristics that distinguish them from other optically active ions: they emit and absorb over narrow wavelength ranges, the wavelengths of the emission and absorption transitions are relatively insensitive to host material, the intensities of these transitions are weak, the lifetimes of metastable states are long, and the quantum efficiencies tend to be high, except in aqueous solutions. These properties all result from the nature of the states involved in these processes and lead to excellent performance of rare earth elements in many optical applications such as lasers and amplifiers restricted to using single-crystal or glass hosts. Whereas in many applications crystalline materials are preferred for reasons that include higher peak cross sections or better thermal conductivities, the versatility of glasses and the broader emission and absorption spectra they provide have led to the use of rare earth doped glasses in many applications [16].

Glasses doped with rare earth elements are of prime importance for the development of fibre lasers, optical amplifiers, lasers, sensors, energy up converters and so on. In this direction, a great amount of investigation has been carried out to optimise new glass matrices containing rare earth elements.

Sankar and Subba Rao [17] investigated luminescence studies on doped borates. Compounds have been synthesized by the solid-state reaction and are subjected to photoluminescence studies after characterization by powder XRD, density, TG/DTA, IR and Diffuse reflectance spectroscopy. The luminescence features of Eu, Sm, Gd, Dy, Bi, and Pb ions were discussed.

Zeng et al. [18] studied luminescence and its temperature effects on Sm^{2+} in alkaline earth borates. Samples of BaB_8O_{13}, SrB_4O_7 and SrB_6O_{10} prepared by an intimate mixture of analytical-grade barium (strontium) carbonates and boric acid (3 mol%

excess) were doped with rare-earth ions. The concentration of the dopant Sm_2O_3 is 2 mol% of Ba^{2+} (Sr^{2+}) ions.

In 2000, Babu and Jayasankar [19,20] investigated the spectroscopic properties of Eu^{3+} and Dy^{3+} ions in lithium borate glasses. The starting materials Li_2CO_3, H_3BO_3 and Eu_2O_3 or Dy_2O_3 mixed in different compositions were thoroughly mixed and melted in an electric furnace in the temperature range 900±950°C for about 30 min in a porcelain crucible. After melting, heating was continued for 15 min to homogenise the melt. The melt was then air-quenched by pouring it on a thick brass plate and pressed with another brass plate. In order to remove strain, the glass samples were annealed for 5 h in an oven at 350°C (above which the sample may lose its glassy nature). Finally, these glass samples were cut for desired dimensions and polished.

Jubera et al. [21] investigated the luminescent properties of Eu^{3+}-activated lithium rare earth borates and oxyborates. The samples were synthesized by solid-state reaction. The starting materials were Ln_2O_3 (Ln=Lanthanides and Y), H_3BO_3, $LiBO_2$, and $LiOH \cdot H_2O$. Stoichiometric amounts of the reactants were dissolved in concentrated nitric acid in order to obtain a homogeneous distribution of the constituents, and then the solutions were evaporated to dryness. The heating procedures consisted in three steps. First, samples were heated at 400°C for 2 h, then to 700°C until all nitric vapours were evacuated. Finally, the products were fired for 15 h at 800°C, in the case of the compounds $Li_6Ln(BO_3)_3$, at 900°C in that of oxyborates and at 1200°C in that of the borates $Li_3Ln_2(BO_3)_3$.

2.3.2. Rare-earth Doped Lithium Triborate

In 2001, Thomazini et al. [22] investigated the structural properties of lithium borate glasses doped with rare earth elements. LBO glass samples were prepared from mixtures of boron oxide and lithium carbonate in the following stoichiometric proportion:

$$3\ B_2O_3 + Li_2CO_3 \rightarrow 2\ LiB_3O_5 + CO_2$$

Some samples were prepared with addition of niobium oxide (Nb_2O_5) to observe the influence of niobium as a network modifier. Then, the LBO samples were doped with Pr^{3+}, Nd^{3+}, and co-doped with Pr^{3+} and Yb^{3+}. The samples were studied by Raman spectroscopy, infrared absorption and differential thermal analysis.

For Pr^{3+}:LBO and Pr^{3+}/Yb^{3+}:LBO glasses, an increase of the glass transition and crystallization temperatures, and a decrease of fusion temperature as a function of the increase of the rare earth doping content were observed. For Nd^{3+}:LBO and Pr^{3+}/Yb^{3+}:LBO+Nb_2O_5 glasses, a decrease of the glass transition was noted. The difference between glass transition and crystallization increases with the addition of rare earth elements, promoting a higher thermal stability of these glasses.

The infrared analyses show that the B-O link is configured in trigonal form. With the addition of rare earth elements, no change related to B-O link or trigonal configuration of boron was observed. The presence of NbO_6 octahedra in the Pr^{3+}/Yb^{3+}:LBO+Nb_2O_5 samples was confirmed by infrared analysis.

Boroxol rings were detected by Raman spectroscopy, confirming the presence of triangles and tetrahedrons of boron. In these samples, vibration modes associated to rare earth elements were not observed, probably due to the small amount of these elements in the matrix. In Pr^{3+}/Yb^{3+}:LBO+Nb_2O_5, the vibrational mode of Nb-O in the NbO_6 octahedra was observed.

2.4. Borates in Nonlinear Optics

The discovery of laser has initiated significant advancements in science and technology. Immediately after the creation of the first laser in 1960 [23], interactions between lasers and materials have been widely investigated. Since then, very intensive research has been carried out in the field of non-linear optical (NLO)

devices, as they are capable of expanding the frequency range provided by common laser sources.

The first NLO borate described was $KB_5O_8.4H_2O$ [24] in 1975, but intense research on NLO borate materials began with the advent of low-temperature β-BaB_2O_4 (BBO) [25,26] and LiB_3O_5 (LBO) [8], which are up to now by far the most frequently used NLO borate materials.

After that, various borate crystals, including $Sr_2B_2Be_2O_7$ (SBBO) [27], BiB_3O_6 (BiBO) [28] and $Ca_4LnO(BO_3)_3$ (CLnOB, where Ln = Gd, La, Y) [29], have been studied as promising NLO crystals. The family of the various borate crystals thus plays a very important role in the field of non-linear optics.

In these fields, great progress has been made since the advent of the first "high-tech" borate material β-BaB_2O_4 and the subsequent discovery of LiB_3O_5 and several further suitable borate compounds. Borates are superior in UV applications to other commonly used NLO materials because of their high UV transmittance [30] combined with a high damage threshold.

LBO, the new NLO crystal offers several advantages such as excellent chemical stability, high damage threshold, wide phase matching angle and remains transparent into the far-UV. These properties allow for an application of the LBO crystals in non-linear optics.

2.5. Borates in Radiation Protection

Developments in the field of radiation protection dosimetry lead to the trend of switching over to thermoluminescence dosimetry (TLD). TLD is generally recognised as the most versatile technique for the measurement of X, gamma and beta radiations, especially in personal monitoring.

Termoluminescence (TL) is the phenomenon of light emission caused by heating a pre-irradiated TL material. In 1981, Pradhan [31] reviewed thermoluminescence dosimetry and its applications. According to Pradhan, for radiation dosimetry it is preferable to have TL detector with:

i. Simple glow curve structure;
ii. High gamma ray sensitivity;
iii. Negligible fading of TL signal;
iv. Emission spectrum around 4500Å;
v. Linear response;
vi. Simple annealing procedure for reuse;
vii. Chemical stability and inertness to extreme climatic variations;
viii. Effective atomic number (Z) close to that of tissue;
ix. Insensitivity to daylight.

In addition to the widely used TL dosimeters, Pradhan has stated the general characteristics of MgB_4O_7:Dy, $Li_2B_4O_7$:Mn, $Li_2B_4O_7$:Cu,Ag, $Li_2B_4O_7$:Cu as promising TL dosimeters especially with their tissue equivalent effective atomic number.

El-Faramawy et al. [32] studied the dosimetric properties of copper doped lithium borate examined using the TL-technique. The temperature at which the TL is observed to be most intense is at 178ºC. Furthermore, this study indicated that this material has low fading and wide linear dose response.

In 2001, Prokic [33] investigated lithium borate solid TL detectors. Dosimetric characteristics of new tissue-equivalent thermoluminescent detectors, $Li_2B_4O_7$: Cu; In; Ag and $Li_2B_4O_7$: Cu; In in the form of sintered pellets were presented. Glow curves consisted of well-defined dosimetric peaks with TL sensitivity were attained.

Furetta et al. [34] presented the dosimetric characteristics of tissue equivalent thermoluminescent solid TL detectors based on lithium borate. Glow-curve shapes, TL sensitivity, photon dose response, minimum detectable dose, relative photon energy response, fading, reproducibility, precision of dose measurements and annealing procedure for $Li_2B_4O_7$:Cu, $Li_2B_4O_7$:Cu,In were given in detail.

CHAPTER III

MATERIALS AND METHODS

3.1. Materials

The following solid powders were used in the synthesis of the products:

Li_2CO_3, H_3BO_3, Gd_2O_3, La_2O_3, Y_2O_3 (From Merck)

In addition to those, spectroscopic grade potassium bromide (KBr) was used for making IR pellets.

3.2. Instrumentation

3.2.1. Powder X-Ray Diffractometer

XRD examinations were performed to identify the structure of the products. XRD patterns were recorded from $10°<2\theta<80°$ by using a Rigaku MiniFlex X-ray Diffractometer with a CuKα radiation source.

Specific d value for each peak was calculated from the corresponding 2θ values by using the Bragg's equation given in *Equation 3.1*. The identification was done by comparing those d values with the characteristic d values in the International Centre for Diffraction Data (ICDD) cards of the appropriate materials.

$$\mathbf{n \cdot \lambda = 2 \cdot d \cdot \sin\theta} \quad (3.1)$$

where,

n: an integer (n = 1, 2, 3, …, n)

λ: the wave length (λ = 1.54056 for Cu anode)

d: the distance between successive parallel planes, Å

θ: the angle of incidence and reflection of the x-ray beam from the given atomic plane.

3.2.2. Infrared Spectrometer

IR examinations were performed to determine the structure of the produced new phases. The infrared spectra of the samples were measured from 400-4000 cm^{-1} with Nicolet 510 FTIR Infrared Spectrometer. IR pellets were prepared using spectroscopic grade KBr with a KBr:Sample ratio of 100mg:3mg. KBr was dried at 180 °C for several hours before the preparation of pellets.

In KBr pellet method, the solid sample is finely pulverized with pure, dry KBr. The mixture is pressed in a hydraulic press to form a transparent pellet, and the spectrum of the pellet is measured. It is important that the solids be extremely finely divided and well mixed. The pellet is pressed in a special die that can be evacuated in order to avoid entrapped air, which causes cloudiness in the pellet.

3.2.3. Differential Thermal Analyser

DTA was carried out to obtain the thermal behaviour of the materials using Setaram Labsys TGA/DTA Simultaneous Thermogravimetrik Analyzer and Differential

Thermal Analyzer. The analyses were performed in aluminium crucibles with a heating rate of 10°C/min under nitrogen.

3.2.4. Scanning Electron Microscope

SEM was carried out to determine the morphology of the samples using JSM-6400 Electron Microscope (JEOL), equipped with NORAN System 6 X-ray Microanalysis System & Semafore Digitizer. The microscope is equipped with secondary and backscattered electron detectors and an X-Ray microanalysis system; it is capable of providing both topographical and compositional information about the specimen.

Samples are coated with a very thin layer of a gold-palladium (Au-Pd) alloy or carbon (C) in this device by using HUMMLE VII Sputter Coating Device (ANATECH).

3.2.5. Thermoluminescence Reader

The dosimetric properties of the samples were determined by using Harshaw TLD Reader Model 3500 with a heating rate of 1 °C/sec, between room temperature and 400 °C. The examined dosimeters were exposed to Beta, 90Sr-90Y radiations at room temperature. The sample amount was 20 mg.

3.2.6. Furnace

Solid-state reactions have been carried out in air by using Protherm furnace. Heating was up to 750 ºC. To avoid melting, reactions started at room temperature.

3.3. Experimental Procedure

3.3.1. Synthesis of Lithium Triborate

Appropriate quantities of Li_2CO_3 and H_3BO_3, weighed separately, were mixed and finely powdered in an agate mortar. Homogenized mixture was transferred into a convenient porcelain crucible and preheated at 300 ºC for 4 hrs to obtain CO_2 and H_2O release. To avoid melting, reactions were started at room temperature, increasing gradually. The mixture is then cooled in a desicator and the weight loss is recorded. After cooling, the mixture was regrinded to help diffusion of atoms. Then, the mixture was heated at 750 ºC for 14 hrs. In between and at the end of the heating process, the mixture was cooled in a desicator and was regrinded. The expected reaction is given below.

$$Li_2CO_3 + 6H_3BO_3 \rightarrow 2LiB_3O_5 + CO_2 + 9H_2O$$

3.3.2. Synthesis of Rare-earth Doped Lithium Triborate

Prepared LiB_3O_5 and Gd_2O_3, La_2O_3 and Y_2O_3 samples were weighed separately at different concentrations and ground together in an agate mortar. The mixtures were then heated at 750 ºC for 7 hrs. The reactions were started at room temperature increasing gradually. Then, the mixtures were cooled in a desicator and were regrinded. The concentrations of rare earth elements doped into LiB_3O_5 are given in the following table.

Table 3.1 *Concentrations of rare earth elements in LiB_3O_5*

Id.	Gd_2O_3 (wt %)	Id.	La_2O_3 (wt %)	Id.	Y_2O_3 (wt %)
3Gd	3	3La	3	3Y	3
5Gd	5	5La	5	5Y	5
7Gd	7	7La	7	7Y	7
9Gd	9	9La	9	9Y	9
11Gd	11	11La	11	11Y	11
15Gd	15	15La	15	15Y	15
20Gd	20	20La	20	20Y	20
25Gd	25	25La	25	25Y	25

CHAPTER IV

RESULTS AND DISCUSSION

4.1. Synthesis of Rare-earth Doped Lithium Triborate

The stoichiometric mixture of reactants with respect to equation given below was heated at 750 ºC for 14 hrs. The desired reaction is given below.

$$Li_2CO_3 + 6H_3BO_3 \rightarrow 2LiB_3O_5 + CO_2 + 9H_2O$$

Rare earth elements with different concentrations stated in *Table 3.1* were doped into LiB_3O_5 samples. Called LBO samples were prepared from the solid-state reactions of Li_2CO_3 with H_3BO_3 as described above. The mixture of reactants was heated at 750 ºC for 7 hrs.

Powder X-Ray Diffraction, Infrared Spectrometry, Differential Thermal Analysis, Scanning Electron Microscopy, and Thermoluminescence studies were used for the characterization of compounds.

4.1.1. Powder X-Ray Diffraction

XRD examinations were carried out to identify the structure of the products. XRD patterns of the prepared samples are given in the following figures. Also, the XRD patterns of each separate sample were given in *Appendix A*. For the patterns in the

Appendices section, peaks abbreviated with (*) represent the peaks of LBO and peaks abbreviated with (0) represents the corresponding RE oxides.

Figure 4.1 represents the XRD pattern of LiB_3O_5 and LiB_3O_5 doped with Gd_2O_3. The pattern at the bottom of the figure belongs to LBO and the patterns above are the patterns of Gd_2O_3 doped LBO. The powder diffraction pattern of the LBO sample is found to match with the powder diffraction data reported in LBO phase [11]. Lithium triborate crystallizes in the orthorhombic system with the space group $Pna2_1$. The unit cell parameters are: a = 8.446 Å, b = 5.13 Å, c = 7.38 Å. This showed that the resulting material was lithium triborate. The powder diffraction pattern of Gd_2O_3 is also found to match with the reported phase [35]. At lower concentrations the peaks of LBO are still dominant but the peaks belonging to rare earth elements are also observed. However, when the concentrations of the rare earth elements increases, with respect to LBO, the peaks of rare earth elements become dominant. On the other hand, LBO peaks still remain. The addition of 5% Gd_2O_3 is the limit in crystallinity because at higher Gd_2O_3 concentrations, peak intensities of LBO decreases.

The XRD patterns of La_2O_3 doped samples were given in *Figure 4.2*. Again, the pattern at the bottom of the figure belongs to LBO. For the patterns at the top of the figure, peaks belonging to La_2O_3 were observed in agreement with the literature [36]. The difference of the La_2O_3 doped samples from the Gd_2O_3 doped ones is that, the addition of 11% La_2O_3 is the limit for the dominance of LBO peaks to remain. It means, when the concentrations of the rare earth elements increases above 11%, the peaks of rare earth elements become dominant, with respect to LBO.

Figure 4.3 represents the XRD pattern of LiB_3O_5 doped with Y_2O_3. Just like Gd_2O_3, the addition of 5% Y_2O_3 is the limit in crystallinity. At higher Y_2O_3 concentrations, peak intensities of LBO decreases and the peaks of rare earth elements become dominant. The powder diffraction pattern of Y_2O_3 peaks observed is found to match with the reported powder diffraction data [37].

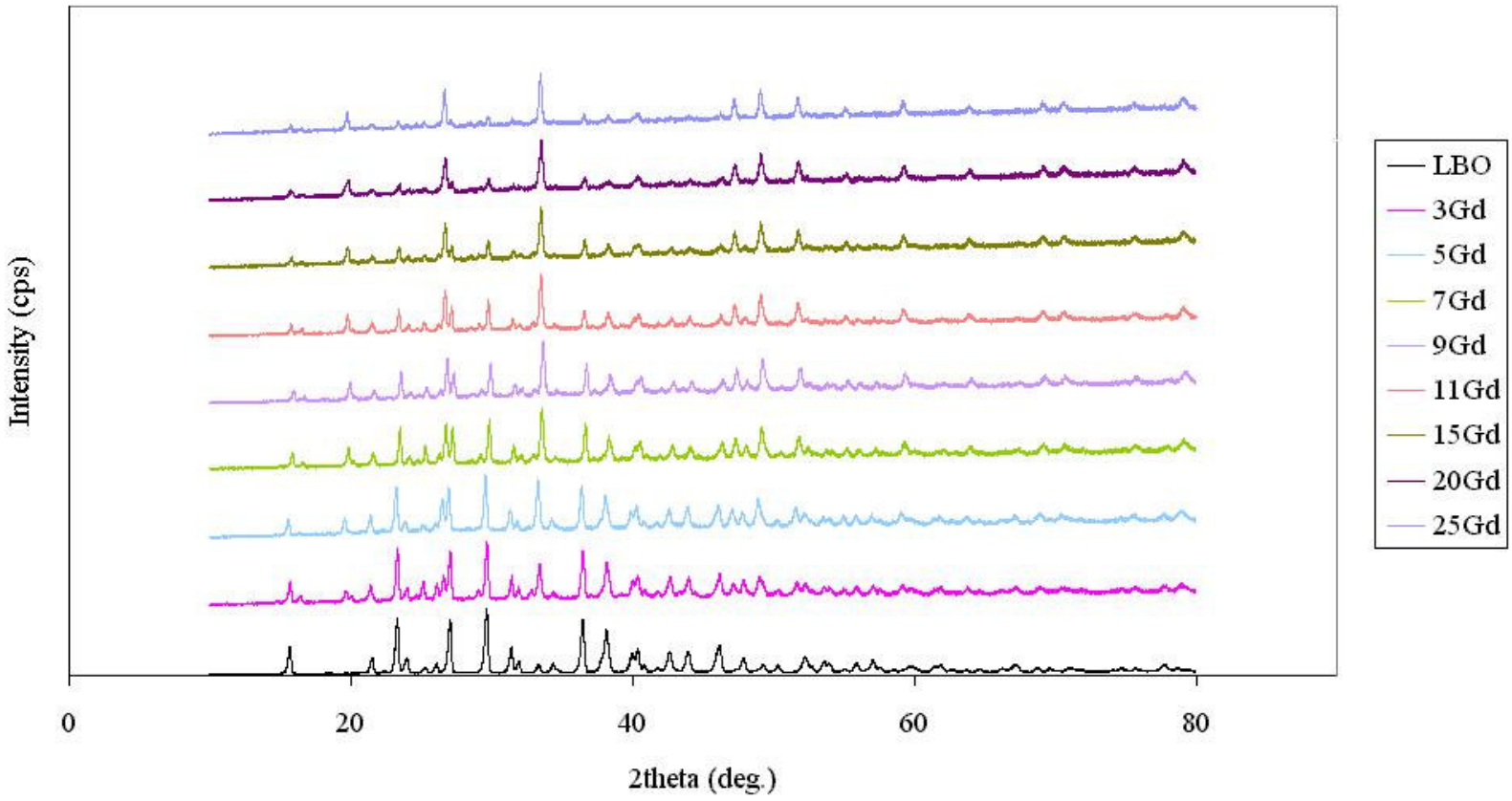

Figure 4.1 *Powder x-ray diffraction pattern of LiB_3O_5 and LiB_3O_5 doped with Gd_2O_3*

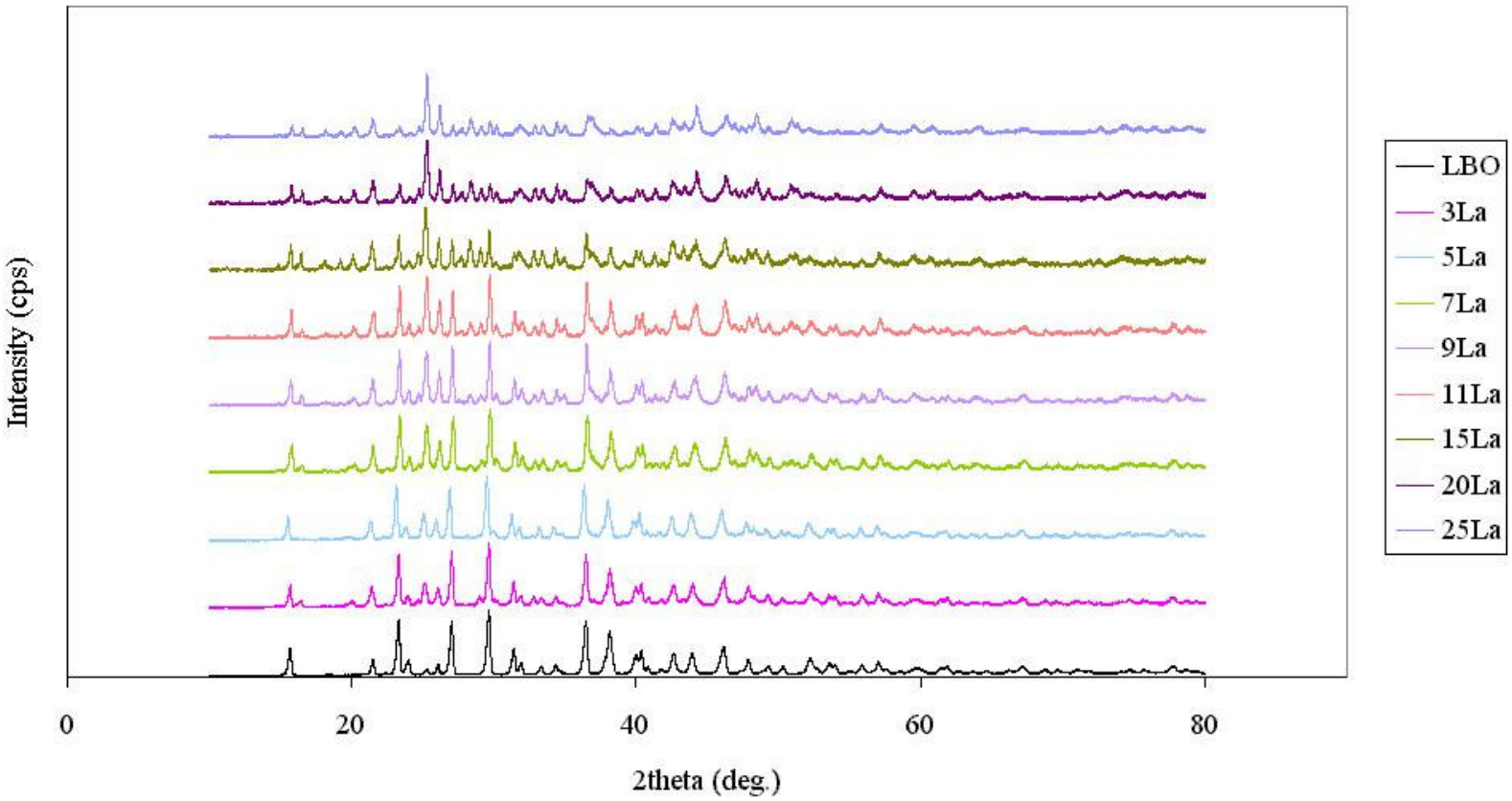

Figure 4.2 *Powder x-ray diffraction pattern of LiB_3O_5 and LiB_3O_5 doped with La_2O_3*

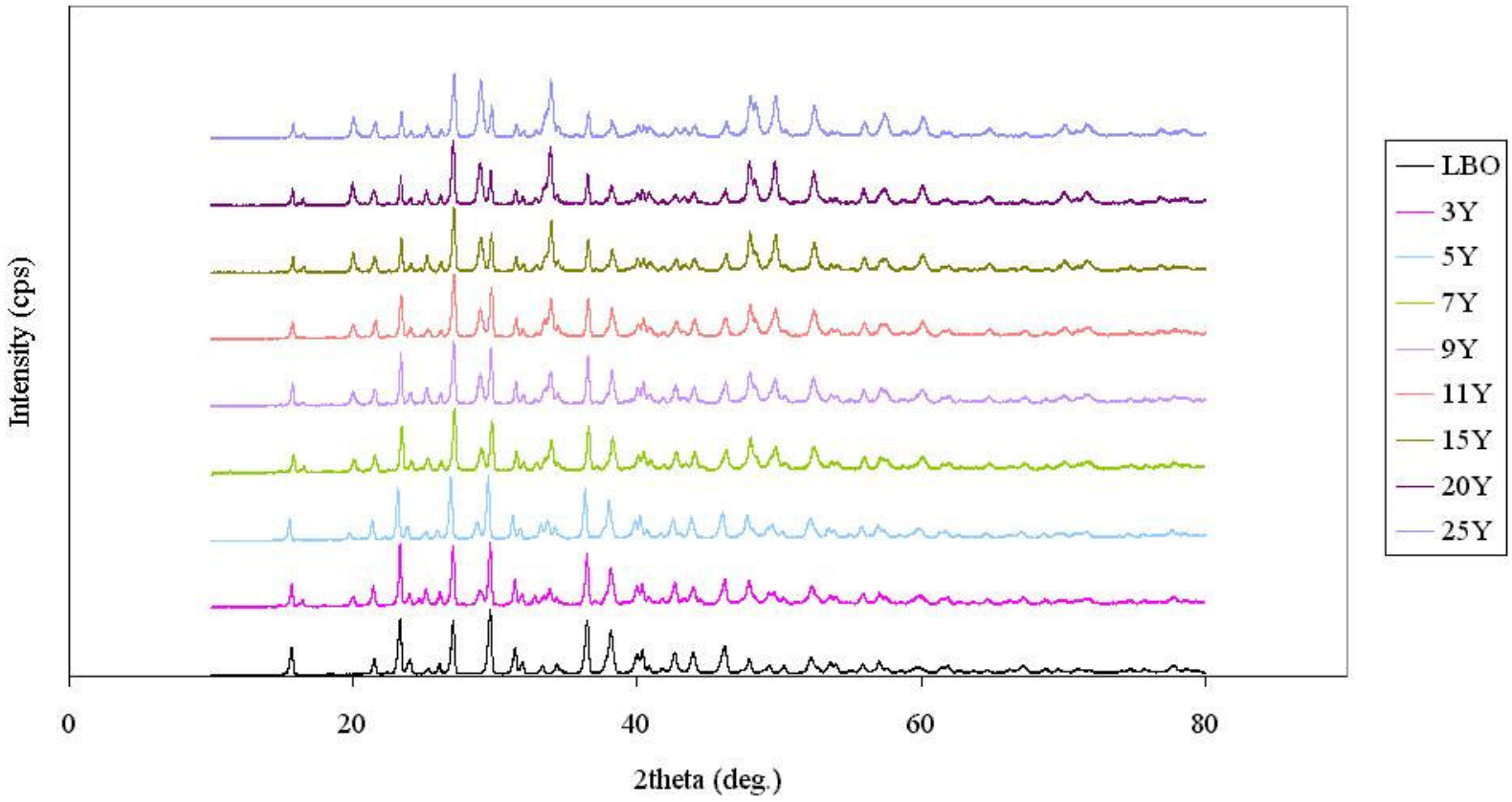

Figure 4.3 *Powder x-ray diffraction pattern of LiB_3O_5 and LiB_3O_5 doped with Y_2O_3*

4.1.2. Infrared Spectra

IR examinations were performed to determine the structure of the produced new phases. The IR spectra of the prepared samples are given in the following figures. Separate IR spectra of each sample were also given in *Appendix B*.

In *Figure 4.4*, the infrared spectra of LBO and LBO doped with Gd_2O_3 were given and *Figures 4.5 and 4.6* show the infrared spectra of LBO and LBO doped with La_2O_3 and Y_2O_3, respectively. In these figures bands are observed in good agreement with the literature [23]. In the LiB_3O_5 compound, the boron atoms have three-fold and four-fold coordination. For the trigonal coordination, the characteristic bands are the stretching bands of the highest intensity, occurring above 1200 cm^{-1} and the weaker bands in the region 700–800 cm^{-1} attributed to scissor vibrations of B-O-B bridges in the boron oxygen network. For the tetrahedral coordination, the typical bands are situated in the 850–1100 cm^{-1} range ascribed to the stretching vibration of B-O.

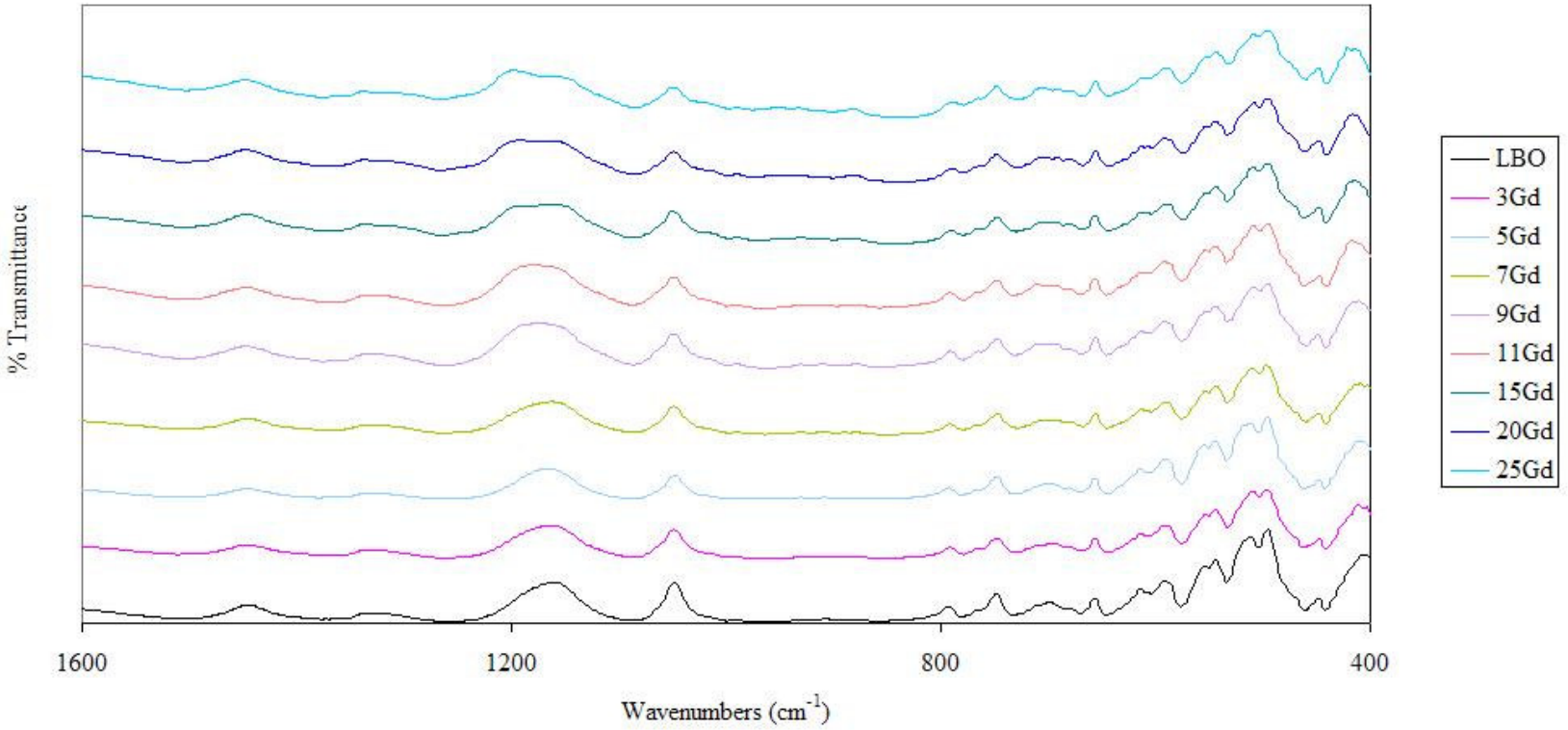

Figure 4.4 *IR spectra of LiB_3O_5 and LiB_3O_5 doped with Gd_2O_3*

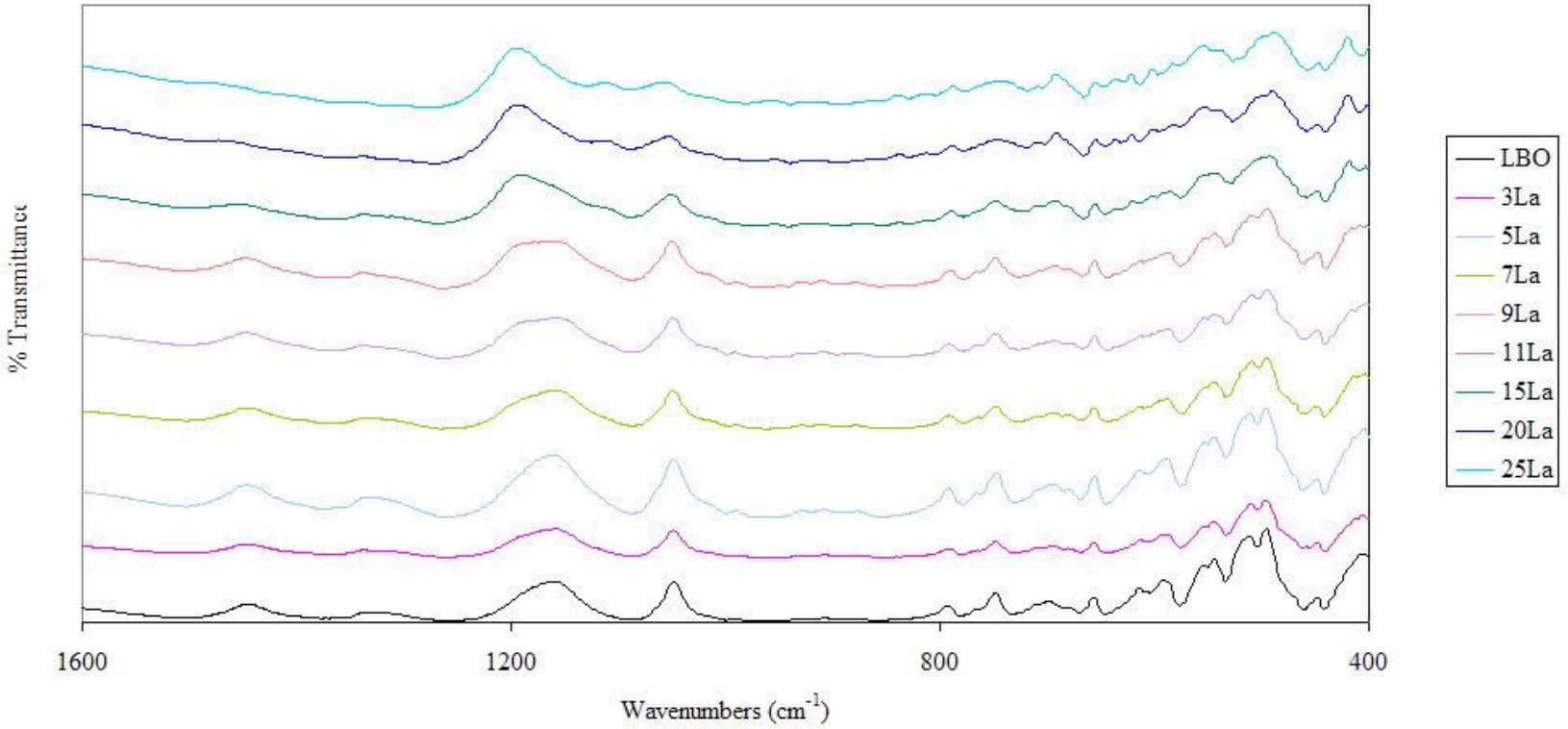

Figure 4.5 *IR spectra of LiB_3O_5 and LiB_3O_5 doped with La_2O_3*

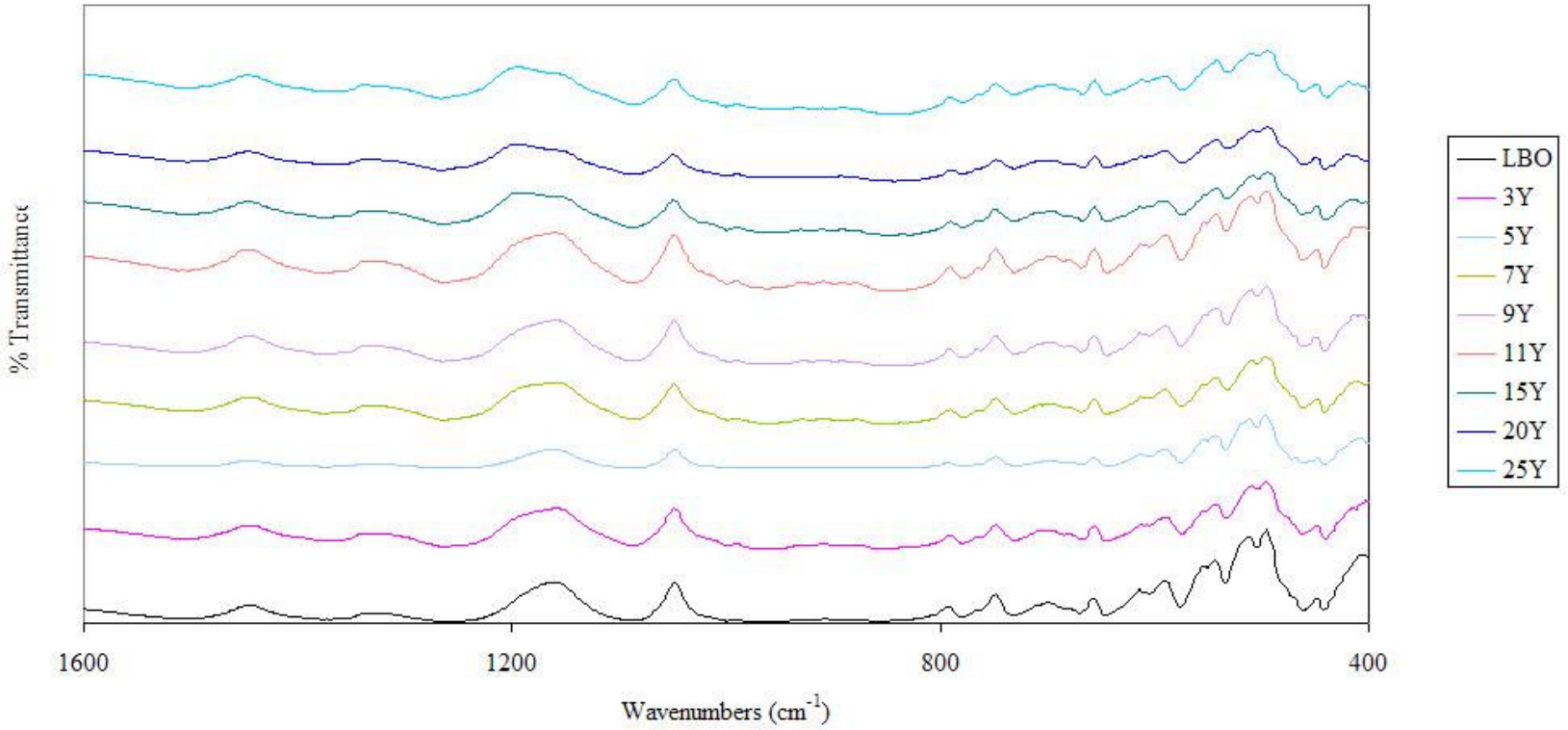

Figure 4.6 *IR spectra of LiB_3O_5 and LiB_3O_5 doped with Y_2O_3*

4.1.3. Differential Thermal Analysis

DTA was carried out to obtain the thermal behaviour of the produced new materials. The DTA curves of the prepared samples are given in the following figures. Also, the DTA curves of each separate sample were given in *Appendix C*.

Figure 4.7 shows the DTA curves of LBO and LBO samples doped with Gd_2O_3. The DTA shows that the compounds are thermally stable up to around 750 °C. For LBO, the peak at 815°C corresponds to the melting point of the product. However, with the addition of 5% Gd_2O_3, the melting point decreases to around 805°C and when the concentration increases to 11% Gd_2O_3, melting point decreases to 804°C. In addition to those, the second peak of doped samples, around 815°C, proves the presence of two phases.

The DTA curves of LBO and LBO samples doped with La_2O_3 were given in *Figure 4.8*. Just like Gd_2O_3 doped LBO, the La_2O_3 doped samples were also thermally stable up to750 °C. With the addition of 5% La_2O_3, the melting point decreases to around 800°C. However, when the concentration increases to 11% La_2O_3, melting point increases to 843°C.

For the LBO samples doped with Y_2O_3, *Figure 4.9* shows the DTA curves. While the melting point of LBO was 815°C, with the addition of 5% Y_2O_3 it decreases to 802°C. When Y_2O_3 concentration increases to 11%, the melting point again shifts to 815°C. The samples were again determined to be thermally stable up to around 750 °C.

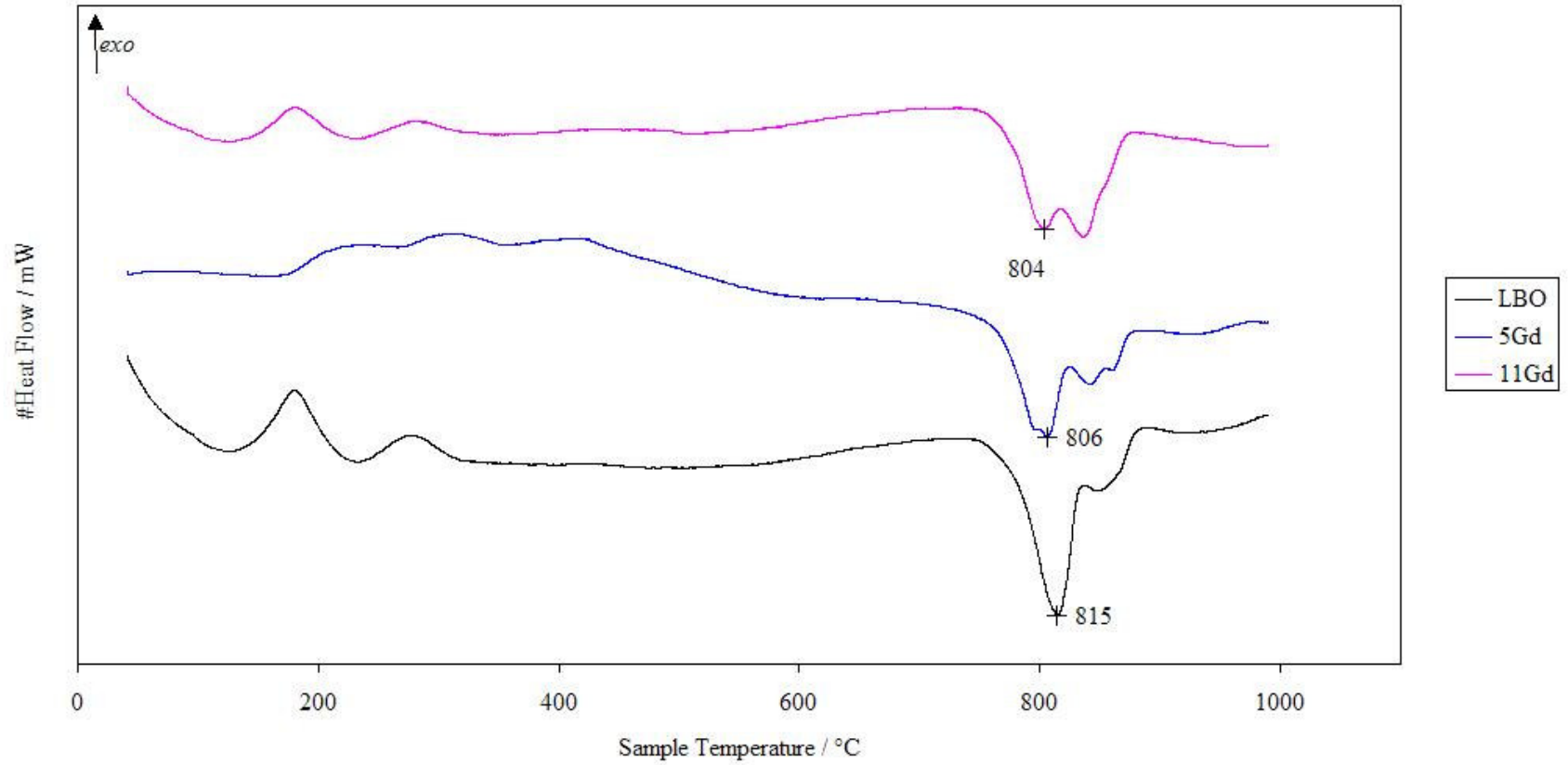

Figure 4.7 *DTA curves of LiB_3O_5 and LiB_3O_5 doped with Gd_2O_3*

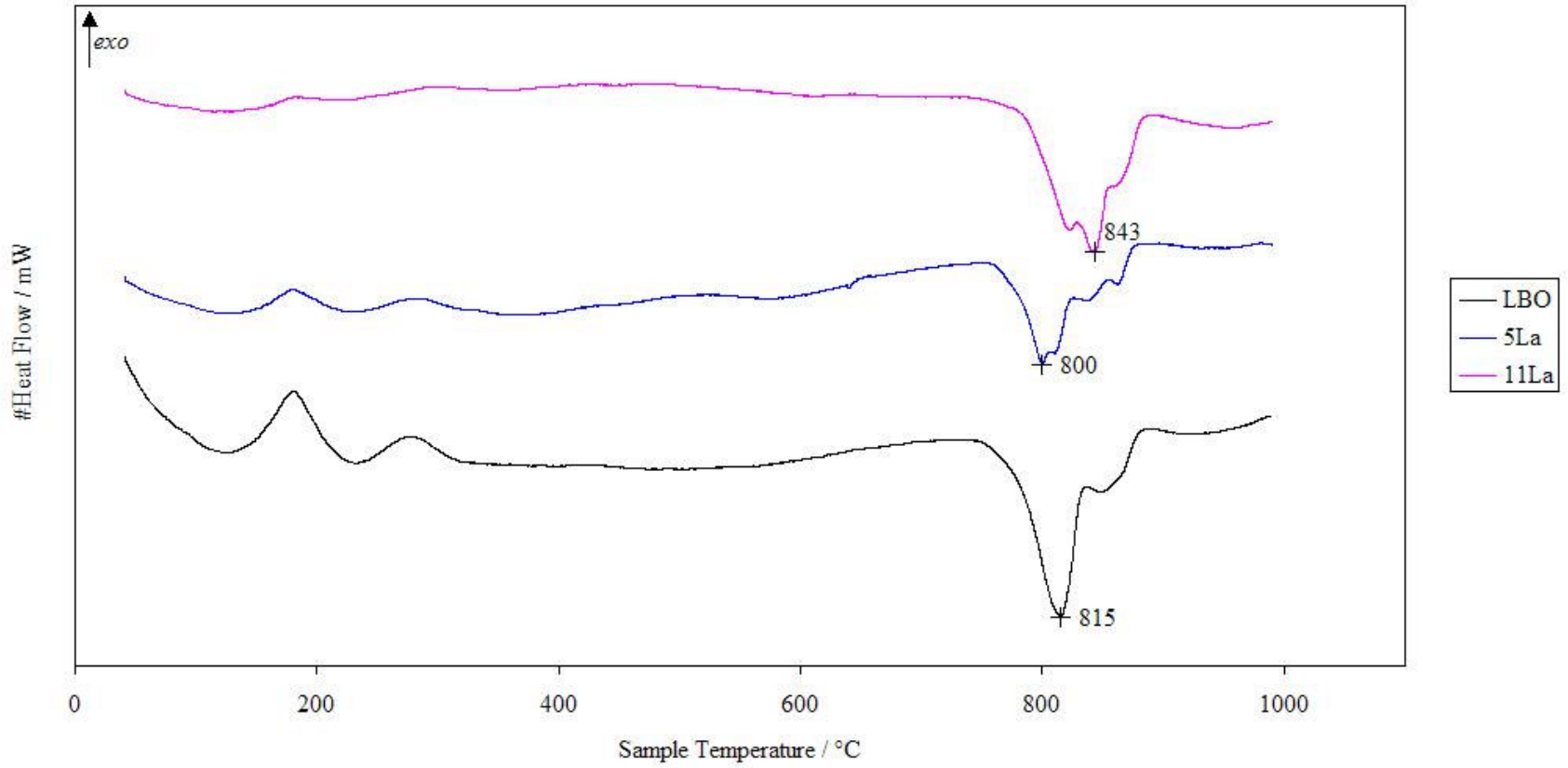

Figure 4.8 *DTA curves of LiB_3O_5 and LiB_3O_5 doped with La_2O_3*

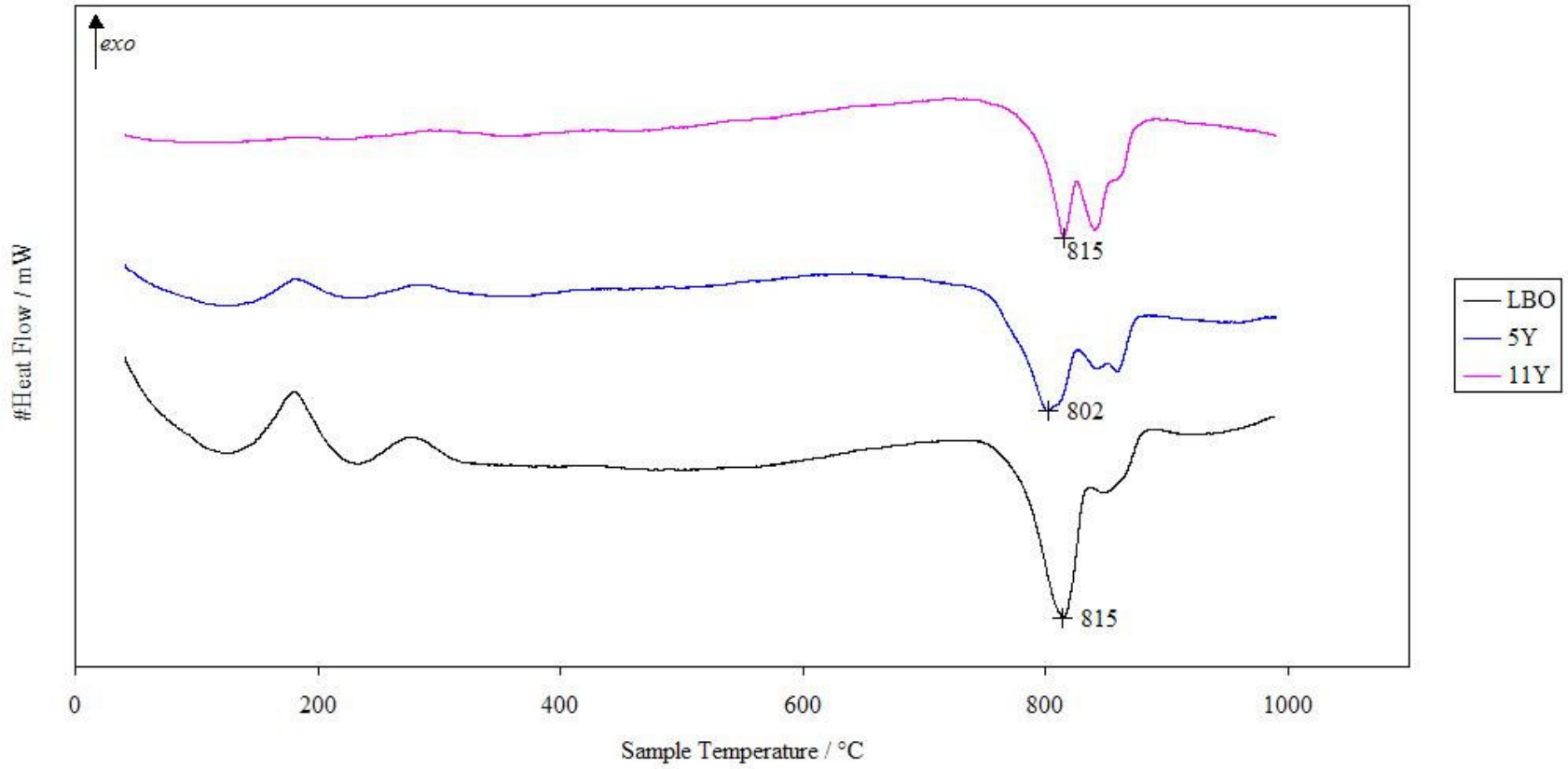

Figure 4.9 *DTA curves of LiB_3O_5 and LiB_3O_5 doped with Y_2O_3*

4.1.4. Scanning Electron Microscopy

SEM was carried out to determine the morphology of the samples. *Figure 4.10* shows the secondary electron image of the LBO samples and *Figure 4.11* shows the LBO samples doped with Gd_2O_3. In *Figures 4.12 and 4.13*, the backscattered electron images of the LBO samples doped with Gd_2O_3 is given. From the figures, the occurrence of Gd_2O_3 particles that stick on LBO can clearly be seen. By using the X-Ray microanalysis system of the microscope, it is proven that the dark coarse particles shown in *Figures 4.12 and 4.13* belong to LBO phase and light fine particles are Gd_2O_3.

For the samples doped with La_2O_3, *Figure 4.14* shows the secondary electron image and *Figures 4.15 and 4.16* show the backscattered electron images of the samples. Again, it can be seen from the figures that the light, fine, La_2O_3 particles were distributed homogeneously on dark, coarse, LBO particles.

Finally *Figure 4.17* represents the secondary electron image of Y_2O_3 doped LBO and *Figures 4.18 and 4.19* show the backscattered electron images of the samples. The only difference of the Y_2O_3 doped LBO from the Gd_2O_3 and La_2O_3 doped ones is that the rare earth particles are not that homogenously distributed on LBO particles.

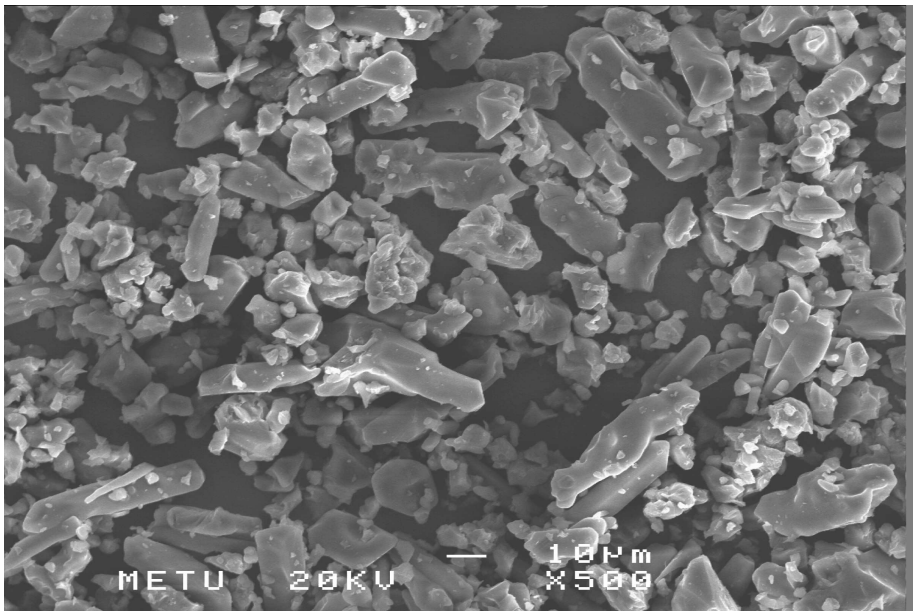

Figure 4.10 *SEM of LiB_3O_5 obtained from the solid-state reaction of Li_2CO_3 and H_3BO_3 at 750℃ for 14 hours*

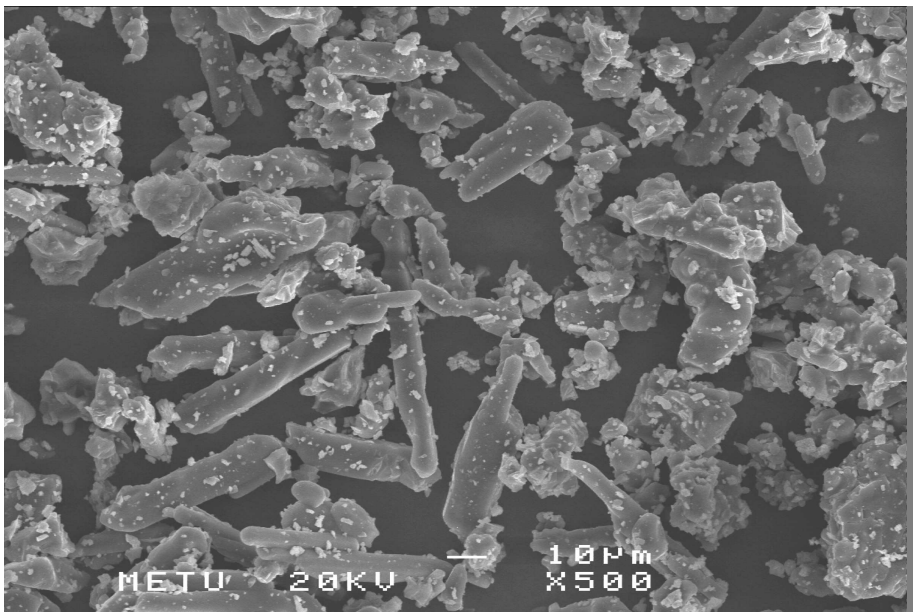

Figure 4.11 *SEM of LiB_3O_5 doped with 11% wt. Gd_2O_3 at 750℃ for 7 hours*

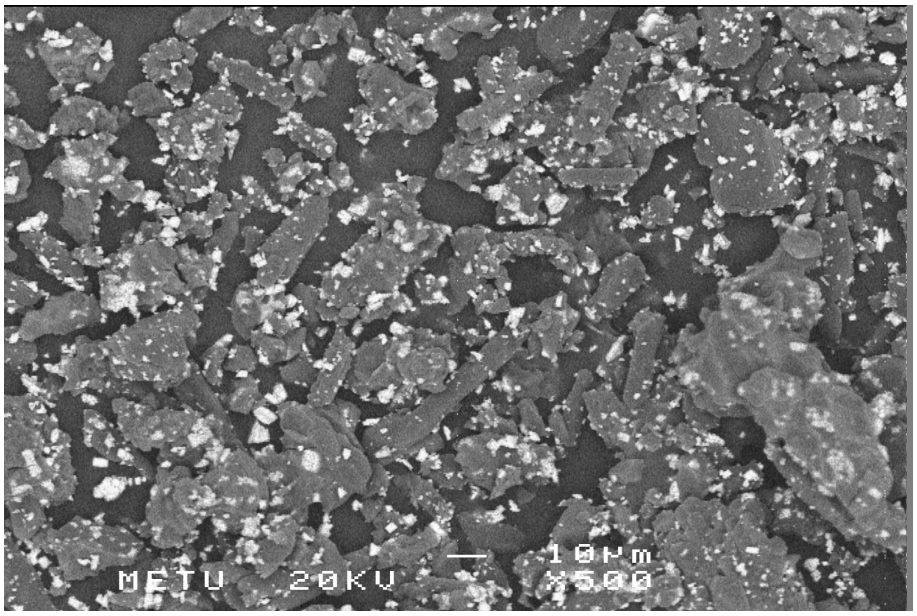

Figure 4.12 *SEM of LiB_3O_5 doped with 11% wt. Gd_2O_3 at 750℃ for 7 hours*

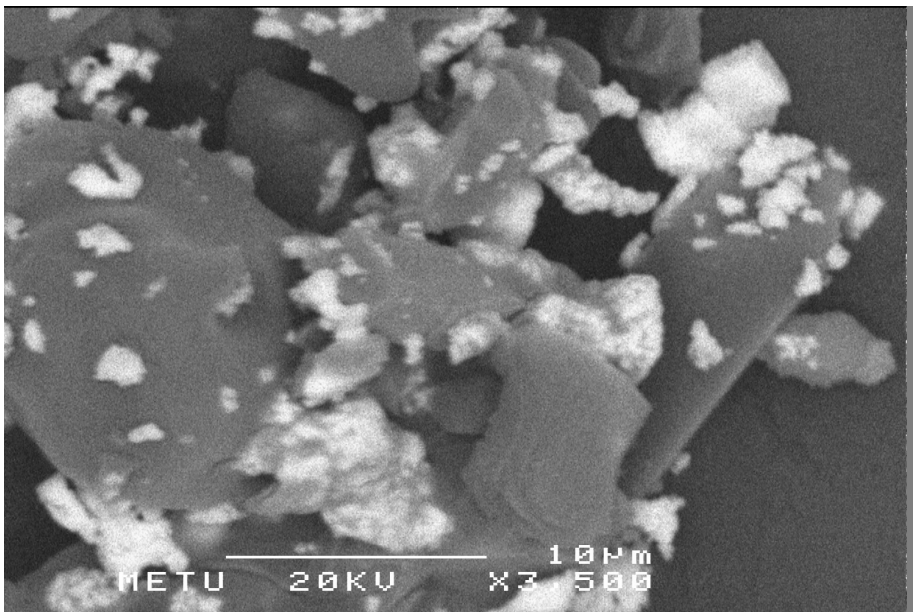

Figure 4.13 *SEM of LiB_3O_5 doped with 11% wt. Gd_2O_3 at 750℃ for 7 hours*

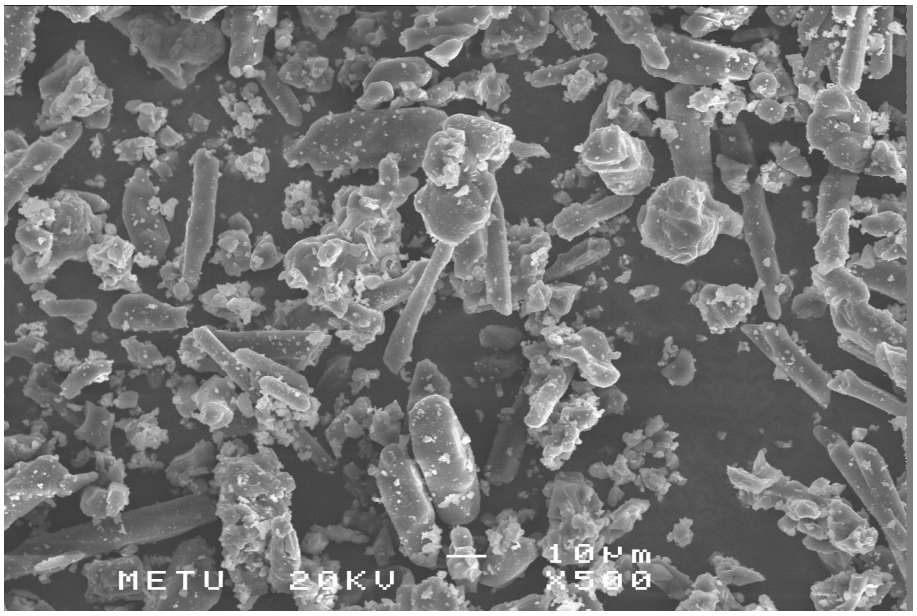

Figure 4.14 *SEM of LiB_3O_5 doped with 11% wt. La_2O_3 at 750℃ for 7 hours*

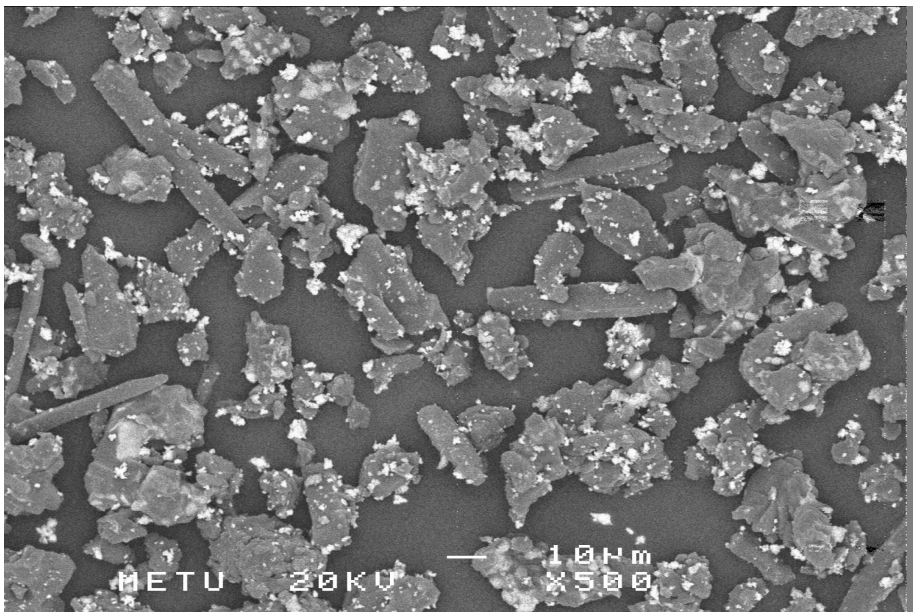

Figure 4.15 *SEM of LiB_3O_5 doped with 11% wt. La_2O_3 at 750℃ for 7 hour*

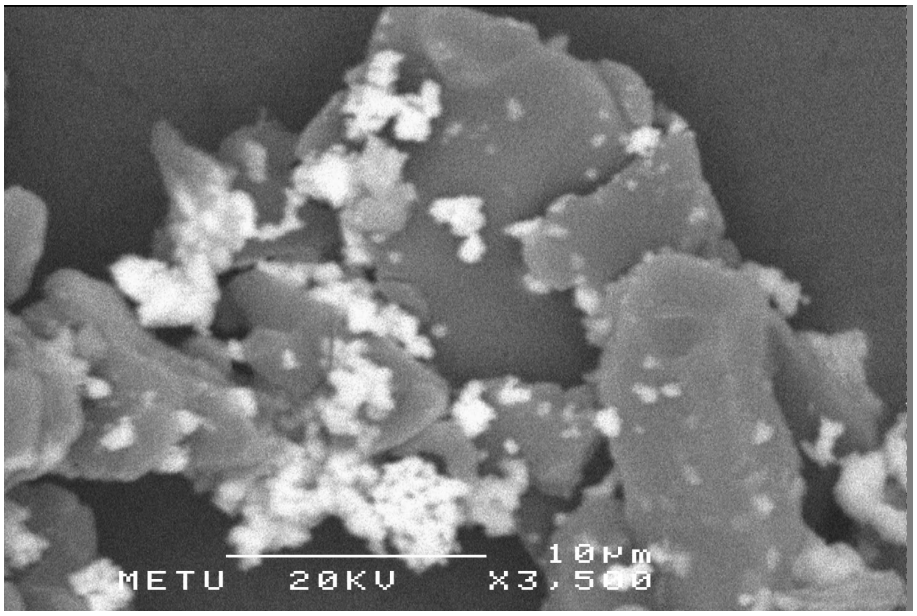

Figure 4.16 *SEM of LiB_3O_5 doped with 11% wt. La_2O_3 at 750℃ for 7 hour*

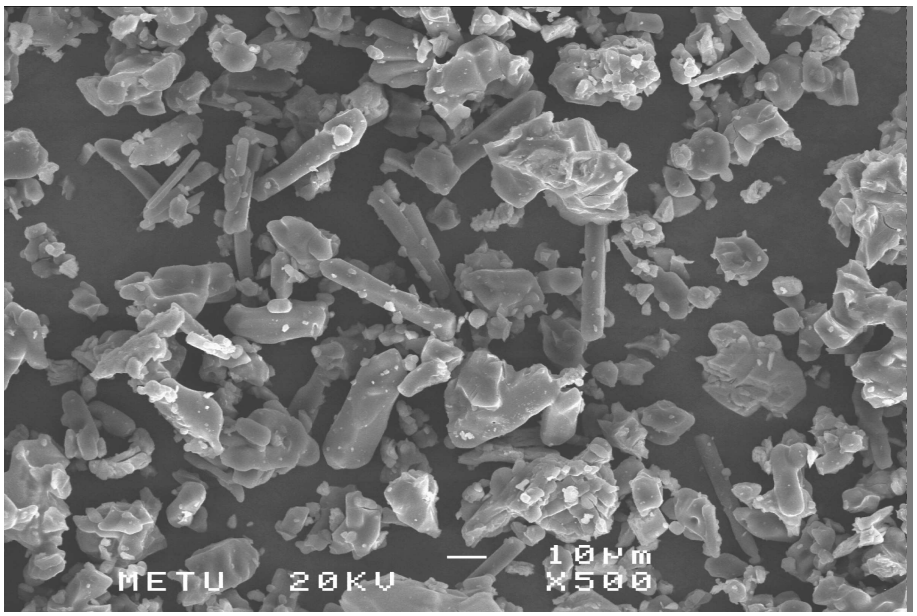

Figure 4.17 *SEM of LiB_3O_5 doped with 11% wt. Y_2O_3 at 750℃ for 7 hours*

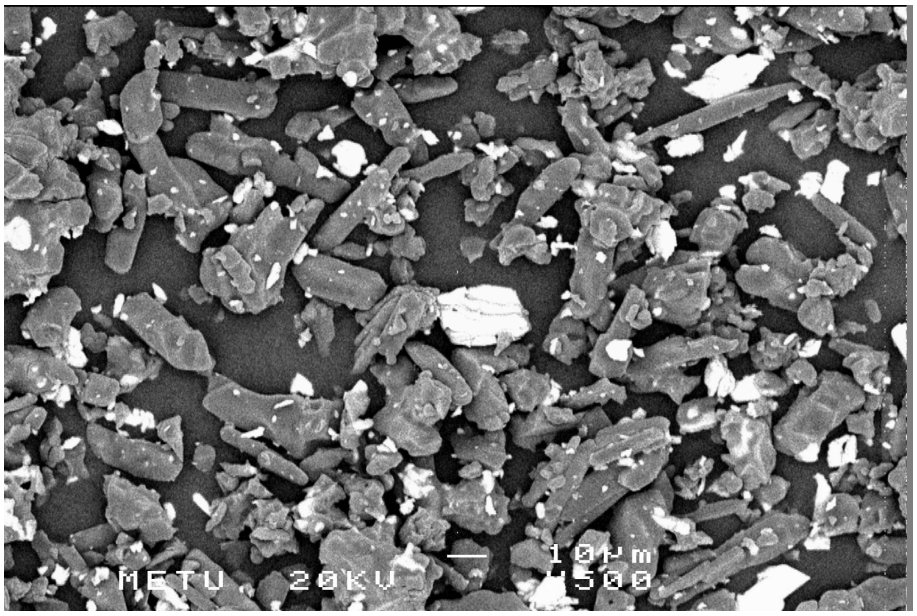

Figure 4.18 *SEM of LiB_3O_5 doped with 11% wt. Y_2O_3 at 750℃ for 7 hours*

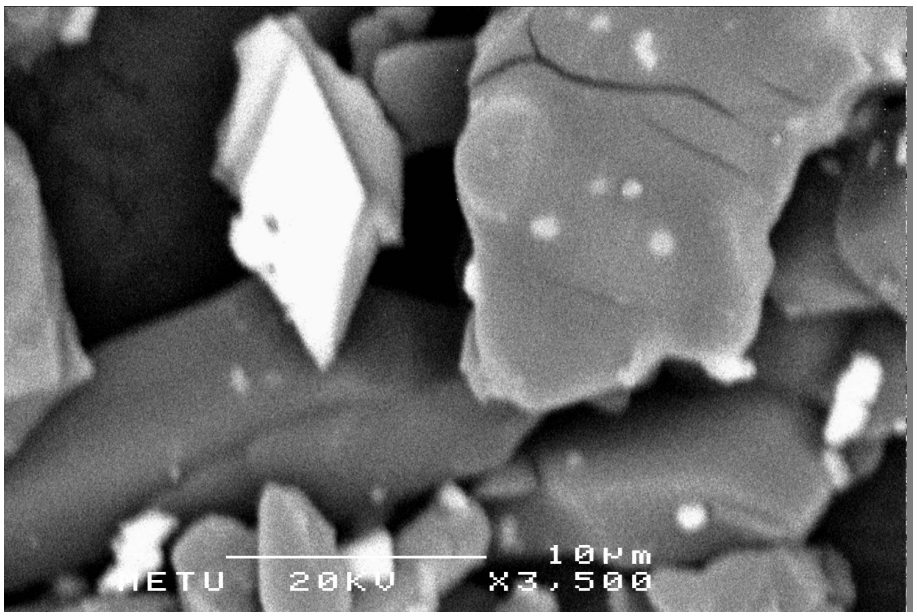

Figure 4.19 *SEM of LiB_3O_5 doped with 11% wt. Y_2O_3 at 750℃ for 7 hours*

4.1.5. Thermoluminescence

In view of excellent dosimetric properties of lithium borates, this thesis study was extended to include the determination of the dosimetric characteristics of LiB_3O_5 doped with RE elements by thermoluminescence (TL) technique. The glow curves of the prepared samples are given in the following figures. Also, the glow curves of each separate sample were given in *Appendix D*.

The glow curve of LiB_3O_5 and LiB_3O_5 samples doped with Gd_2O_3 is illustrated in *Figure 4.20* where two peaks are apparent. The maximum TL responses of the two peaks are at 110 and 190 ºC. As expected from the very low temperature of the peak, the peak at 110 ºC is affected by fading. It means that the dose response of the samples decreases with time. Further studies are needed to improve the dosimetric properties. For the doped samples highest TL response is obtained for 7% Gd_2O_3 doped LiB_3O_5.

For La_2O_3 doped LiB_3O_5, the glow curve consisting of two peaks is illustrated in *Figure 4.21*. The highest TL response obtained for those samples were from 11% doped. However, again, the peak at 110 ºC is affected by fading.

Figure 4.22 illustrated the glow curve of LiB_3O_5 and LiB_3O_5 samples doped with Y_2O_3. Likewise, Gd_2O_3 and La_2O_3, TL curve of Y_2O_3 consists of two peaks at 110 and 190 ºC, with the lower one affected by fading. In the case of, Y_2O_3 doped LiB_3O_5; highest TL response is obtained for 11% doped samples.

In *Figures 4.20, 4.21 and 4.22*, the dotted lines represent the samples of the same colour irradiated after 24 hours.

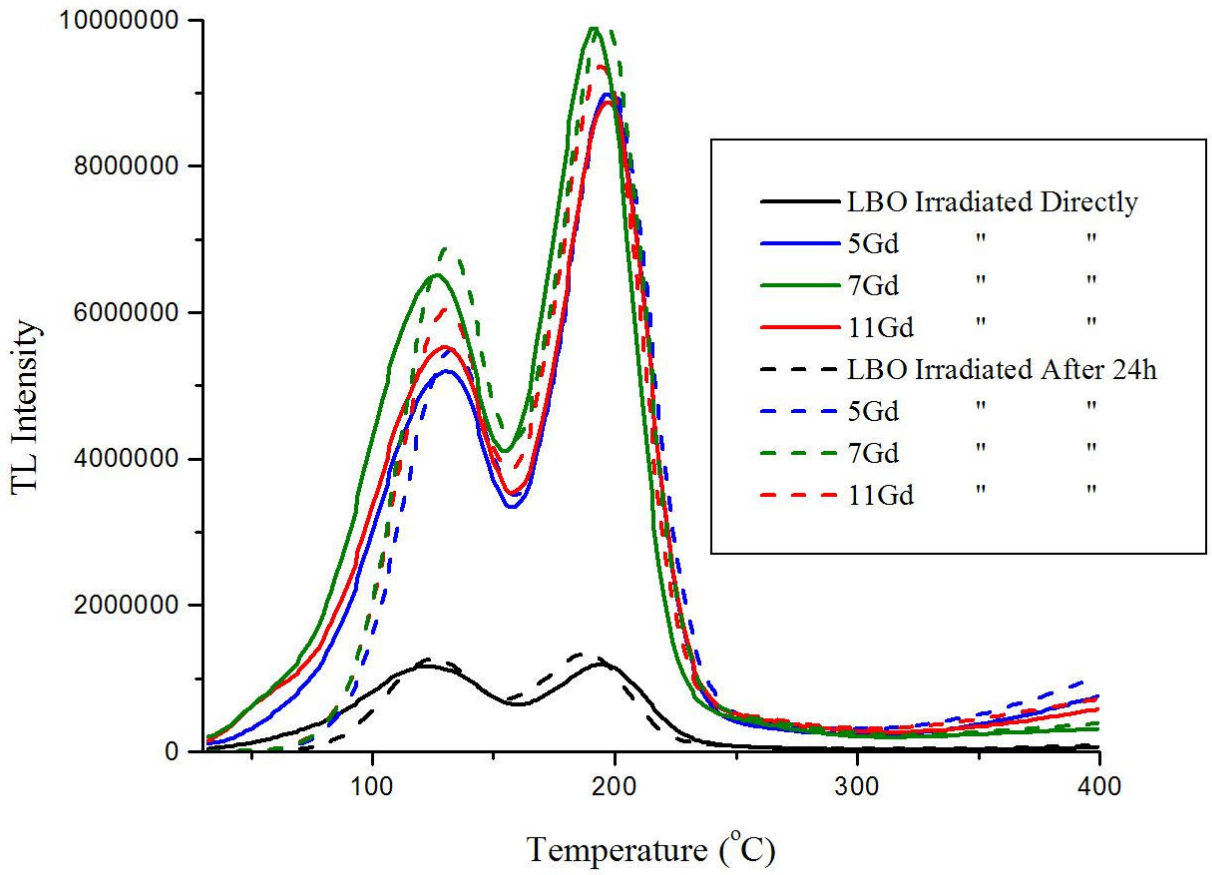

Figure 4.20 *The glow curve of LiB_3O_5 and LiB_3O_5 samples doped with Gd_2O_3*

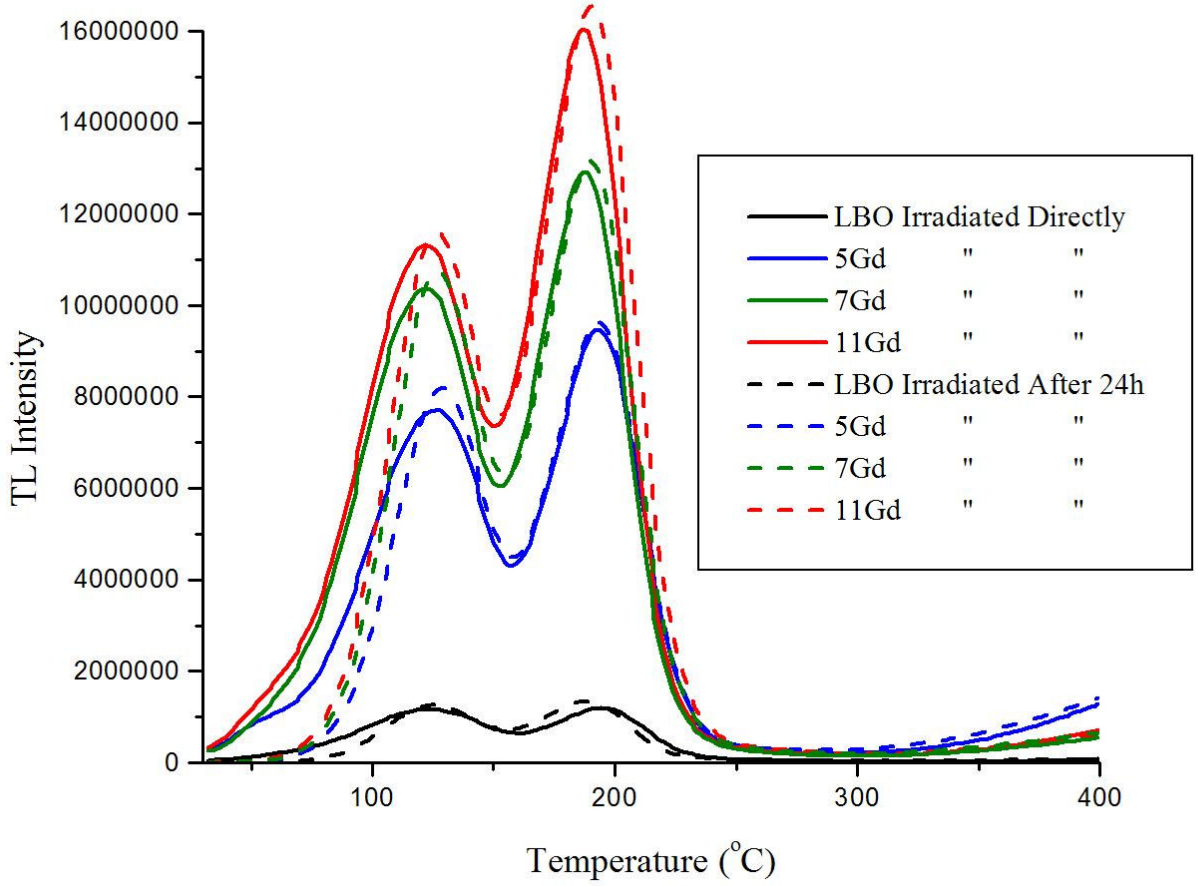

Figure 4.21 *The glow curve of LiB_3O_5 and LiB_3O_5 samples doped with La_2O_3*

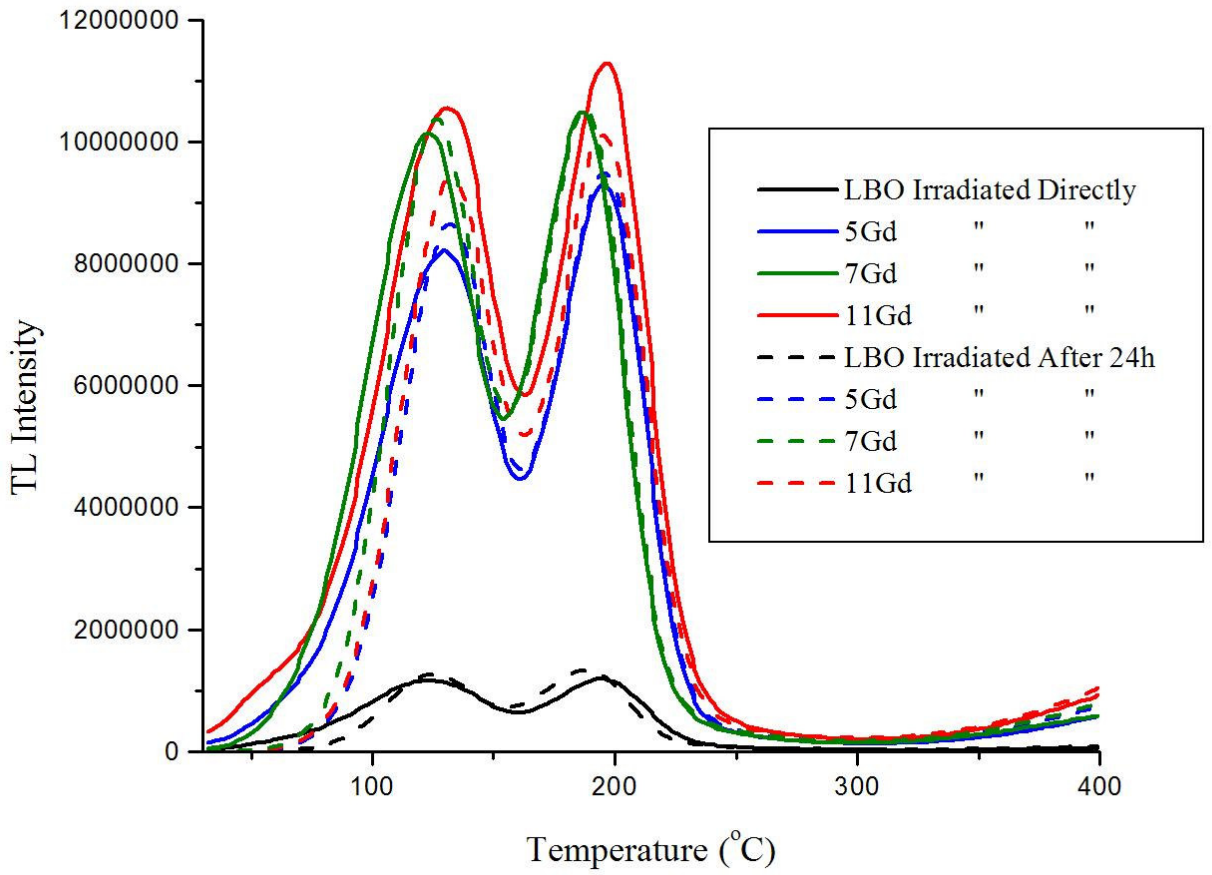

Figure 4.22 The glow curve of LiB_3O_5 and LiB_3O_5 samples doped with Y_2O_3

CHAPTER V

CONCLUSIONS AND RECOMMENDATIONS

The aim of the study is to synthesize and characterize rare-earth doped lithium triborate by solid-state synthesis method and to investigate the possible applications of the materials.

In this study it is found that,

1. LiB_3O_5 was produced successfully from the solid-state reaction of Li_2CO_3 and H_3BO_3 at 750ºC, and LBO samples were, then, doped with Gd_2O_3, La_2O_3, and Y_2O_3.

2. XRD analysis showed that due to the rare-earth addition, peaks belonging to rare-earth elements are observed. However, LBO peaks are still dominant. On the other hand, when the concentrations of the rare earth elements increases, with respect to LBO, the peaks of rare earth elements become dominant.

3. IR analyses indicated that with the addition of rare earth elements, no change related to B-O link was observed.

4. The DTA analysis showed that the compounds are thermally stable up to 750°C. The melting point of LBO decreases with addition of 5% wt. rare-earth elements. When the concentration of rare-earth elements increases to 11%, the melting point of Gd_2O_3 doped samples decreases but La_2O_3 and Y_2O_3 dopes samples increases.

5. In the SEM image two phases belonging to LBO and RE elements are observed clearly.

6. With the TL analysis, it is considered that the samples show dose response. Besides, the response of the materials is affected by fading.

7. Studies may be extended to determine other potential applications of the products.

REFERENCES

[1] D. R. Lide, *CRC Handbook of Chemistry and Physics*, CRC Press, LLC, **2004**.

[2] D. E. Garrett, *Borates, Handbook of Deposits, Processing, and Use*, Academic Press, London, **1998**.

[3] Boren, *Bor Hakkında*, From http://www.boren.gov.tr/expin.htm#rezerv, Retrieved June 24, **2005**.

[4] C. Mazzetti, F. D. Carli, *Gazetta Chimica Italiana* **1926**, *56*, 23.

[5] A. P. Rollet, R. Bouaziz, *Comptes Rendus* **1955**, *240*, 2417.

[6] B. S. R. Sastry, F.A. Hummel, *Journal of the American Ceramic Society* **1958**, *41*, 11.

[7] H. König, R. Hoppe, *Zeitschrift fur Anorganische und Allgemeine Chemie* **1978**, *439*, 71.

[8] C. Chen, Y.Wu, A. Jiang, B.Wu, G. You, R. Li, S. Lin, *Journal of the Optical Society of America B* **1989**, *6*, 616.

[9] E. Bétourné, M. Touboul, *Journal of Alloys and Compounds* **1997**, *255*, 91.

[10] S. C. Sabharwal, B. Tiwari, Sangeeta, *Journal of Crystal Growth* **2003**, *249*, 502.

[11] Powder diffraction file No. 50–0061 JCPDS-ICDD, USA.

[12] S. C. Sabharwal, B. Tiwari, Sangeeta, *Journal of Crystal Growth* **2004**, *263*, 327.

[13] Powder diffraction file No. 40–0505 JCPDS-ICDD, USA.

[14] Powder diffraction file No. 16–0200 JCPDS-ICDD, USA.

[15] U. Moryc, W. S. Ptak, *Journal of Molecular Structure*, **1999**, 511-512, 241.

[16] M. J. F. Digonnet, *Rare Earth Doped Fiber Lasers and Amplifiers*, Marcel Dekker Incorporated, New York, **2001**.

[17] R. Sankar , G. V. Subba Rao, *Journal of Alloys and Compounds* **1998**, *281*, 126.

[18] Q. Zeng, Z. Pei, Q. Su, S. Huang, *Physica Status Solidi B* **1999**, *212*, 207.

[19] P. Babu, C. K. Jayasankar, *Physica B* **2000**, *279*, 262.

[20] P. Babu, C. K. Jayasankar, *Optical Materials* **2000**, *15*, 65.

[21] V. Jubera, J. P. Chaminade, A. Garcia, F. Guillen, C. Fouassier, *Journal of Luminescence* **2003**, *101*, 1.

[22] D. Thomazini, F. Lanciotti Jr., A. S. B. Sombra, *Cerâmica*, **2001**, *47*, 88.

[23] T. H. Maiman, *Nature* **1960**, *187*, 493.

[24] C. F. Dewey, W. R. Cook, R. T. Hodgson, J. J. Wynne, *Applied Physics Letters* **1975**, *26*, 714.

[25] C. Chen, B. Wu, A. Jiang, G. You, *Scienctia Sinica B* **1985**, *28*, 235.

[26] J. Liebertz, S. Stahr, *Zeitschrift fuer Kristallographie* **1983**, *165*, 91.

[27] C. Chen, Y. Wang, B. Wu, K. Wu, W. Zeng, L. Yu, *Nature* **1995**, *373*, 322.

[28] H. Hellwig, J. Liebertz, L. Bohatu´, *Solid State Communications* **1999**, *109*, 249.

[29] G. Aka, A. Kahn-Harari, D. Vivien, J. M. Benitez, F. Salin, J. Godard, *European Journal of Solid State and Inorganic Chemistry* **1996**, *33*, 727.

[30] K. Kato, *IEEE Journal of Quantum Electronics* **1990**, *26*, 1173.

[31] A. S. Pradhan, *Radiation Protection Dosimetry* **1981**, *1*, 153.

[32] N.A. El-Faramawy, S.U. El-Kameesy, A. El-Agramy, G. Metwally, *Radiation Physics and Chemistry* **2000**, *58*, 9.

[33] M. Prokic, *Radiation Measurements* **2001**, *33*, 393.

[34] C. Furetta, M. Prokic, R. Salamon, V. Prokic, G. Kitis, *Nuclear Instruments and Methods in Physics Research A* **2001**, *456*, 411.

[35] Powder diffraction file No. 42–1465 JCPDS-ICDD, USA.

[36] Powder diffraction file No. 22–0641 JCPDS-ICDD, USA.

[37] Powder diffraction file No. 44–0399 JCPDS-ICDD, USA.

APPENDIX A

XRD PATTERNS OF THE PRODUCED MATERIALS

XRD pattern of the each separate sample are given in the following figures. In those figures, peaks abbreviated with (*) represent the peaks of LBO and peaks abbreviated with (0) represents the corresponding rare-earth oxides.

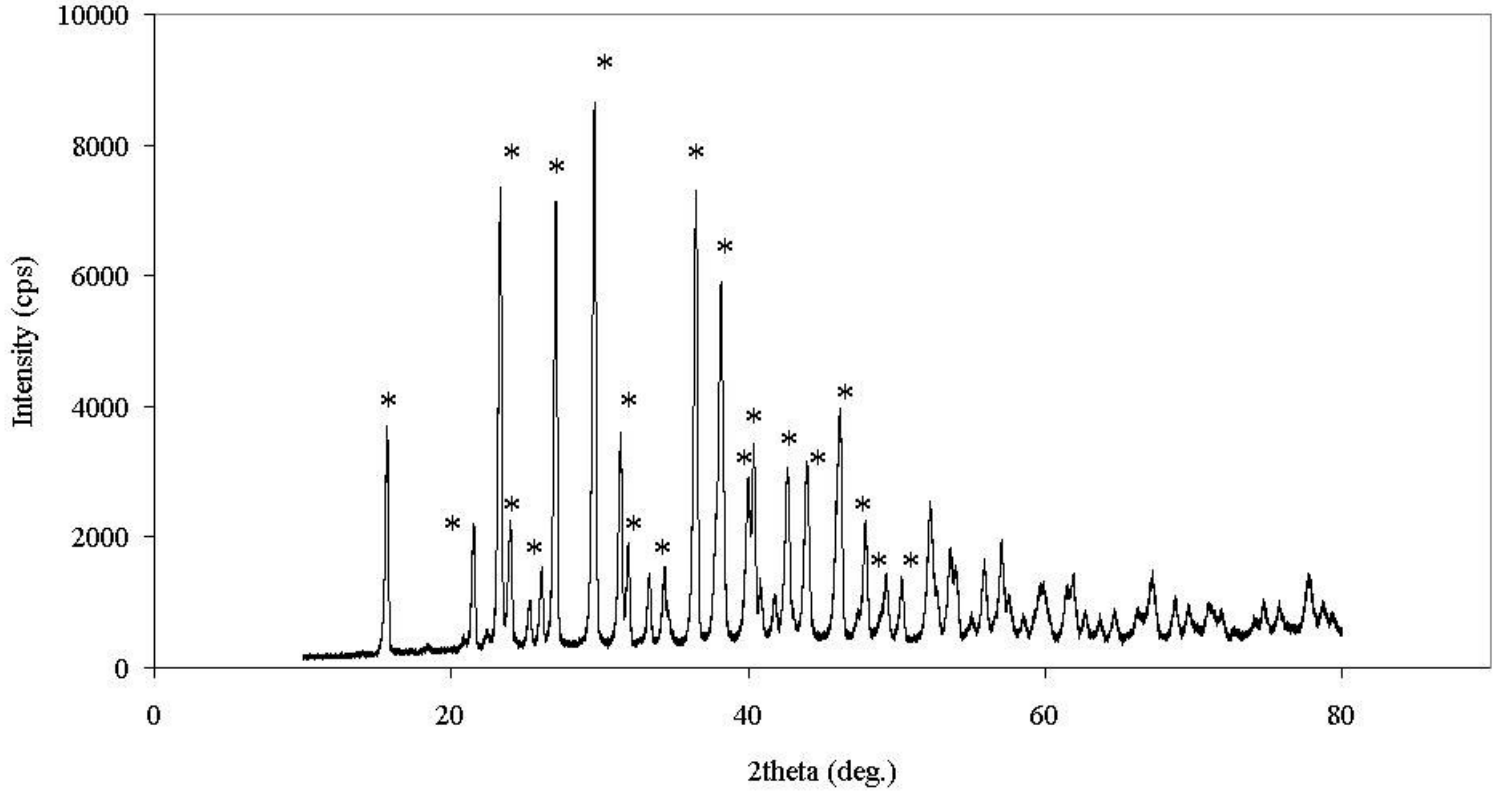

Figure B.1 *Powder x-ray diffraction pattern of LiB_3O_5 (*: LBO)*

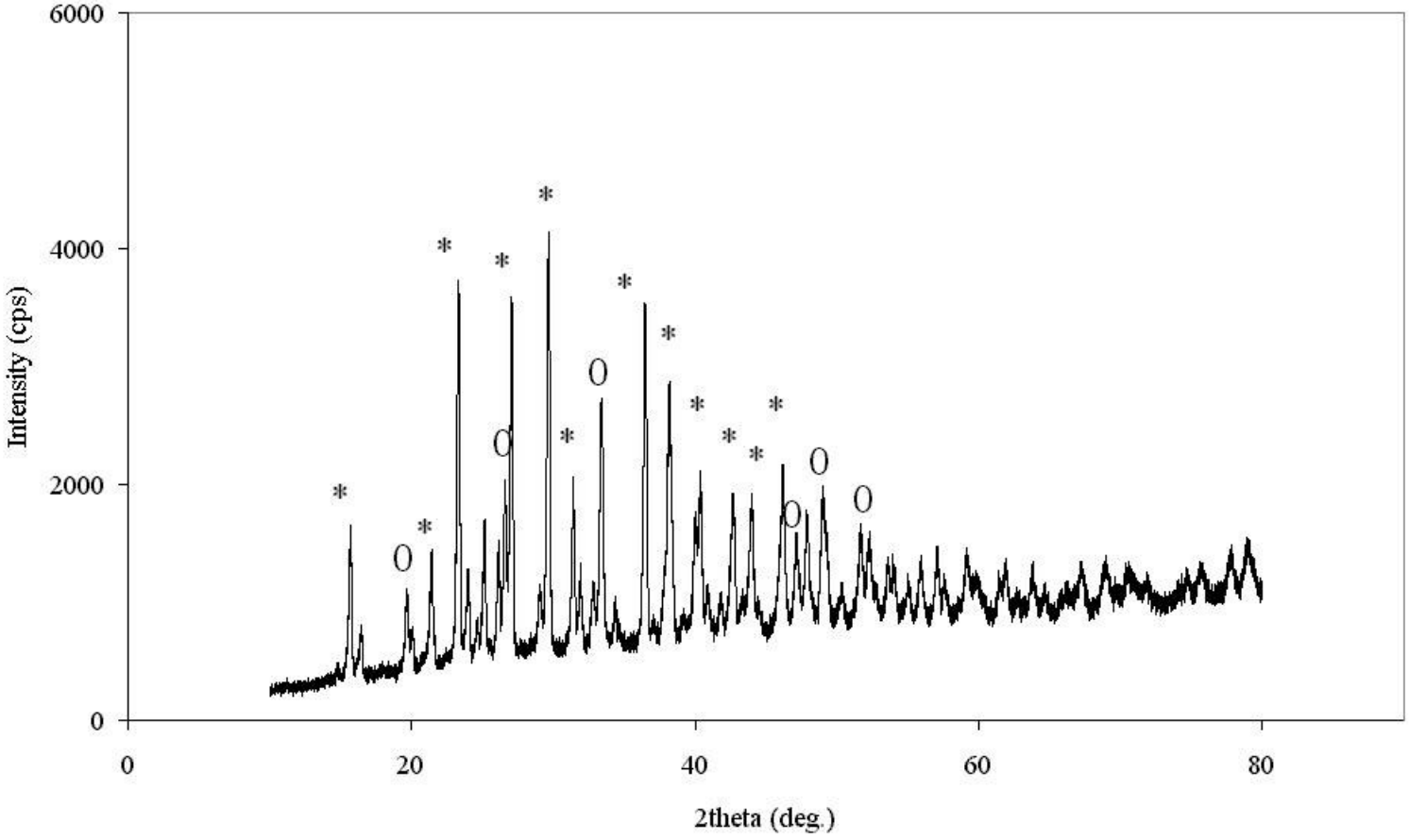

Figure B.2 *Powder x-ray diffraction pattern of LiB_3O_5 doped with 3% wt. Gd_2O_3*

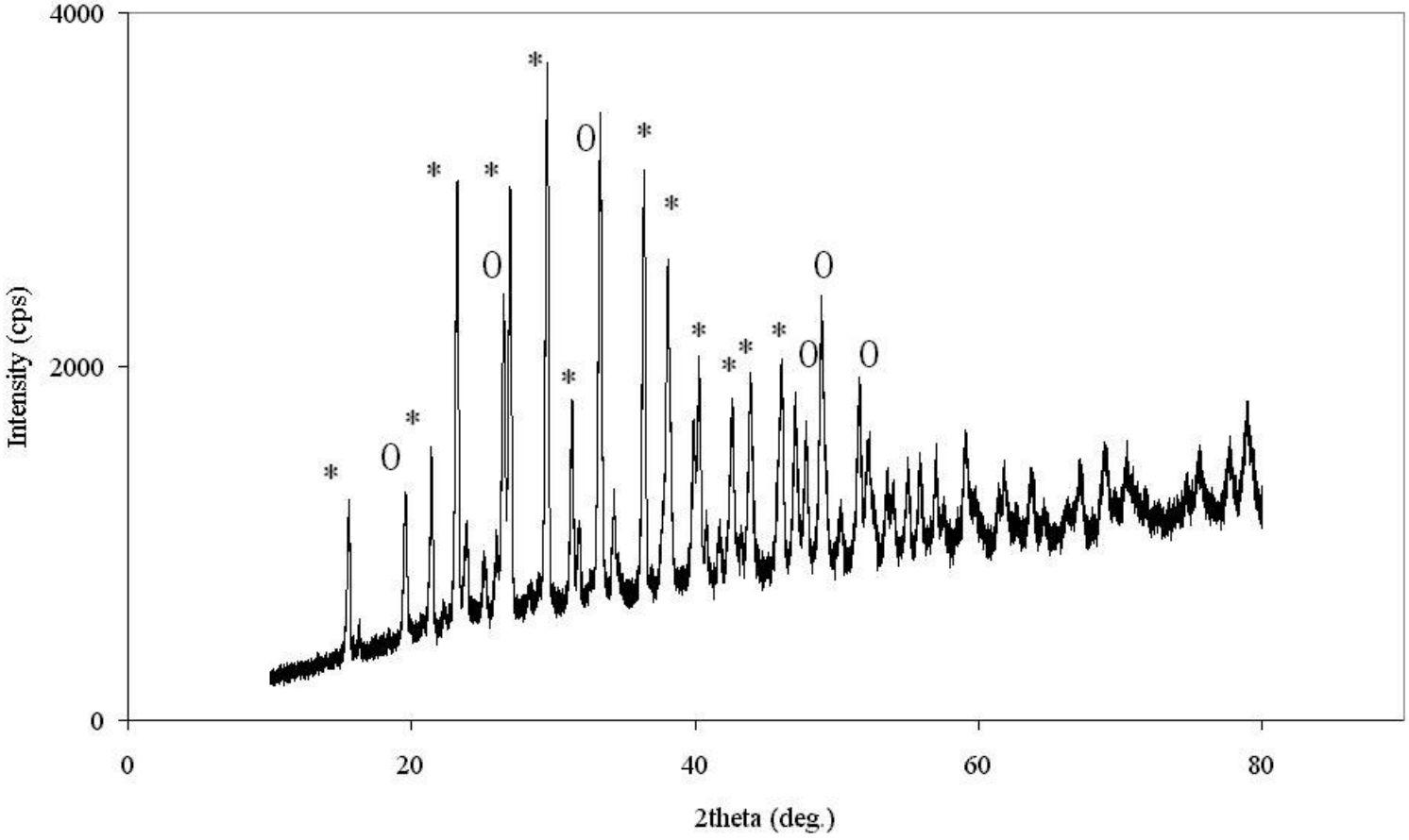

Figure B.3 *Powder x-ray diffraction pattern of LiB_3O_5 doped with 5% wt. Gd_2O_3*

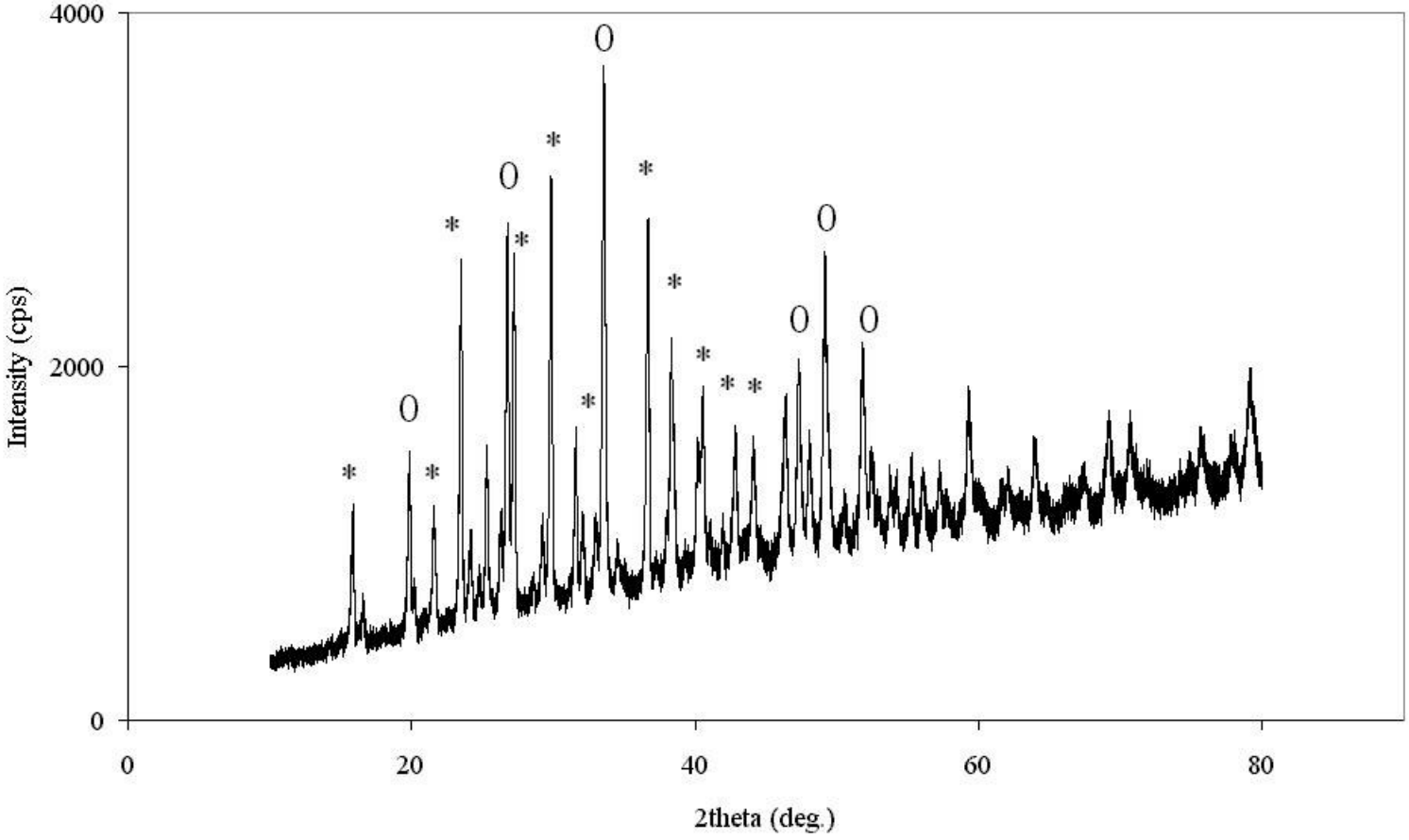

Figure B.4 *Powder x-ray diffraction pattern of LiB_3O_5 doped with 7% wt. Gd_2O_3*

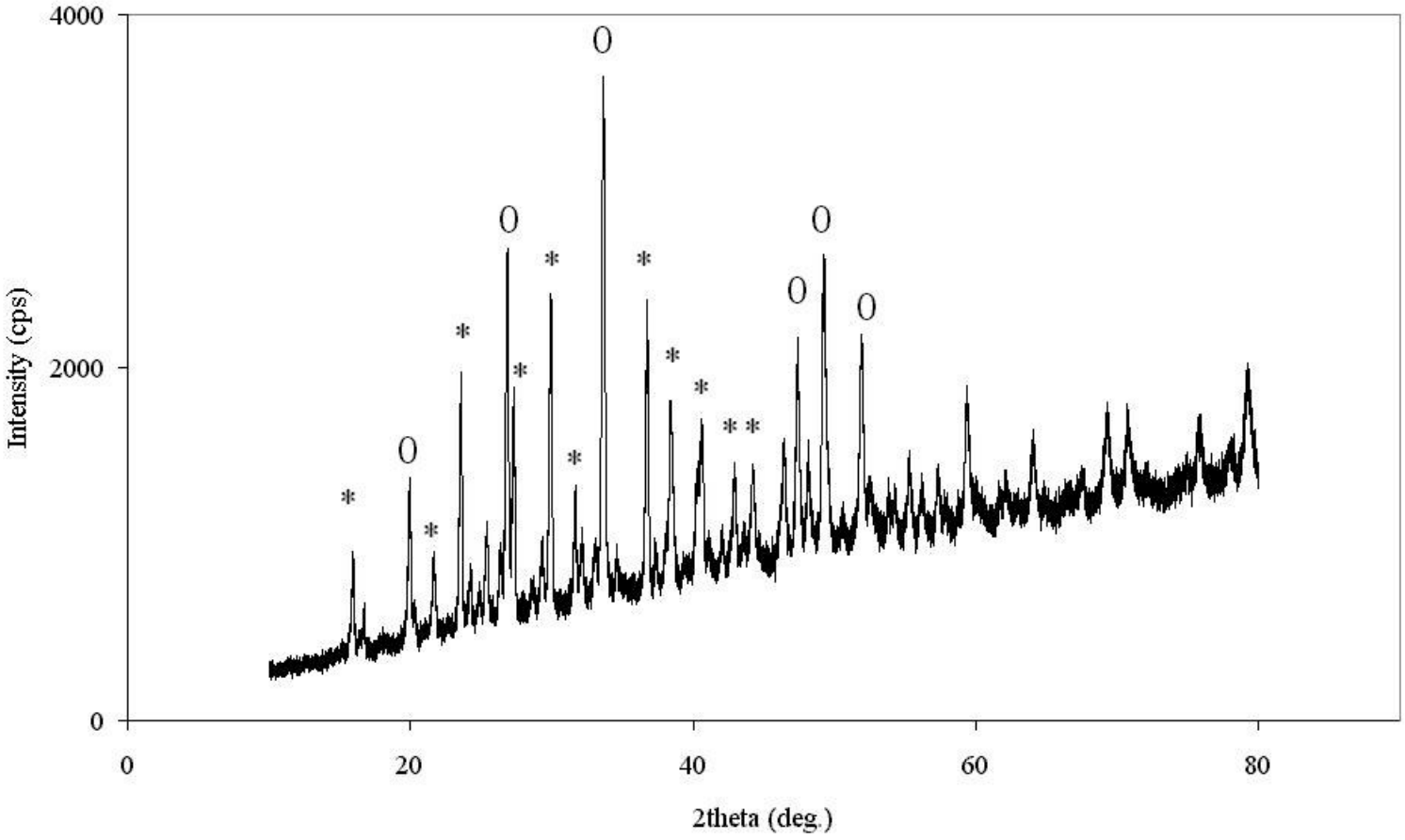

Figure B.5 *Powder x-ray diffraction pattern of LiB_3O_5 doped with 9% wt. Gd_2O_3*

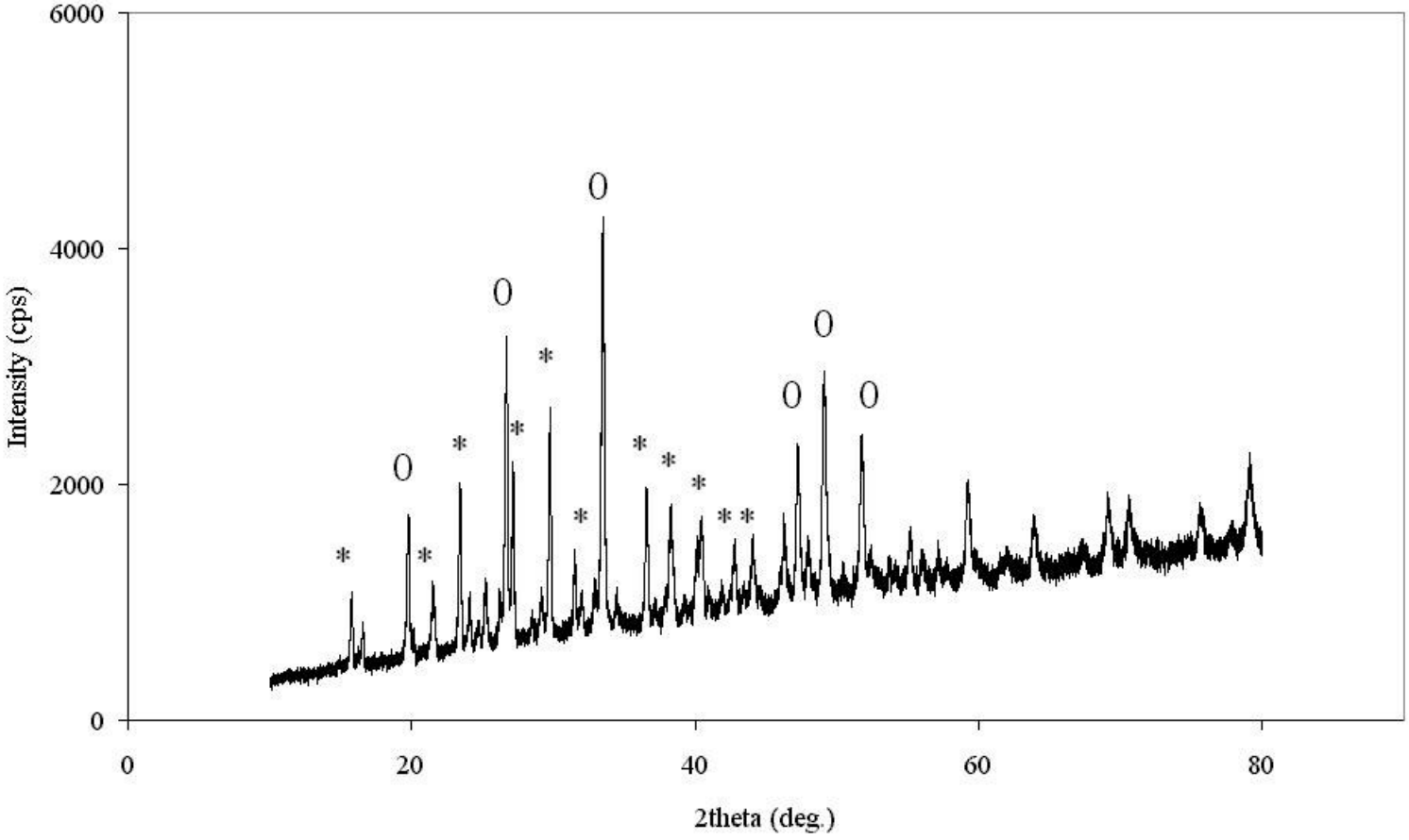

Figure B.6 *Powder x-ray diffraction pattern of LiB_3O_5 doped with 11% wt. Gd_2O_3*

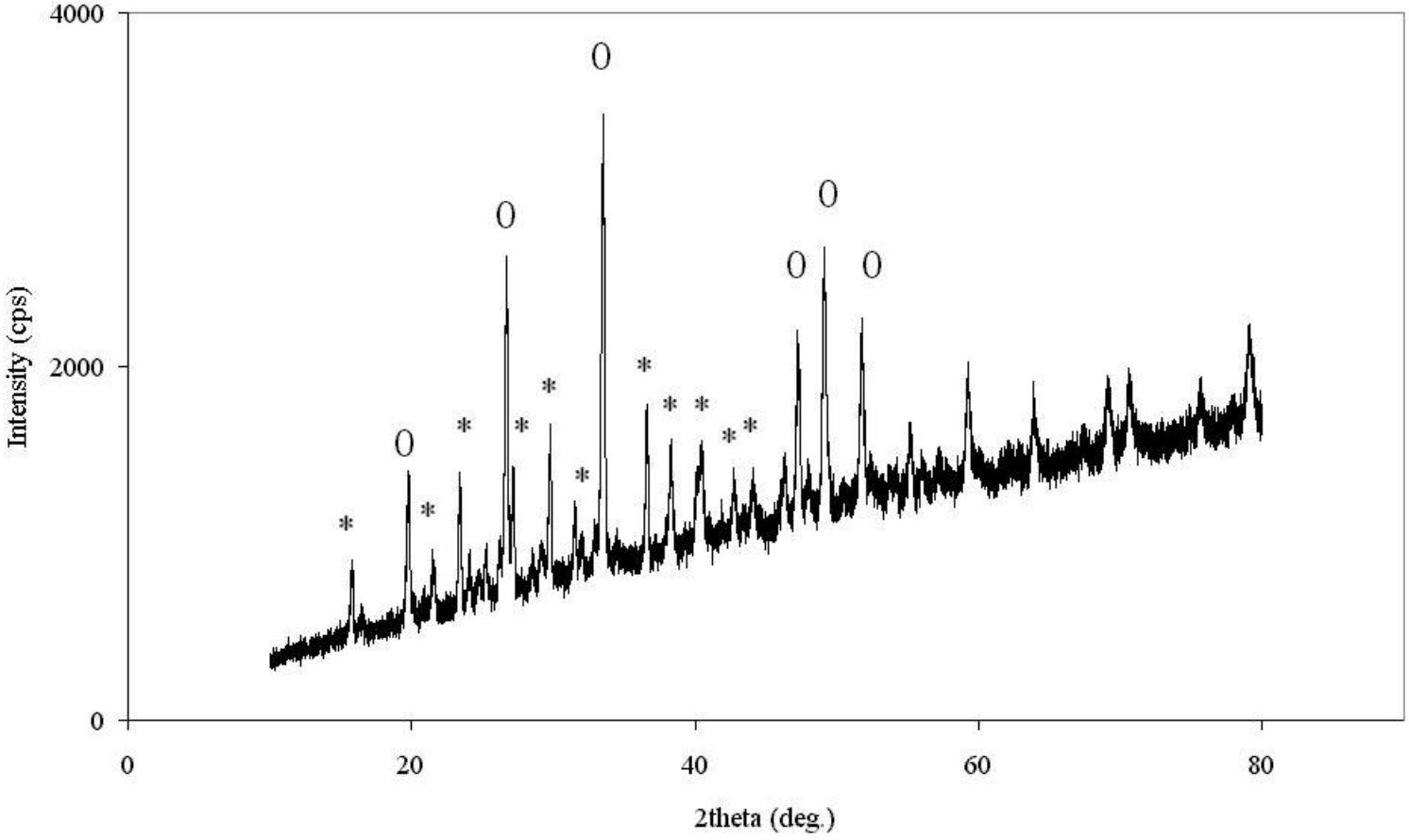

Figure B.7 *Powder x-ray diffraction pattern of LiB_3O_5 doped with 15% wt. Gd_2O_3*

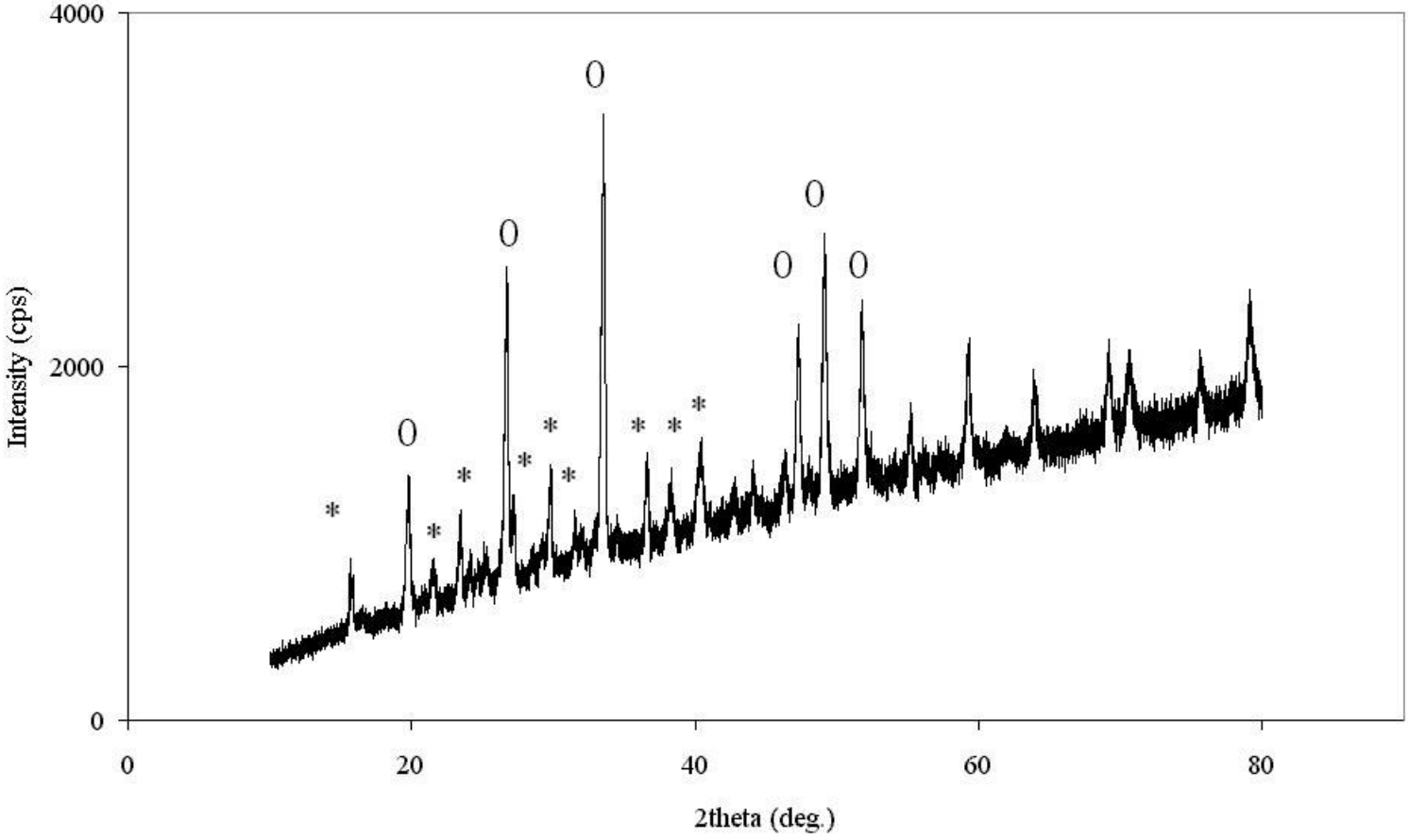

Figure B.8 *Powder x-ray diffraction pattern of LiB_3O_5 doped with 20% wt. Gd_2O_3*

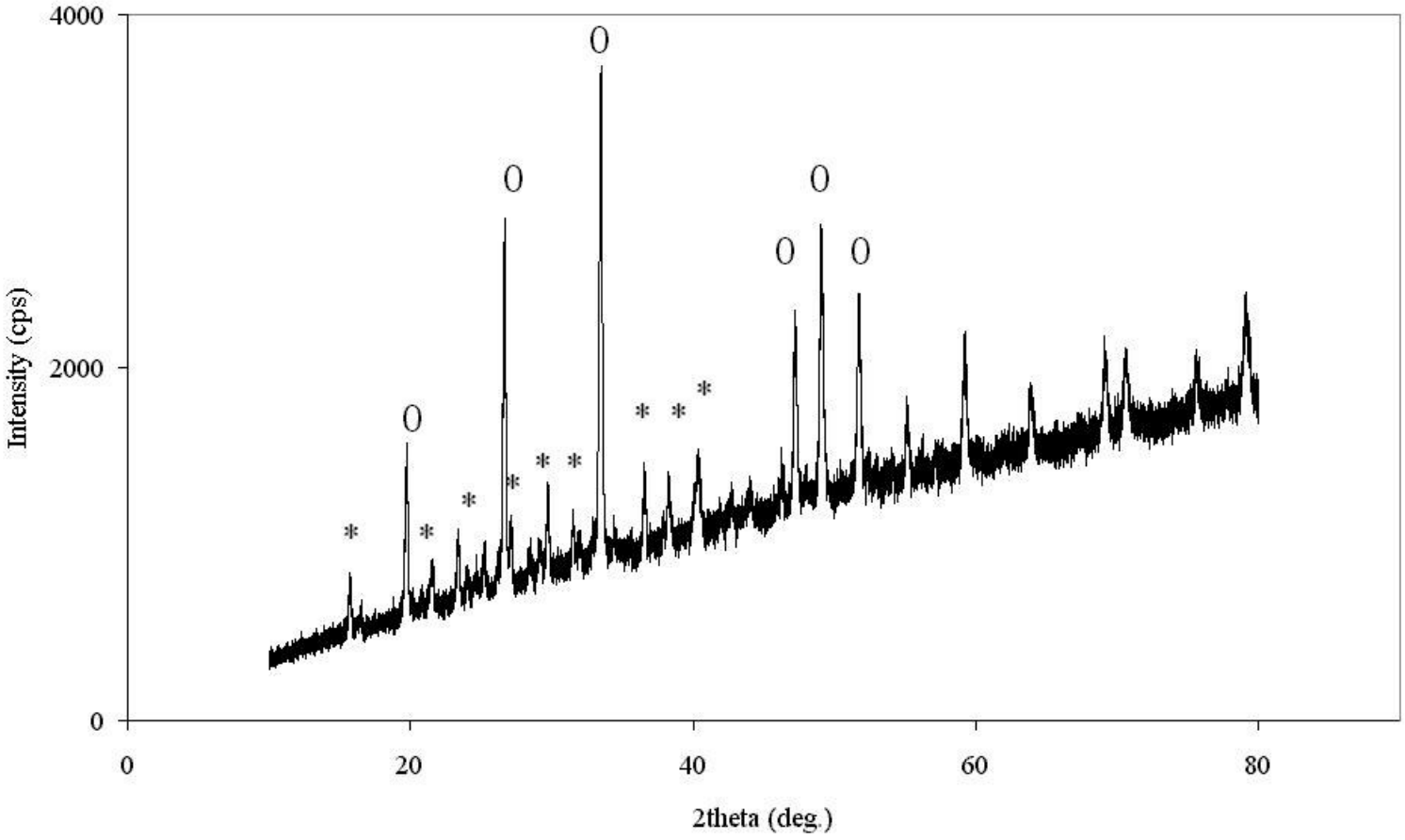

Figure B.9 *Powder x-ray diffraction pattern of LiB_3O_5 doped with 25% wt. Gd_2O_3*

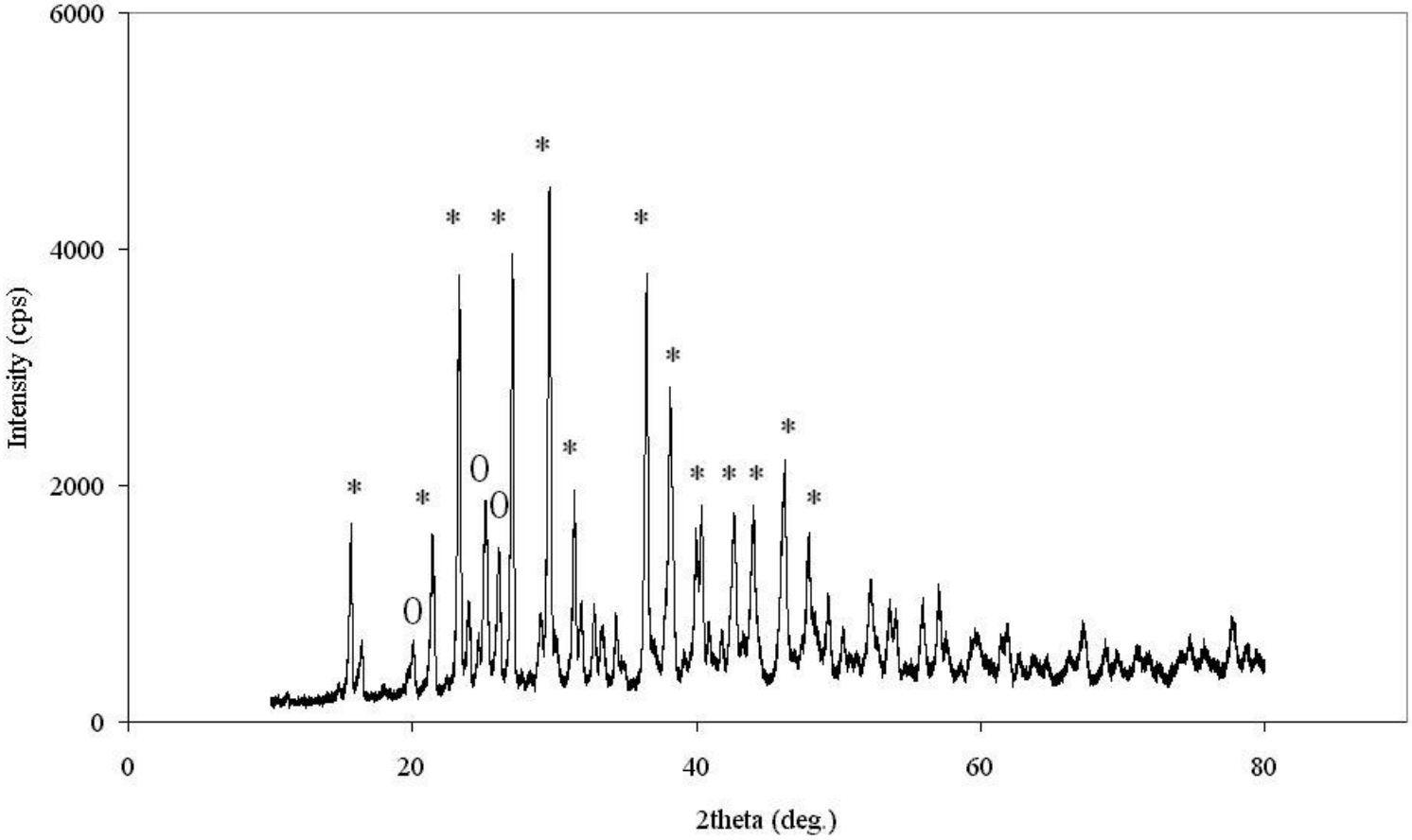

Figure B.10 *Powder x-ray diffraction pattern of LiB_3O_5 doped with 3% wt. La_2O_3*

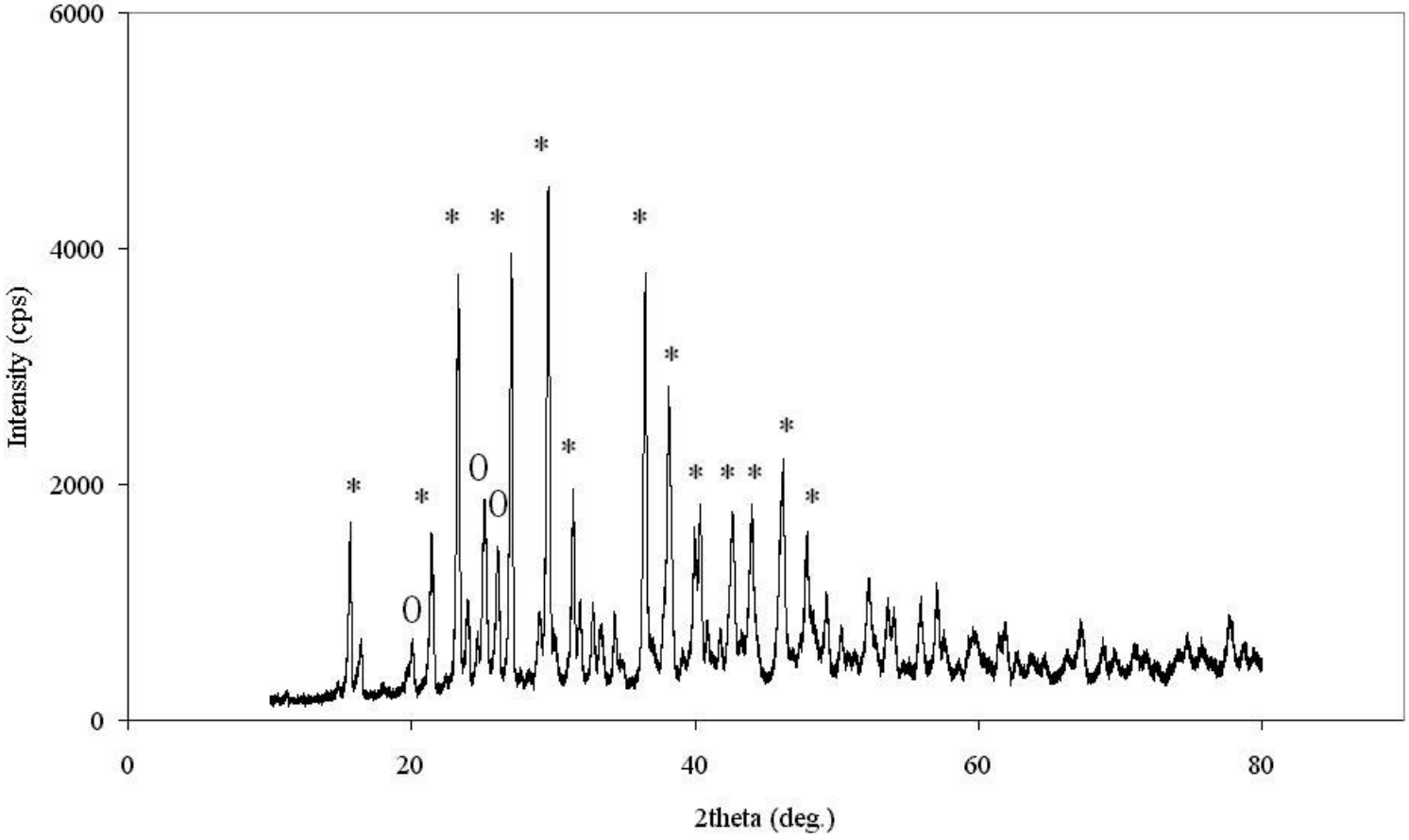

Figure B.11 *Powder x-ray diffraction pattern of LiB_3O_5 doped with 5% wt. La_2O_3*

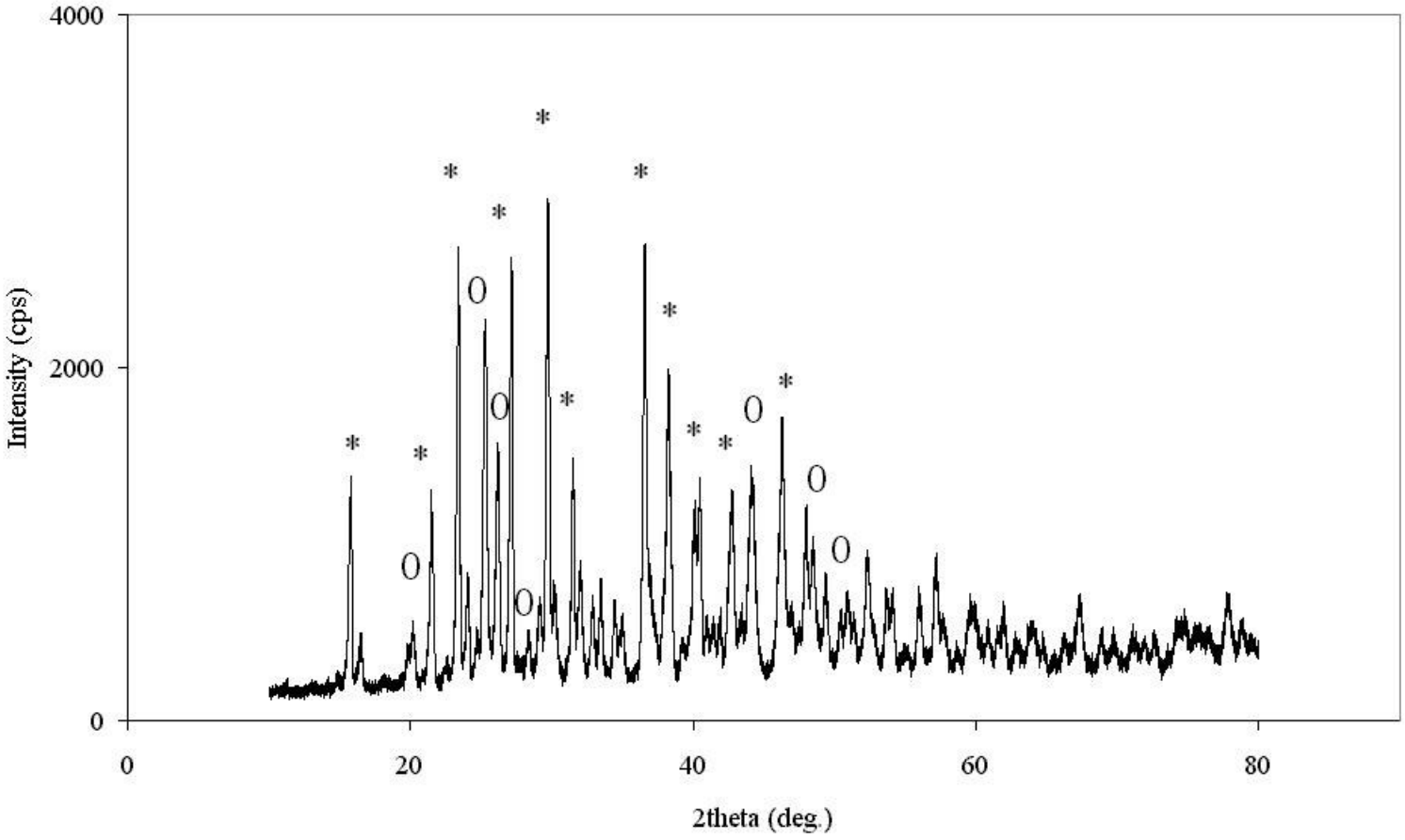

Figure B.12 *Powder x-ray diffraction pattern of LiB_3O_5 doped with 7% wt. La_2O_3*

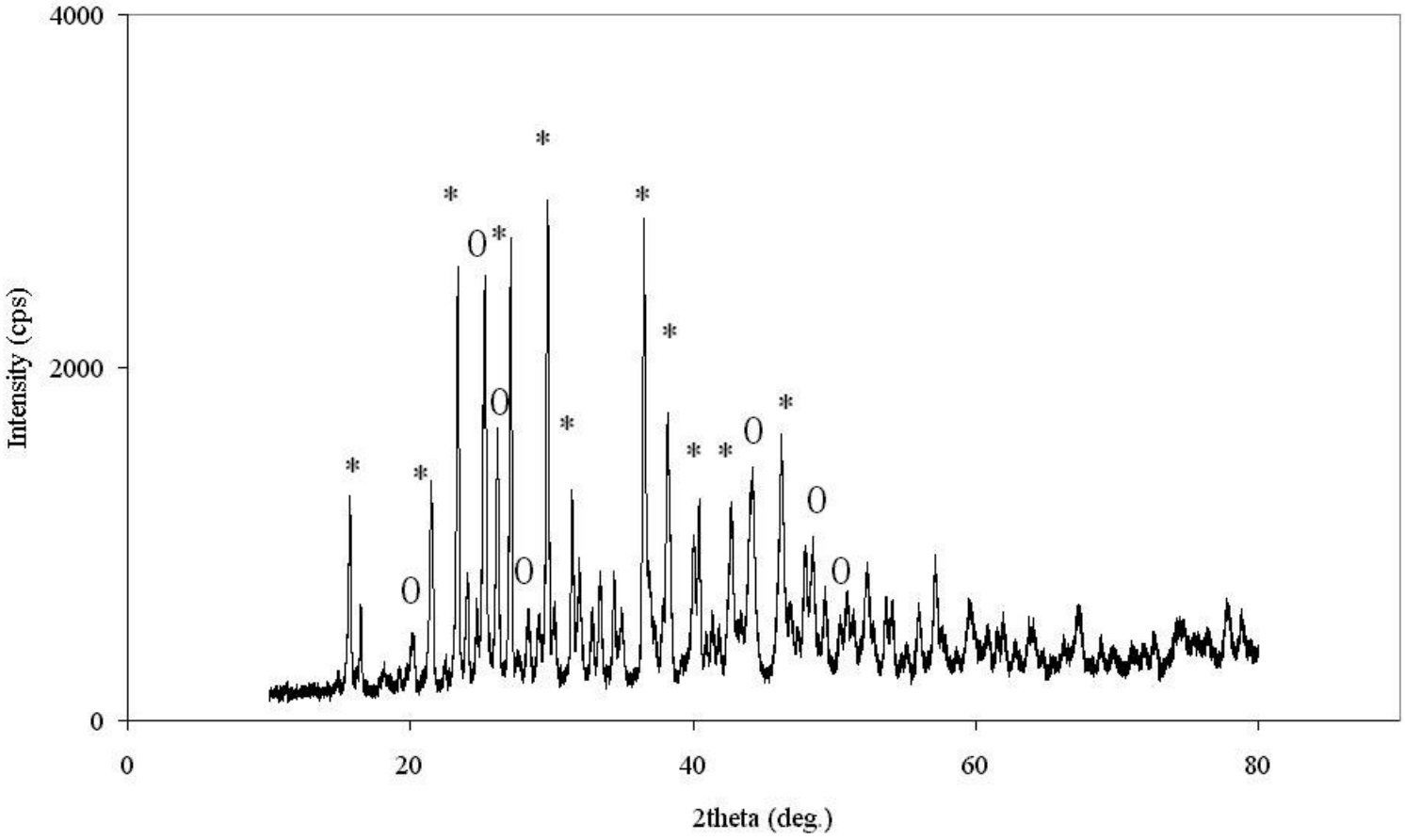

Figure B.13 *Powder x-ray diffraction pattern of LiB_3O_5 doped with 9% wt. La_2O_3*

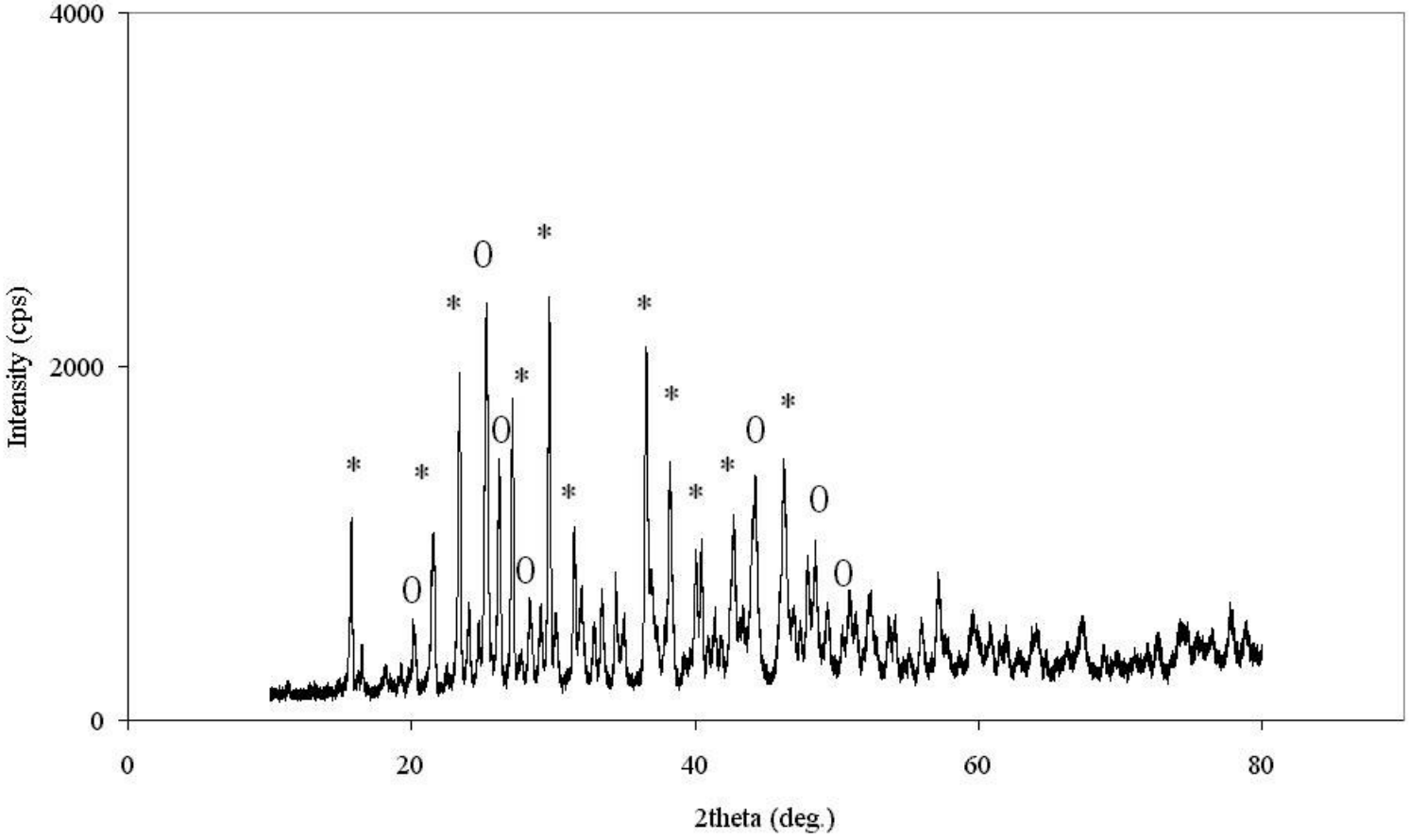

Figure B.14 *Powder x-ray diffraction pattern of LiB_3O_5 doped with 11% wt. La_2O_3*

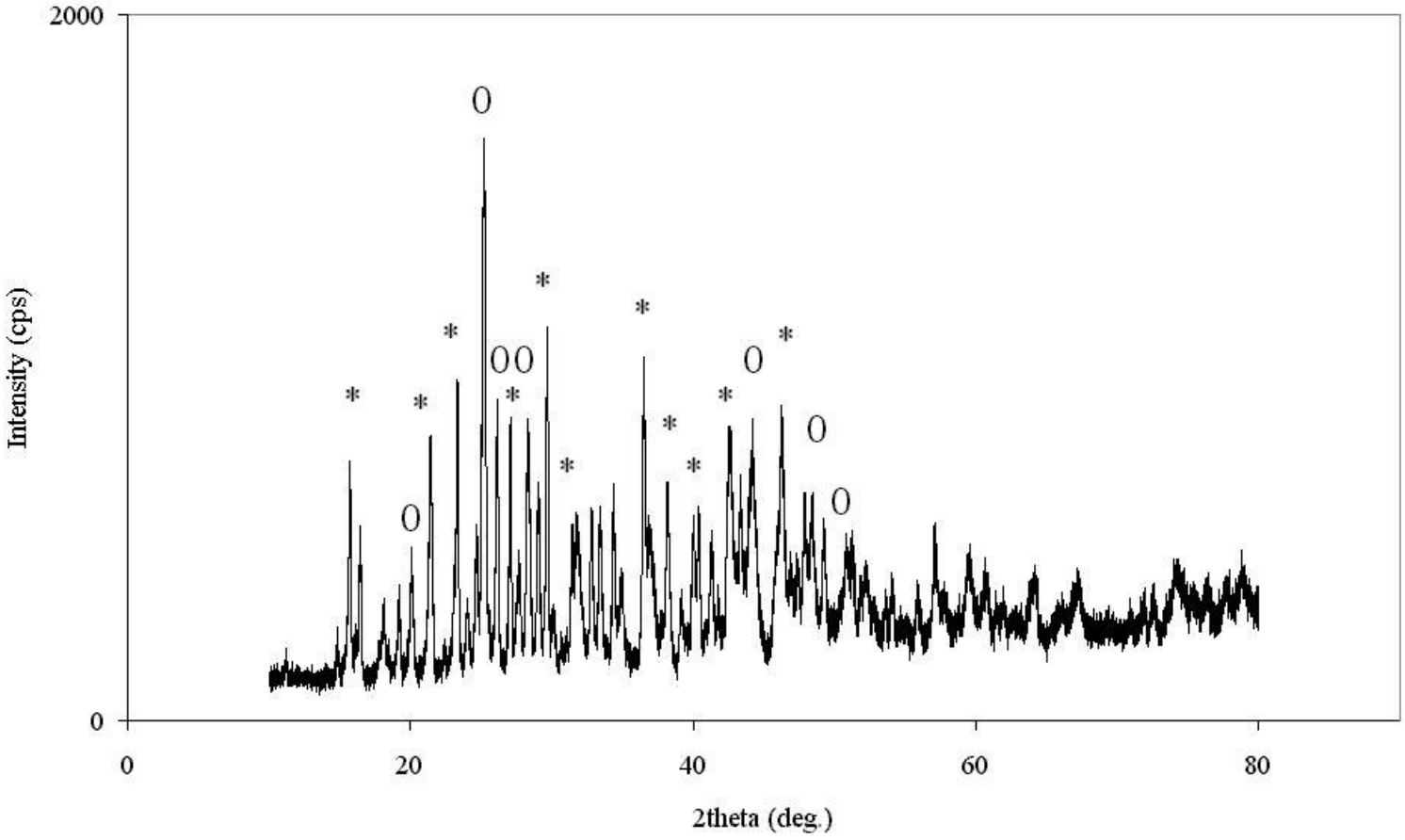

Figure B.15 *Powder x-ray diffraction pattern of LiB_3O_5 doped with 15% wt. La_2O_3*

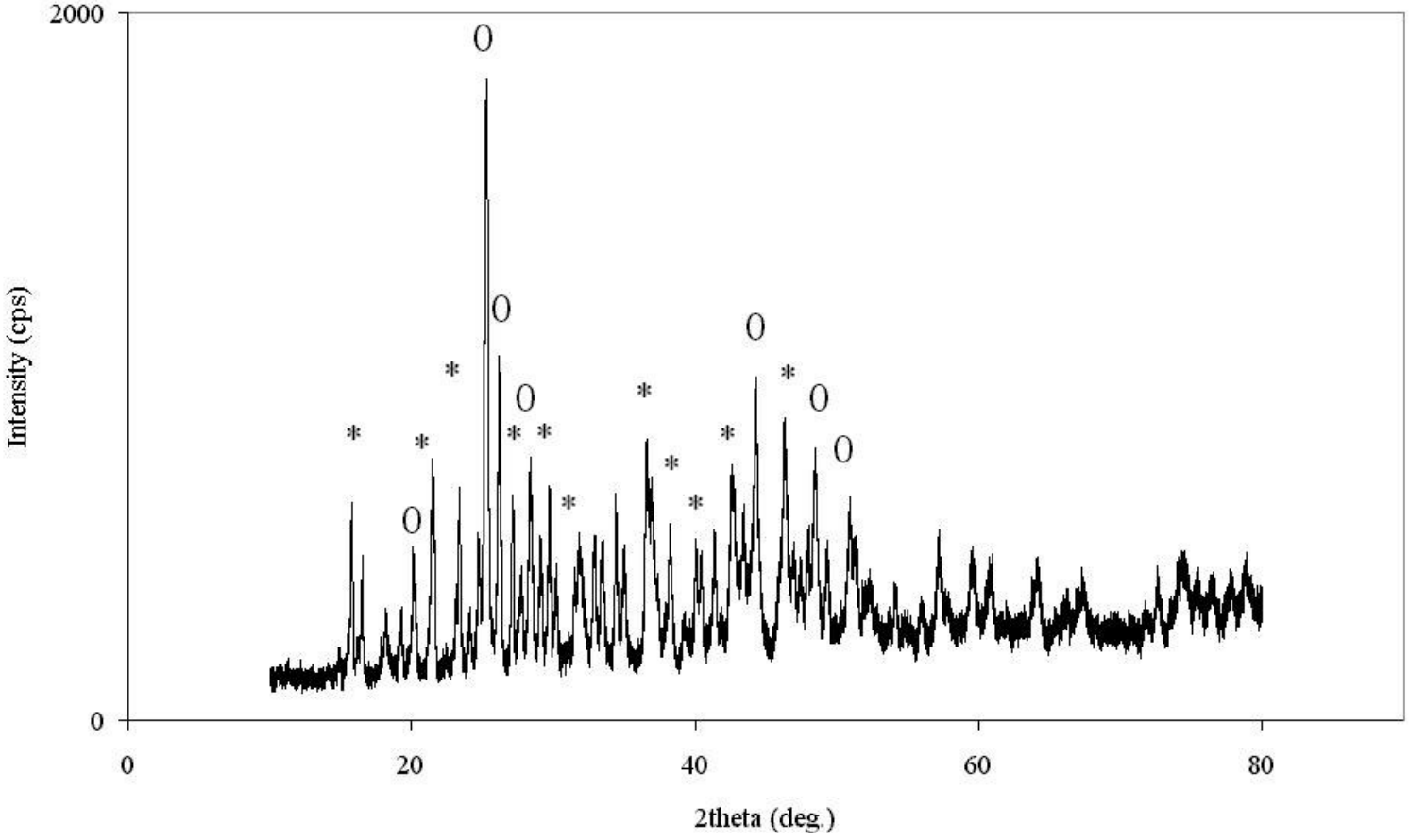

Figure B.16 *Powder x-ray diffraction pattern of LiB_3O_5 doped with 20% wt. La_2O_3*

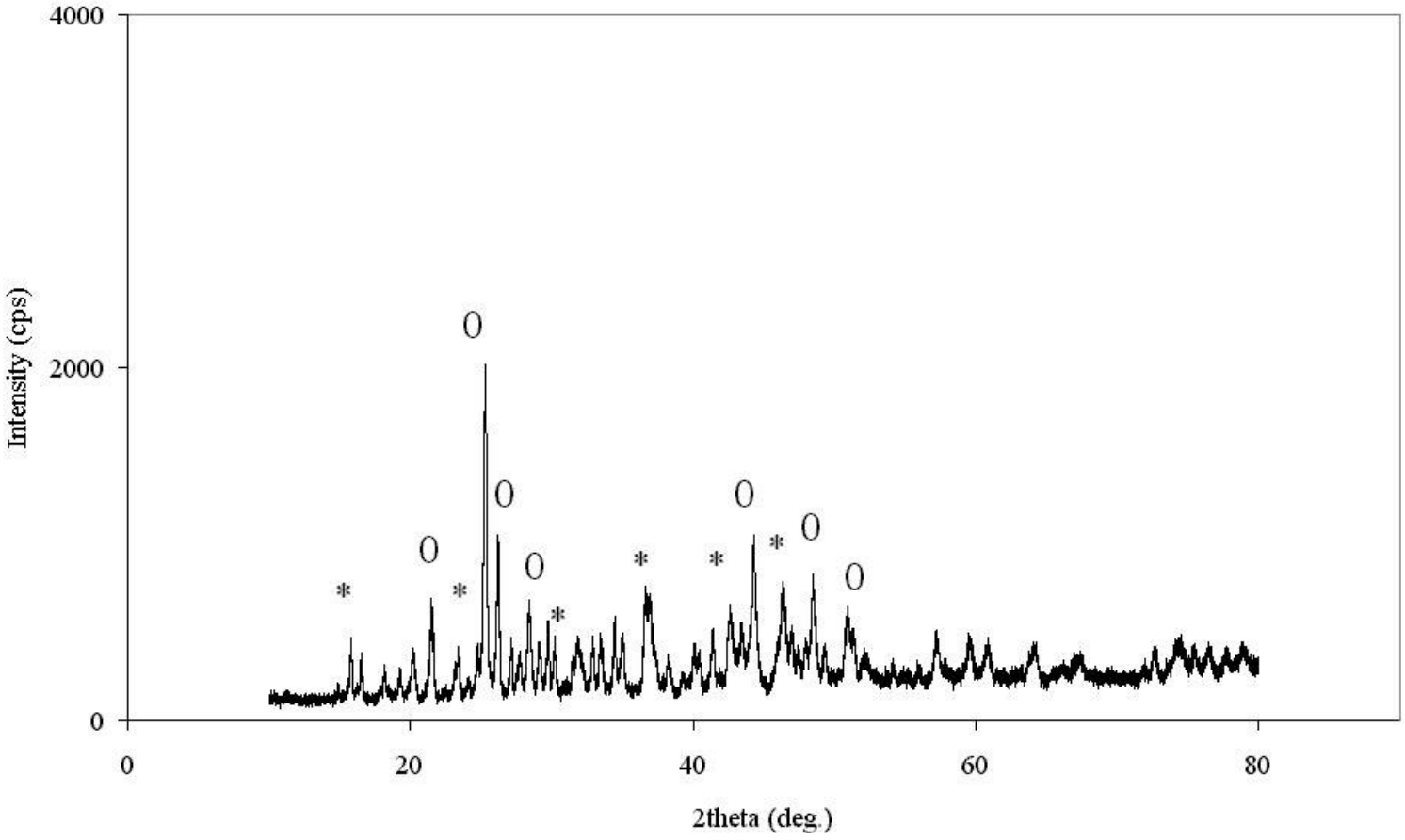

Figure B.17 *Powder x-ray diffraction pattern of LiB_3O_5 doped with 25% wt. La_2O_3*

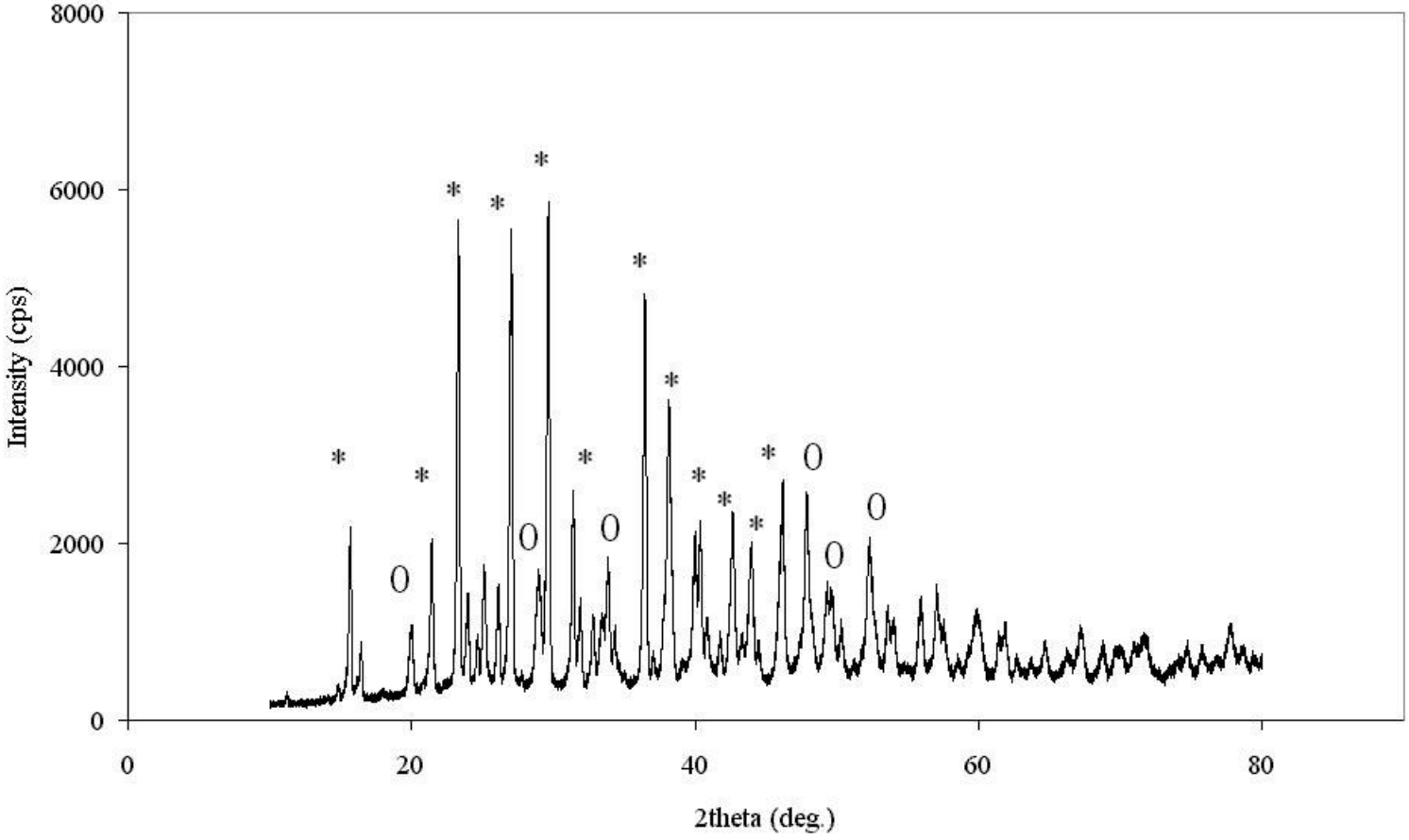

Figure B.18 *Powder x-ray diffraction pattern of LiB_3O_5 doped with 3% wt. Y_2O_3*

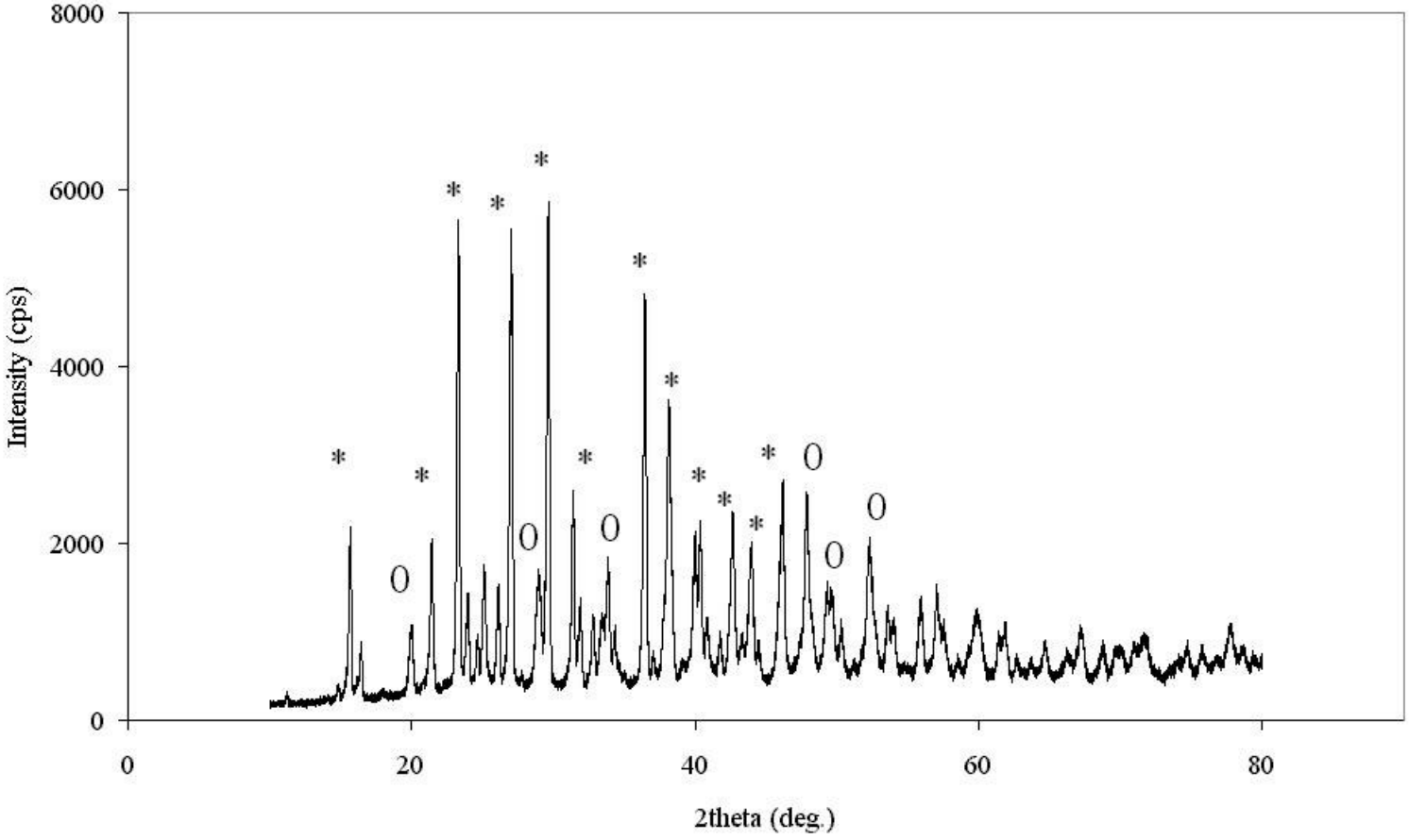

Figure B.19 *Powder x-ray diffraction pattern of LiB_3O_5 doped with 5% wt. Y_2O_3*

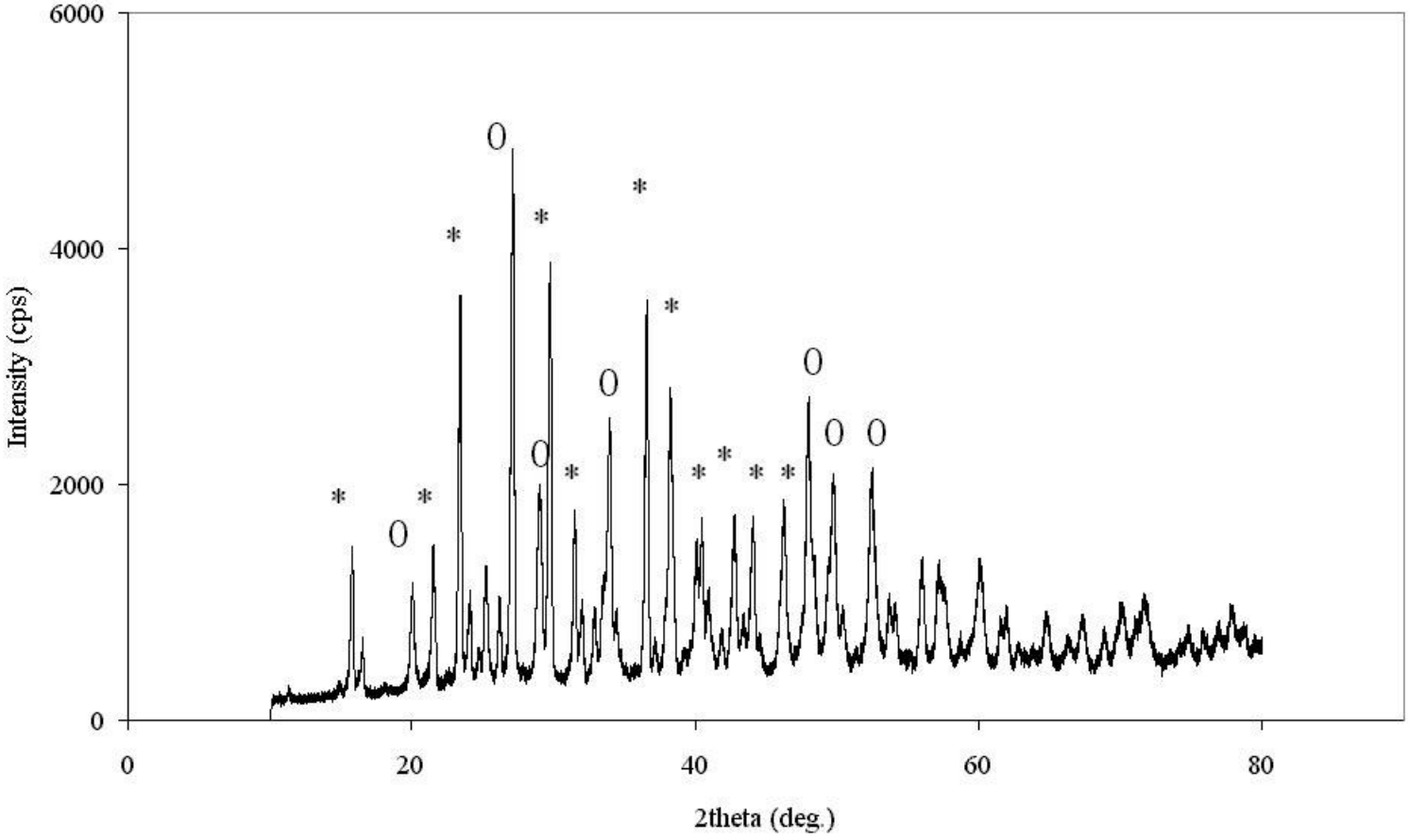

Figure B.20 *Powder x-ray diffraction pattern of LiB_3O_5 doped with 7% wt. Y_2O_3*

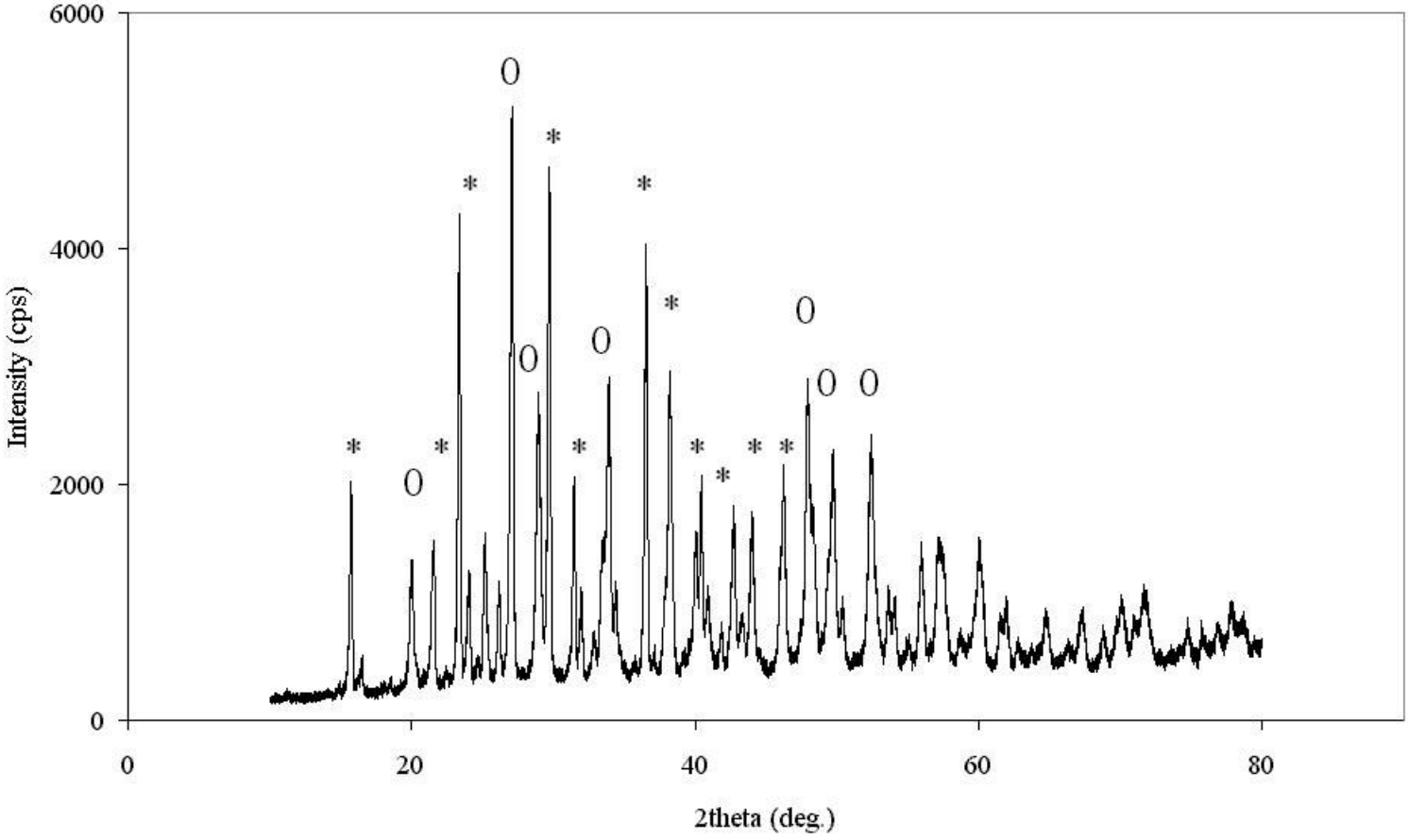

Figure B.21 *Powder x-ray diffraction pattern of LiB_3O_5 doped with 9% wt. Y_2O_3*

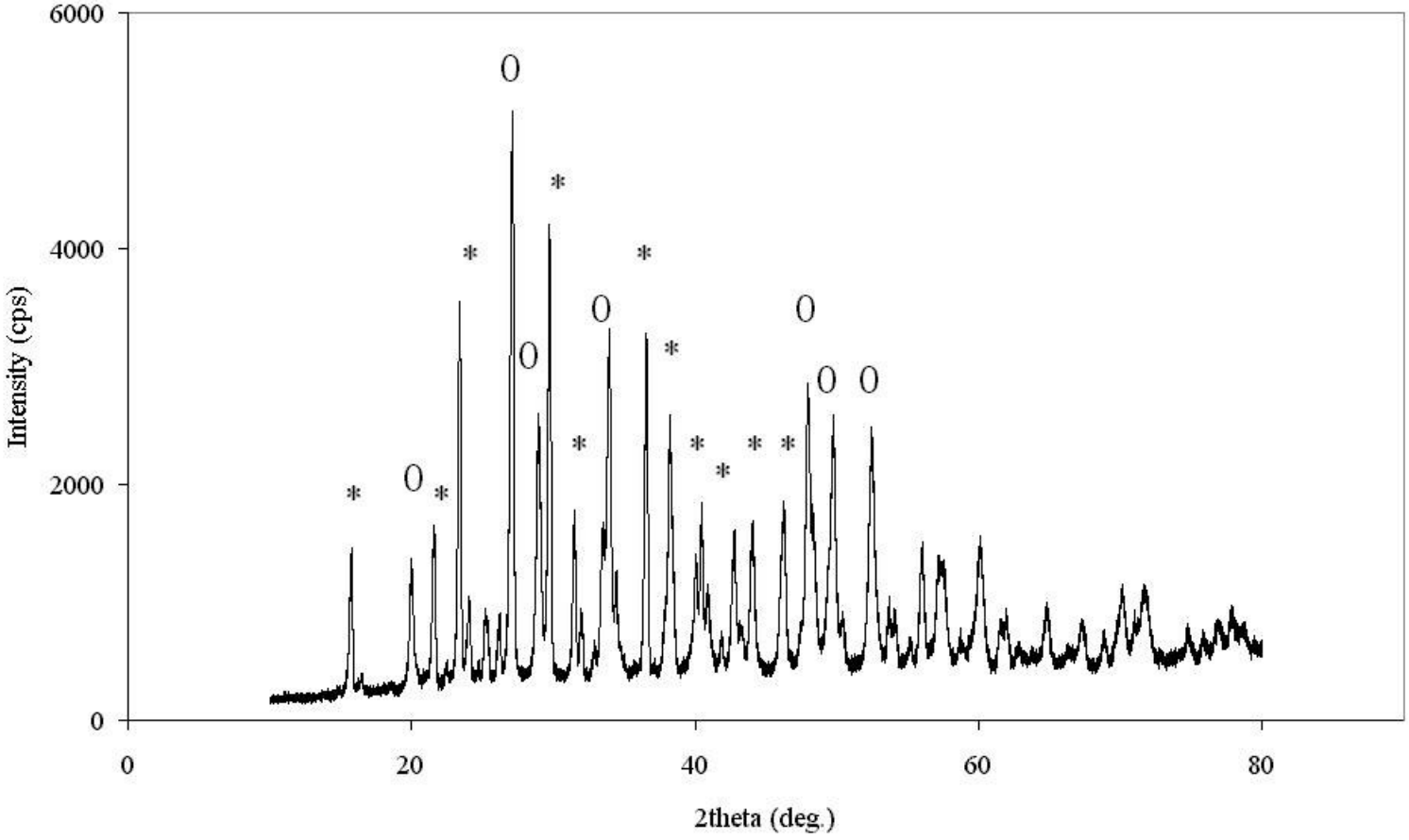

Figure B.22 *Powder x-ray diffraction pattern of LiB_3O_5 doped with 11% wt. Y_2O_3*

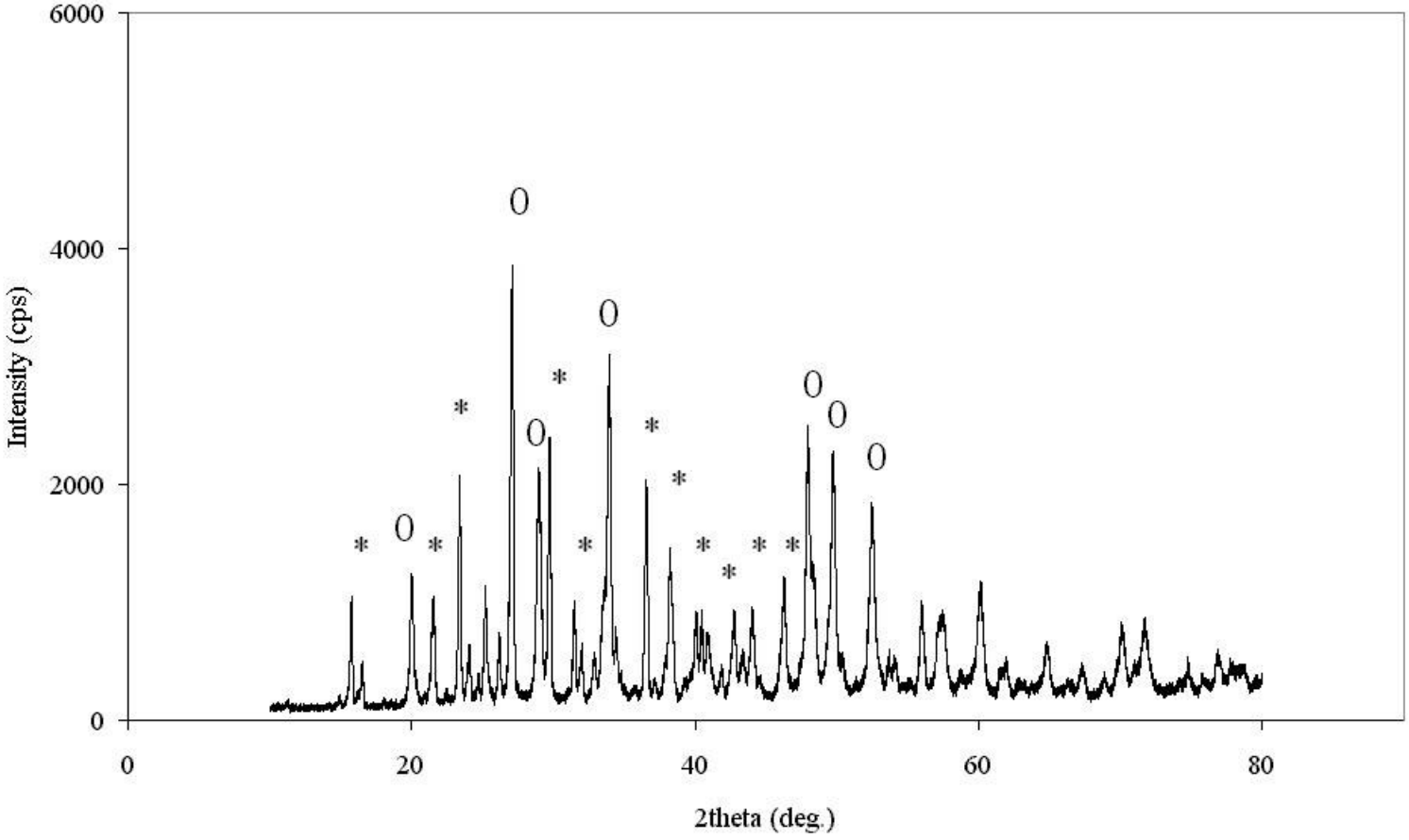

Figure B.23 *Powder x-ray diffraction pattern of LiB_3O_5 doped with 15% wt. Y_2O_3*

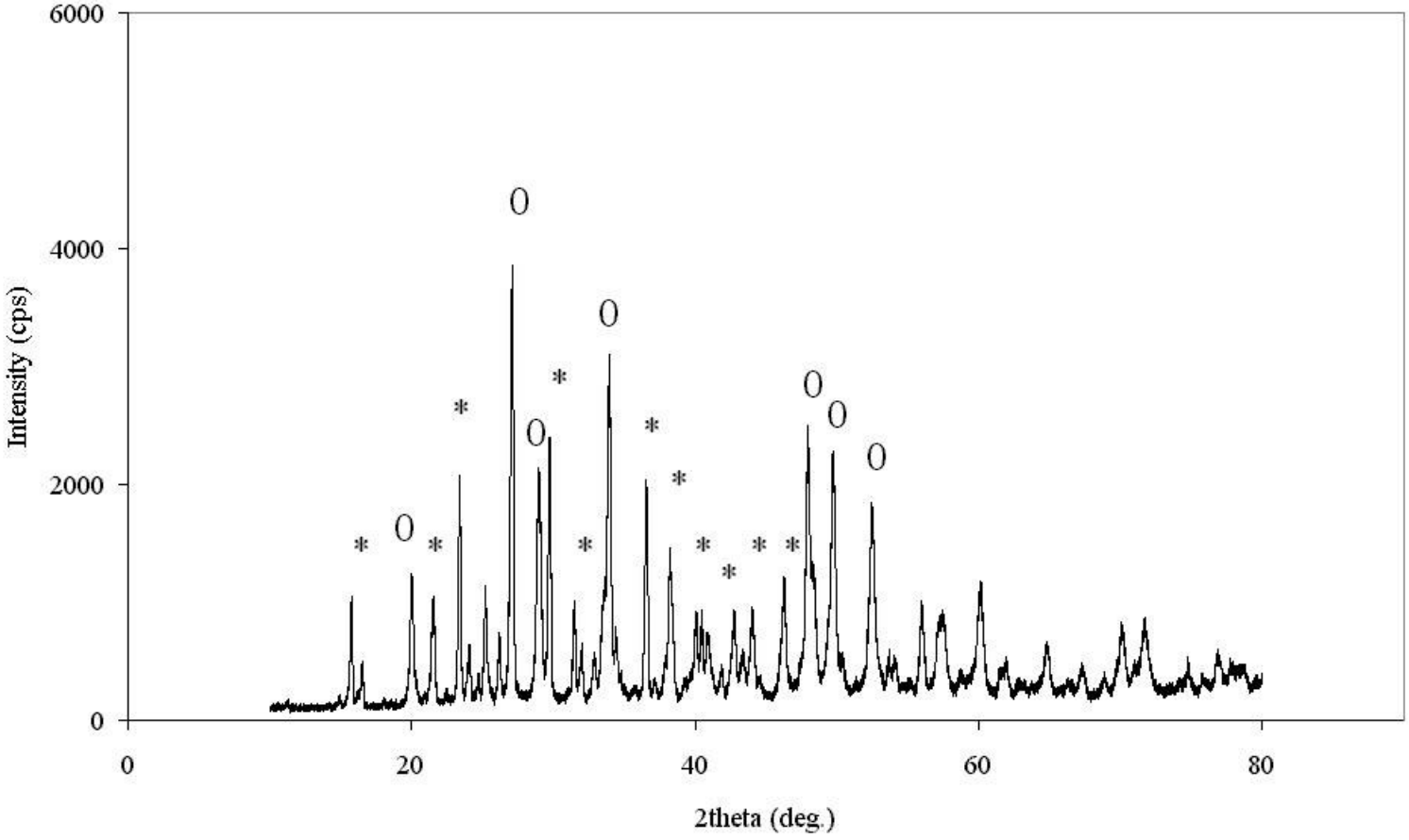

Figure B.24 *Powder x-ray diffraction pattern of LiB_3O_5 doped with 20% wt. Y_2O_3*

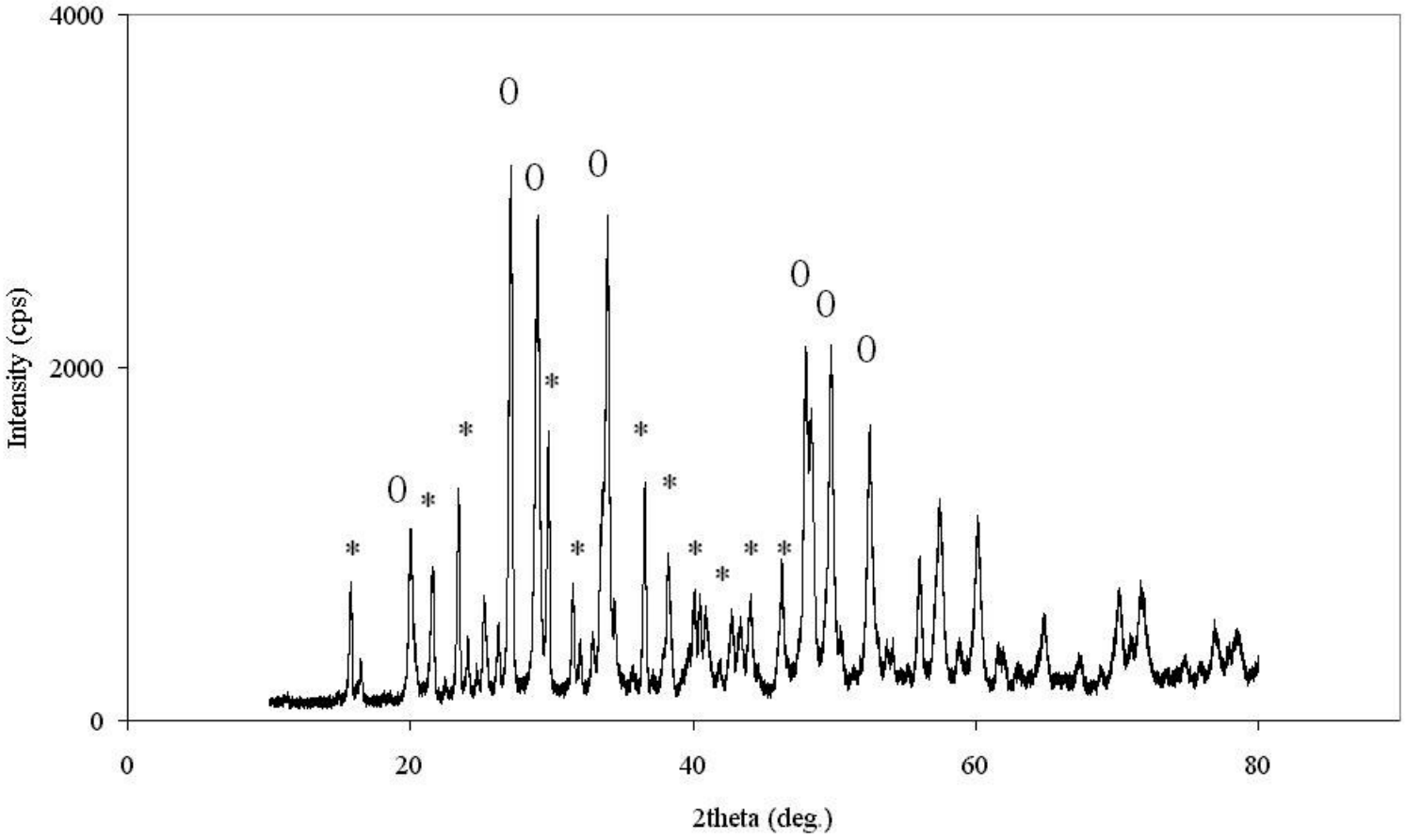

Figure B.25 *Powder x-ray diffraction pattern of LiB_3O_5 doped with 25% wt. Y_2O_3*

APPENDIX B

IR SPECTRA OF THE PRODUCED MATERIALS

The IR spectra of LBO and LBO samples doped with rare-earth elements given separately are shown in the following figures.

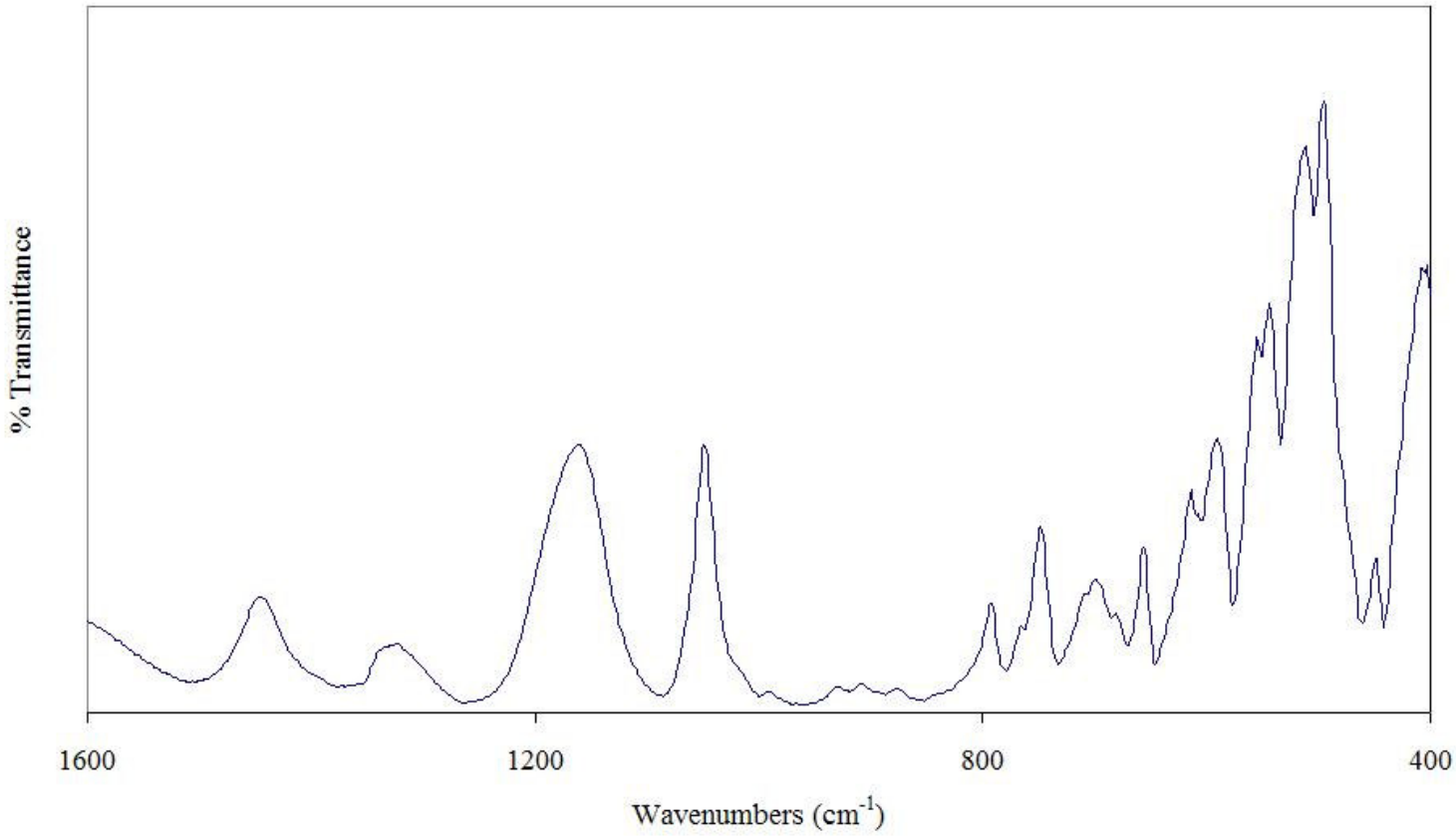

Figure C.1 *IR spectrum of LiB_3O_5 obtained from the solid-state reaction of Li_2CO_3 and H_3BO_3 at 750℃ for 14 hours*

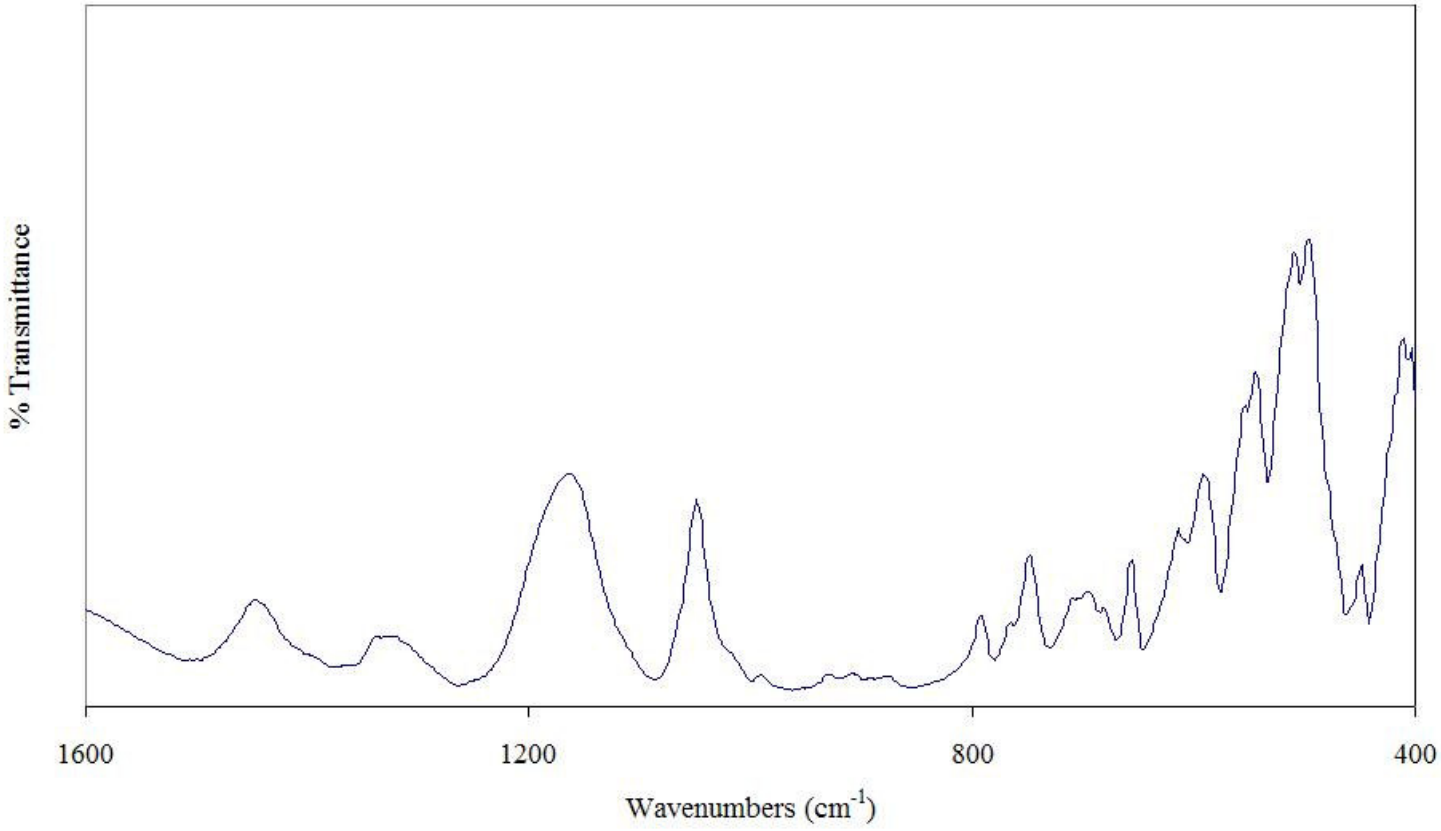

Figure C.2 *IR spectrum of LiB_3O_5 doped with 3% wt. Gd_2O_3 at 750℃ for 7 hours*

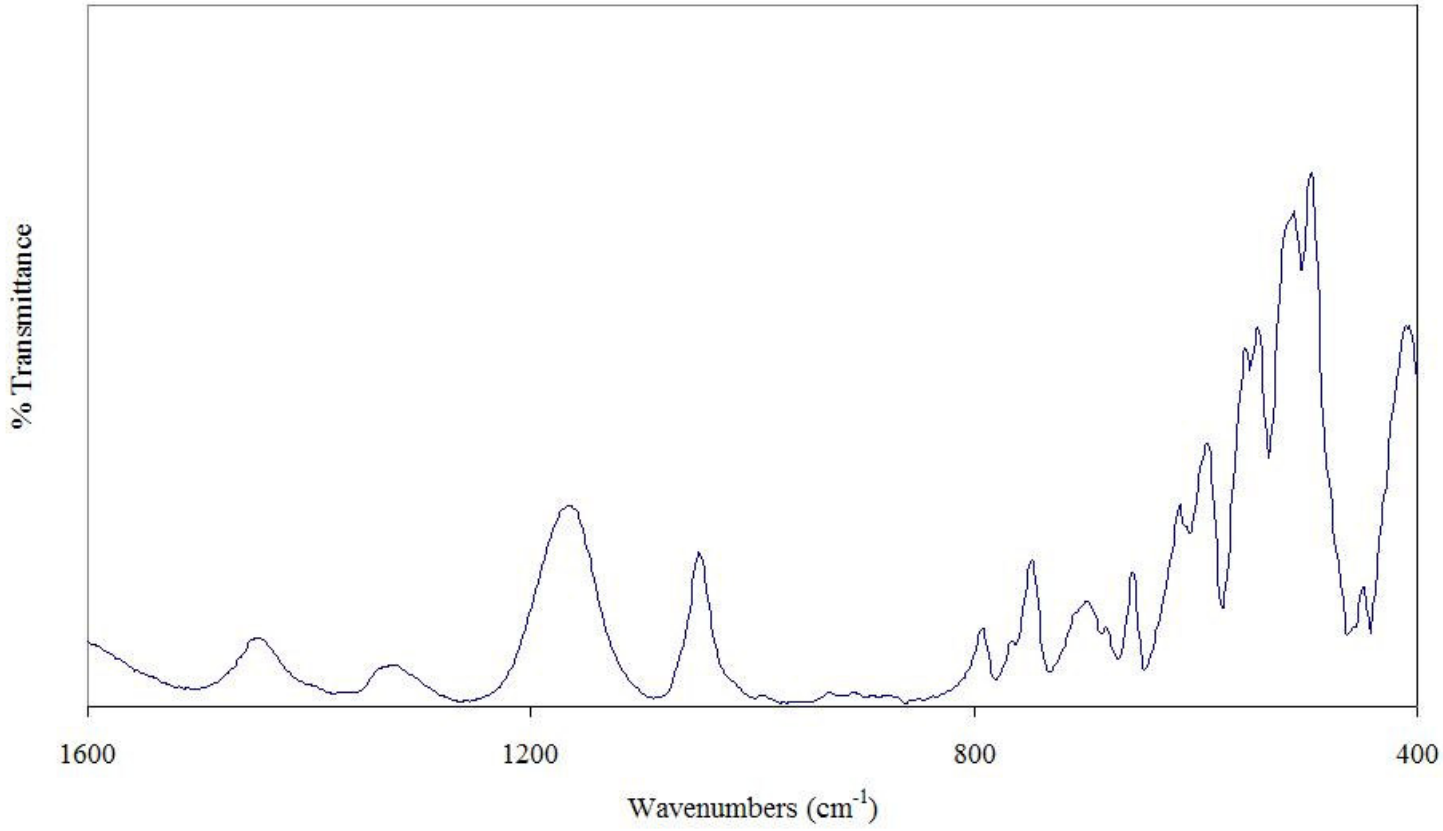

Figure C.3 *IR spectrum of LiB_3O_5 doped with 5% wt. Gd_2O_3 at 750℃ for 7 hours*

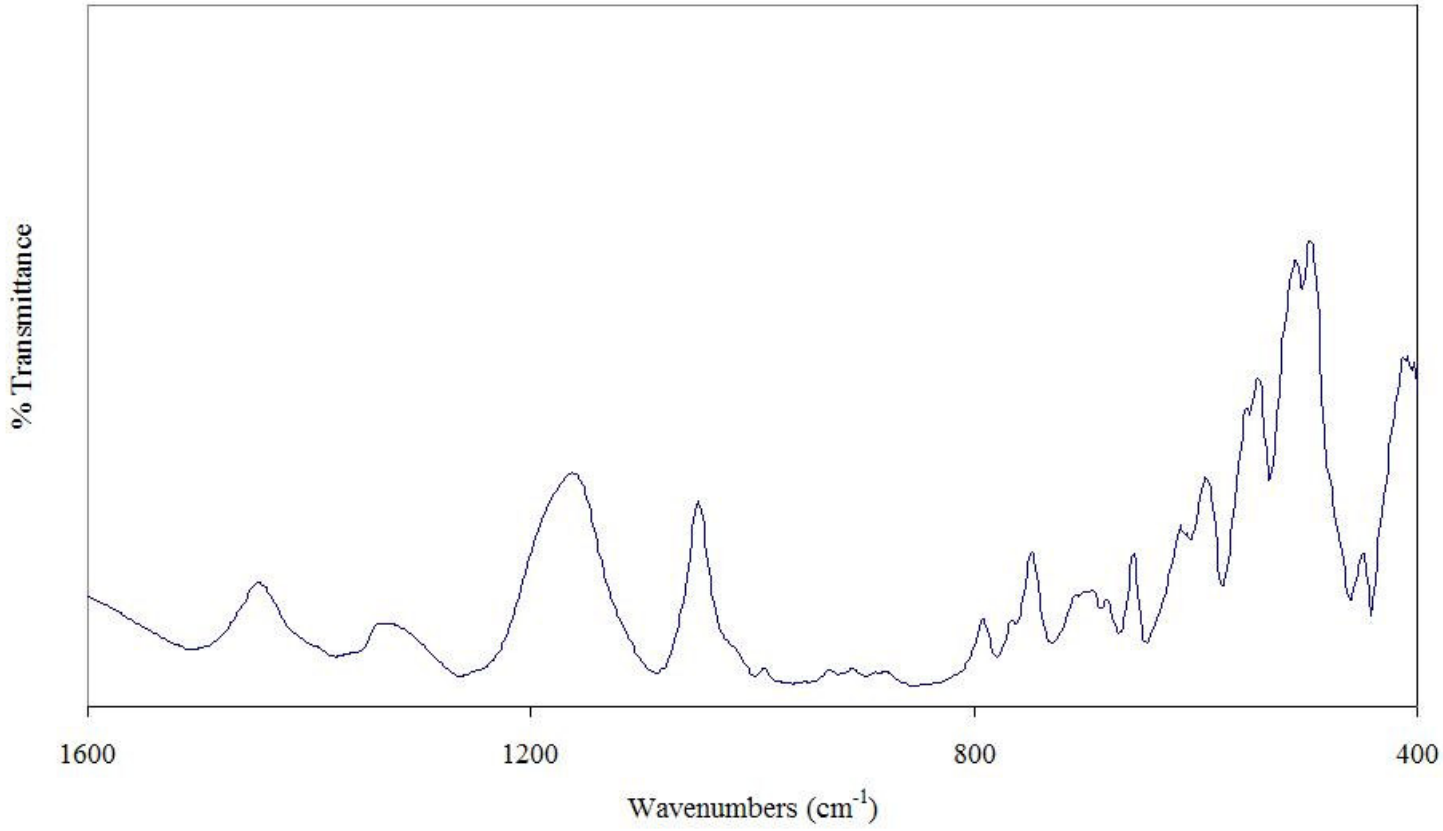

Figure C.4 *IR spectrum of LiB_3O_5 doped with 7% wt. Gd_2O_3 at 750℃ for 7 hours*

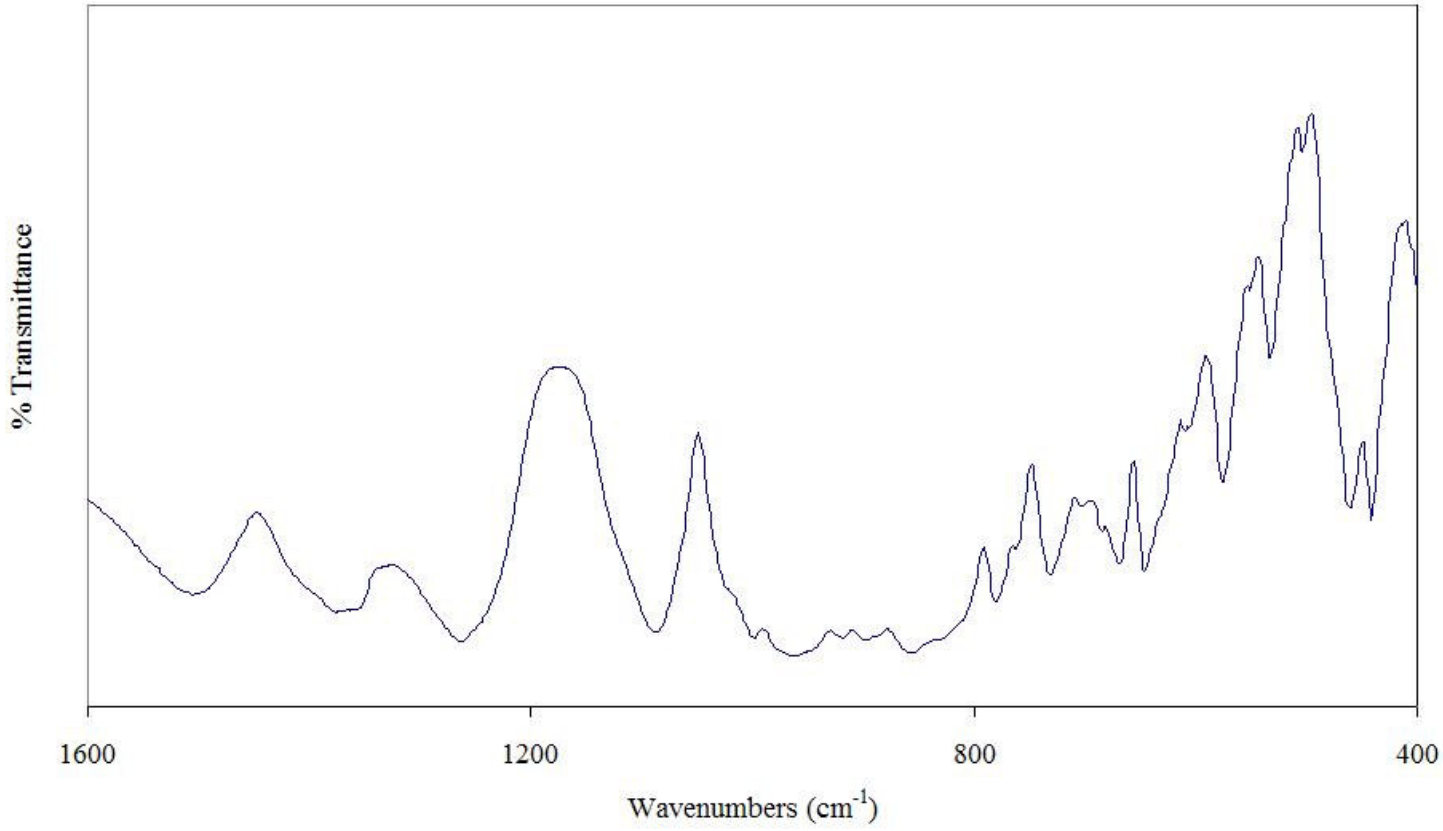

Figure C.5 *IR spectrum of LiB_3O_5 doped with 9% wt. Gd_2O_3 at 750℃ for 7 hours*

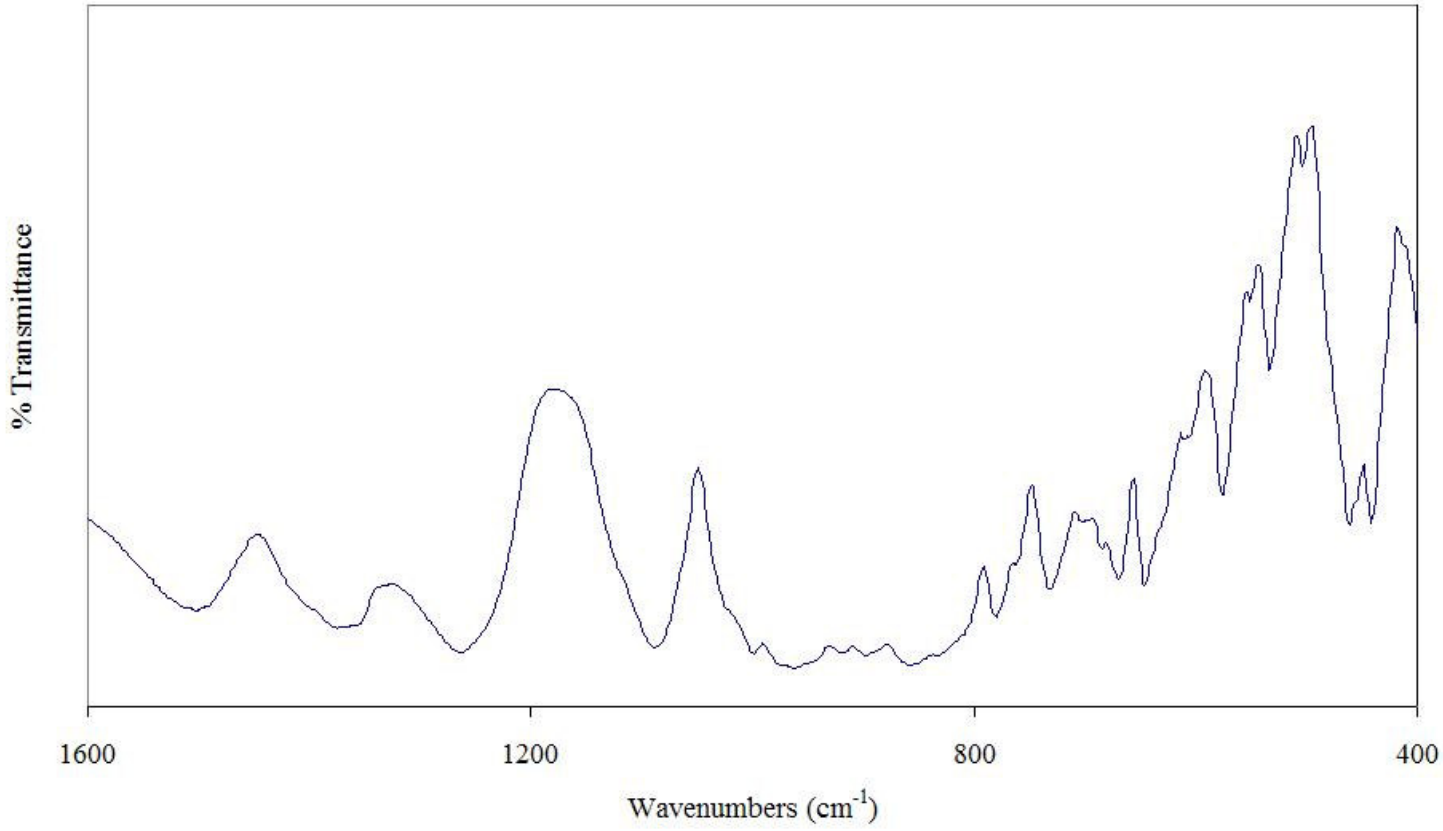

Figure C.6 *IR spectrum of LiB_3O_5 doped with 11% wt. Gd_2O_3 at 750℃ for 7 hours*

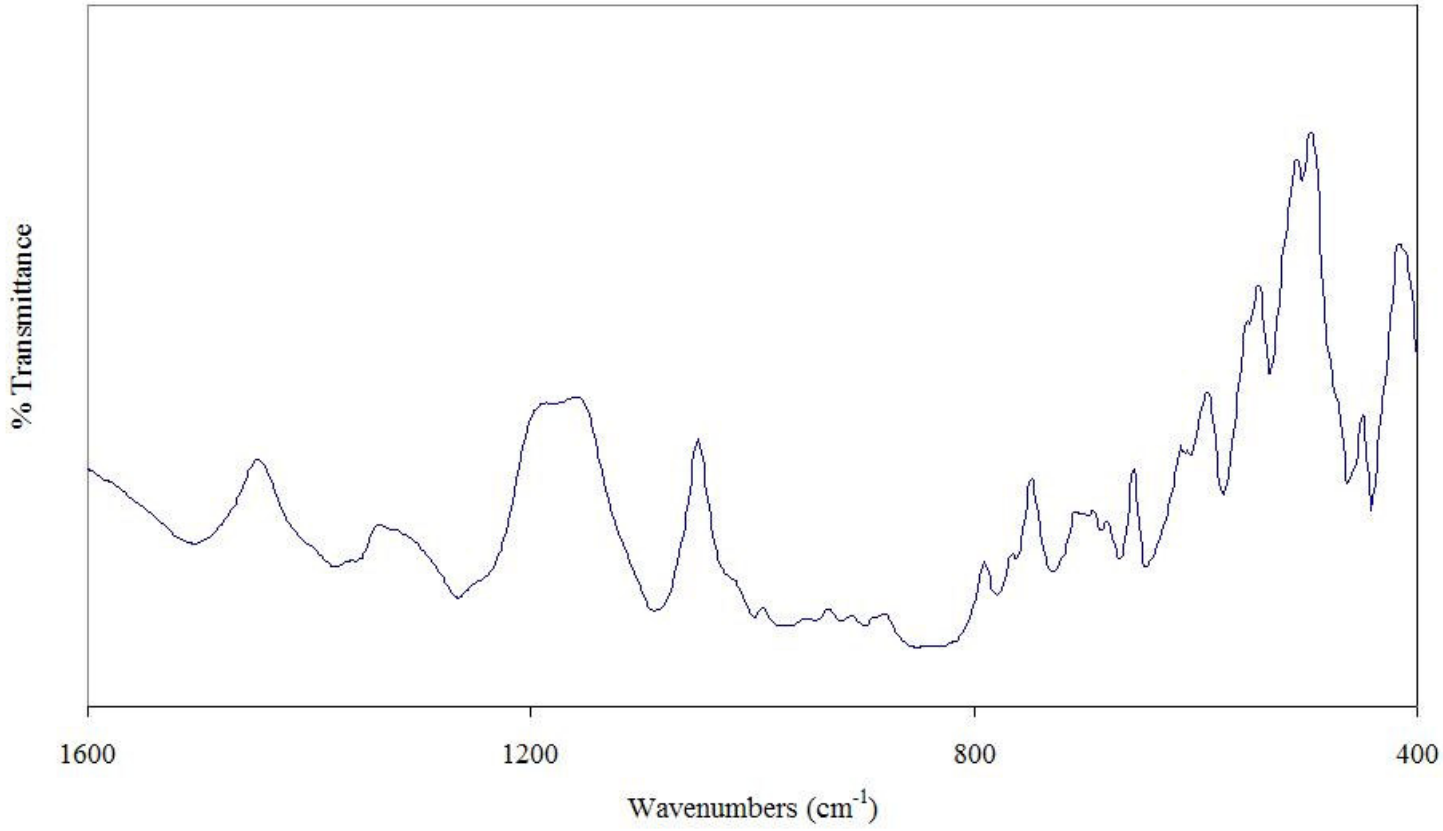

Figure C.7 *IR spectrum of LiB_3O_5 doped with 15% wt. Gd_2O_3 at 750℃ for 7 hours*

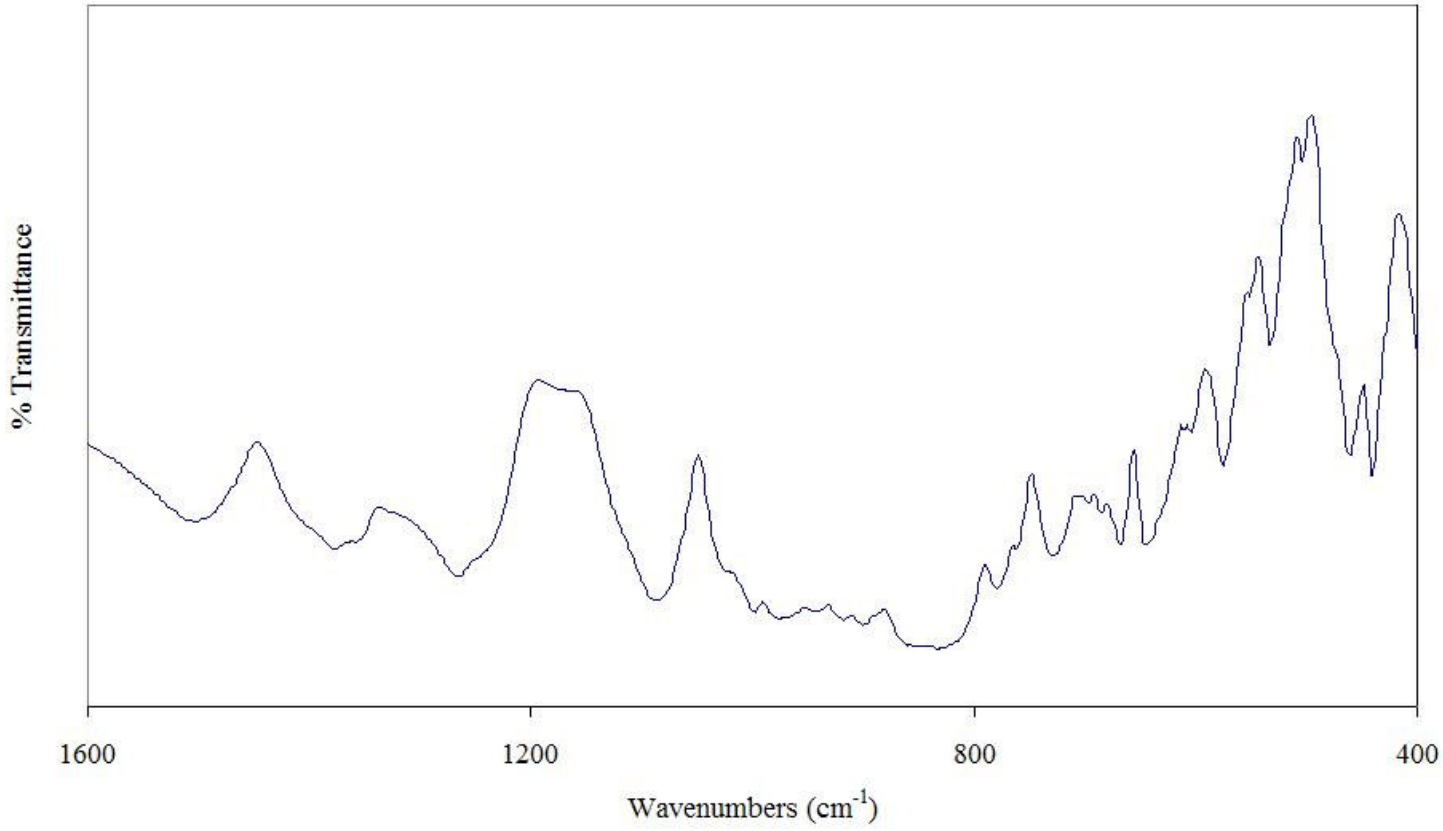

Figure C.8 *IR spectrum of LiB_3O_5 doped with 20% wt. Gd_2O_3 at 750℃ for 7 hours*

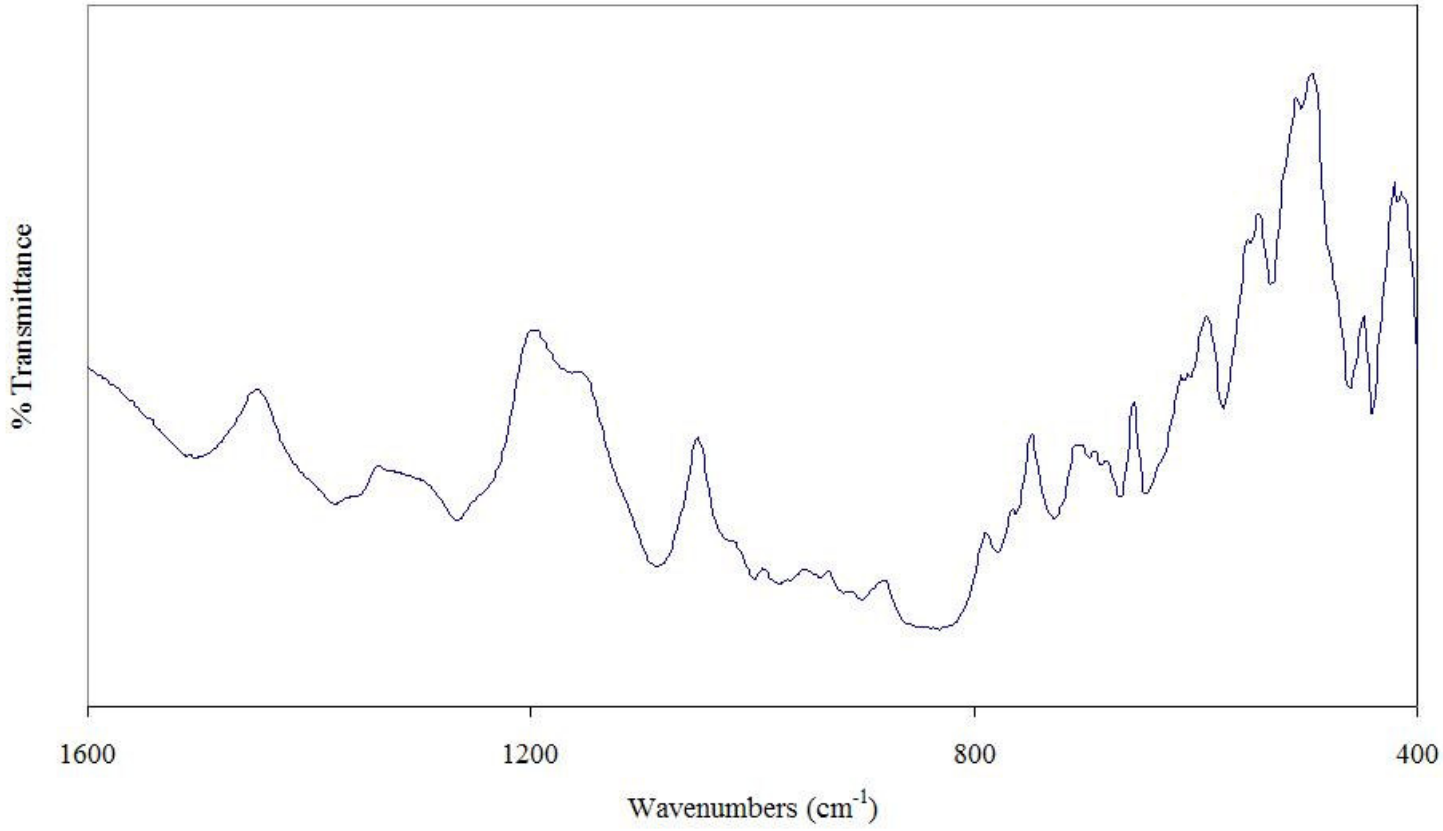

Figure C.9 *IR spectrum of LiB_3O_5 doped with 25% wt. Gd_2O_3 at 750℃ for 7 hours*

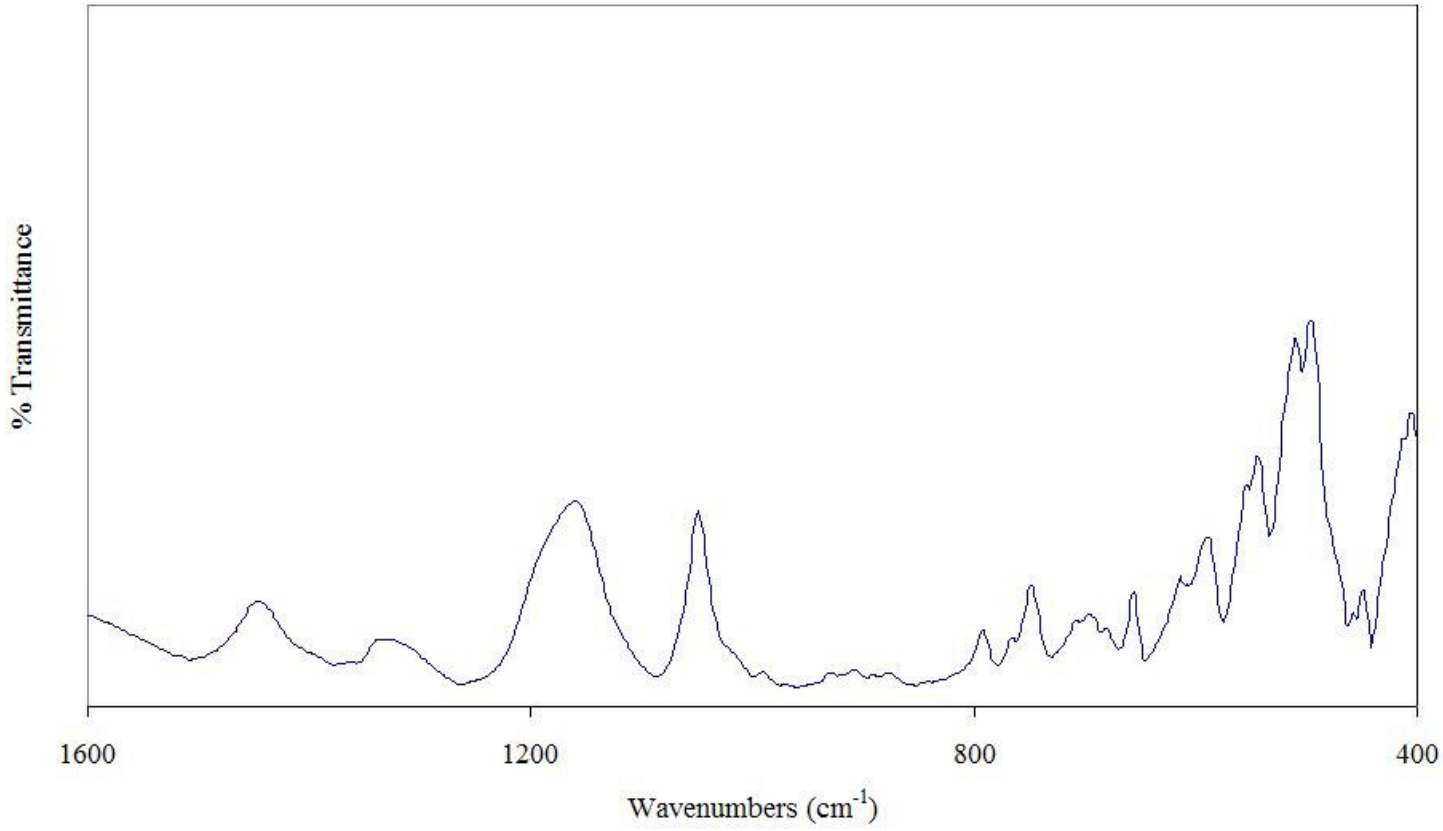

Figure C.10 *IR spectrum of LiB_3O_5 doped with 3% wt. La_2O_3 at 750℃ for 7 hours*

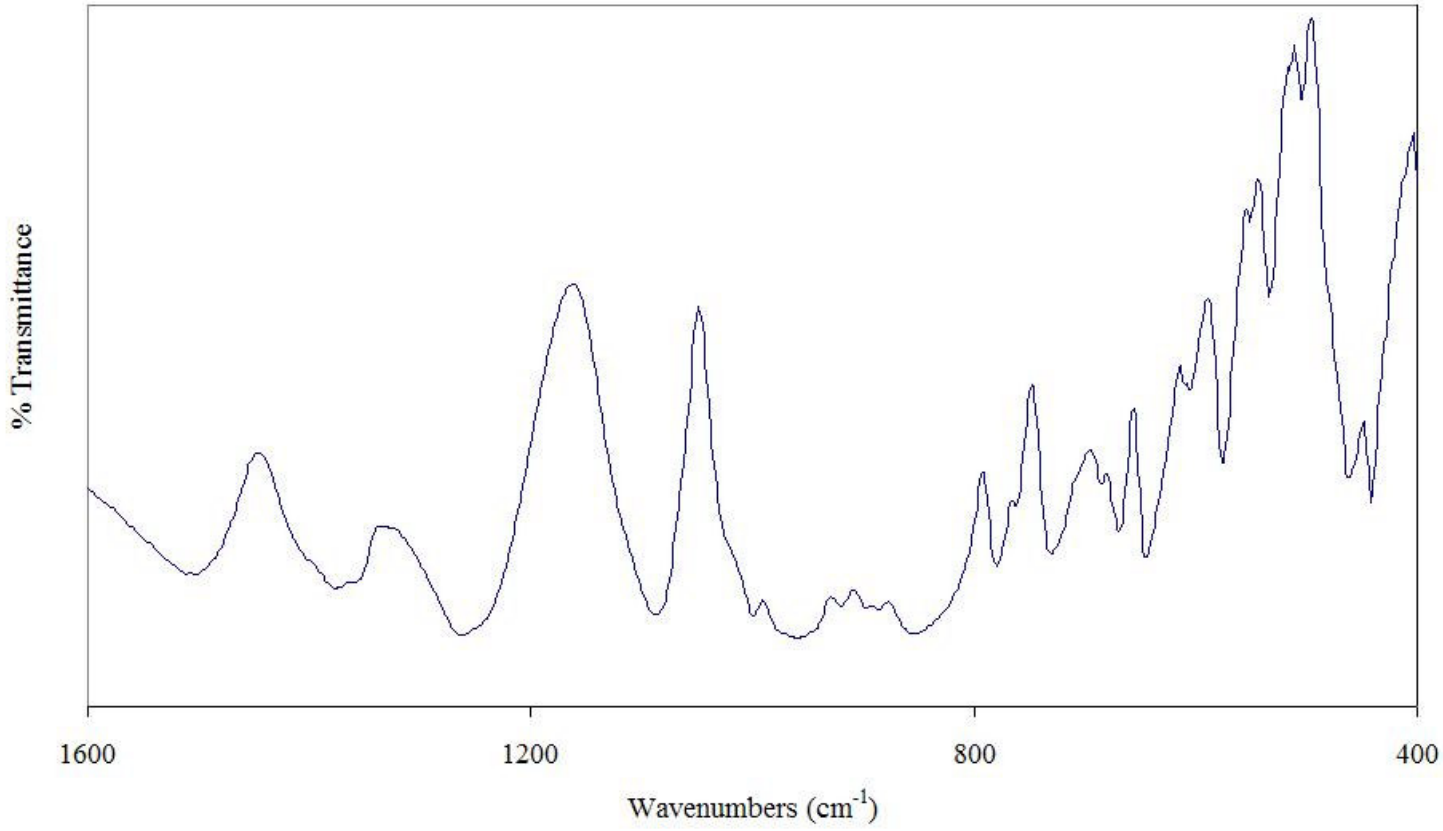

Figure C.11 *IR spectrum of LiB_3O_5 doped with 5% wt. La_2O_3 at 750℃ for 7 hours*

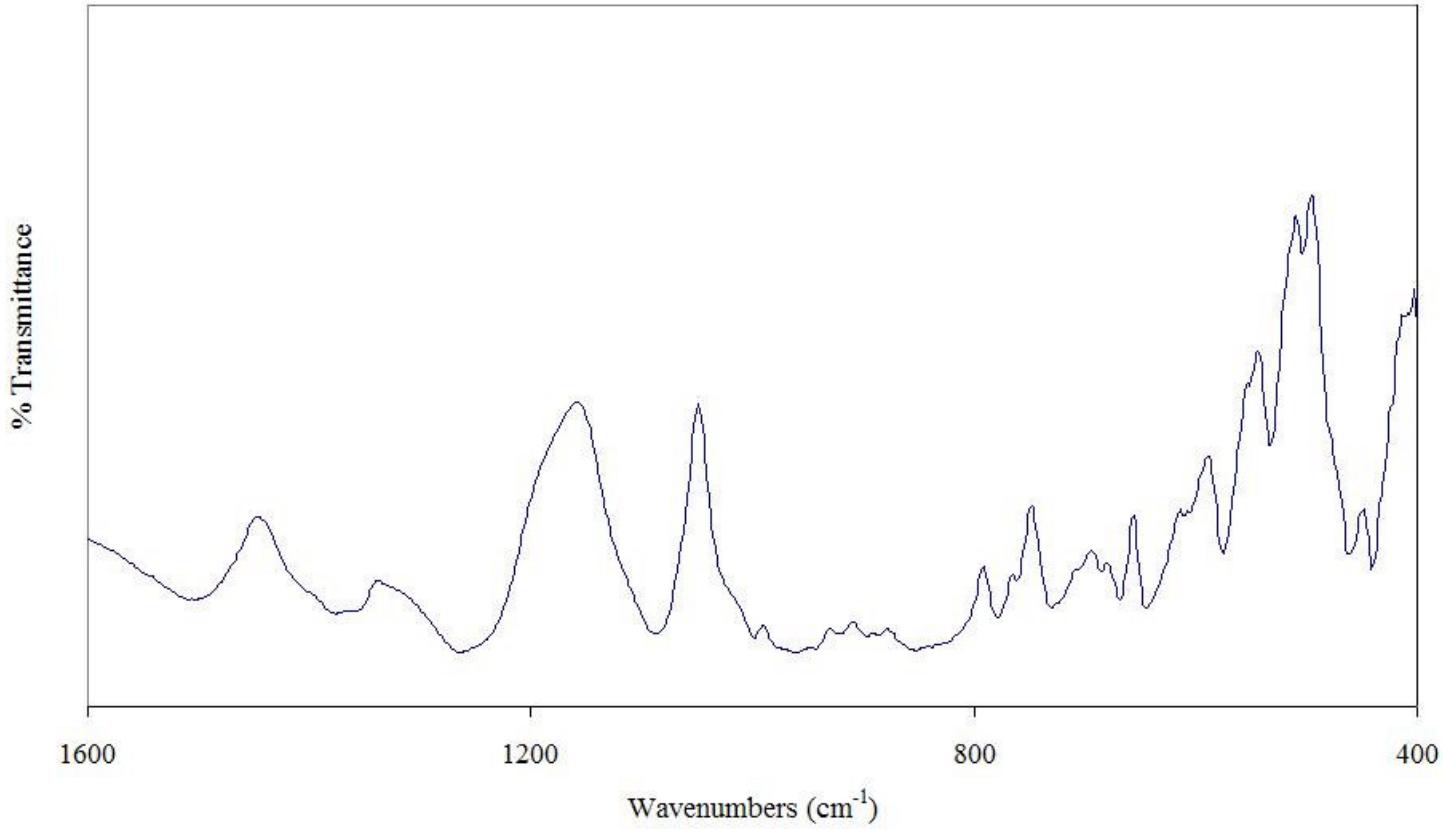

Figure C.12 *IR spectrum of LiB_3O_5 doped with 7% wt. La_2O_3 at 750℃ for 7 hours*

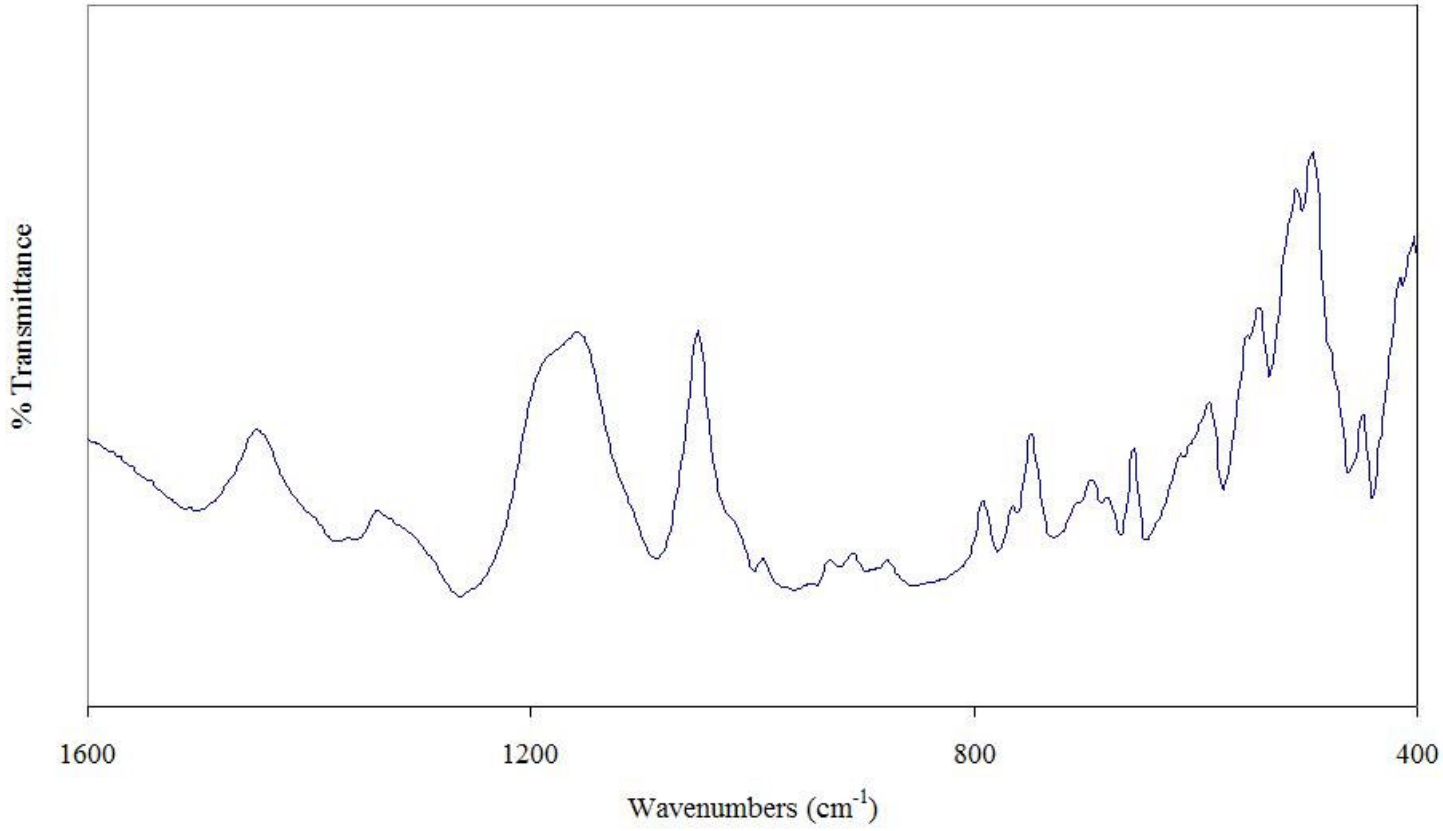

Figure C.13 *IR spectrum of LiB_3O_5 doped with 9% wt. La_2O_3 at 750℃ for 7 hours*

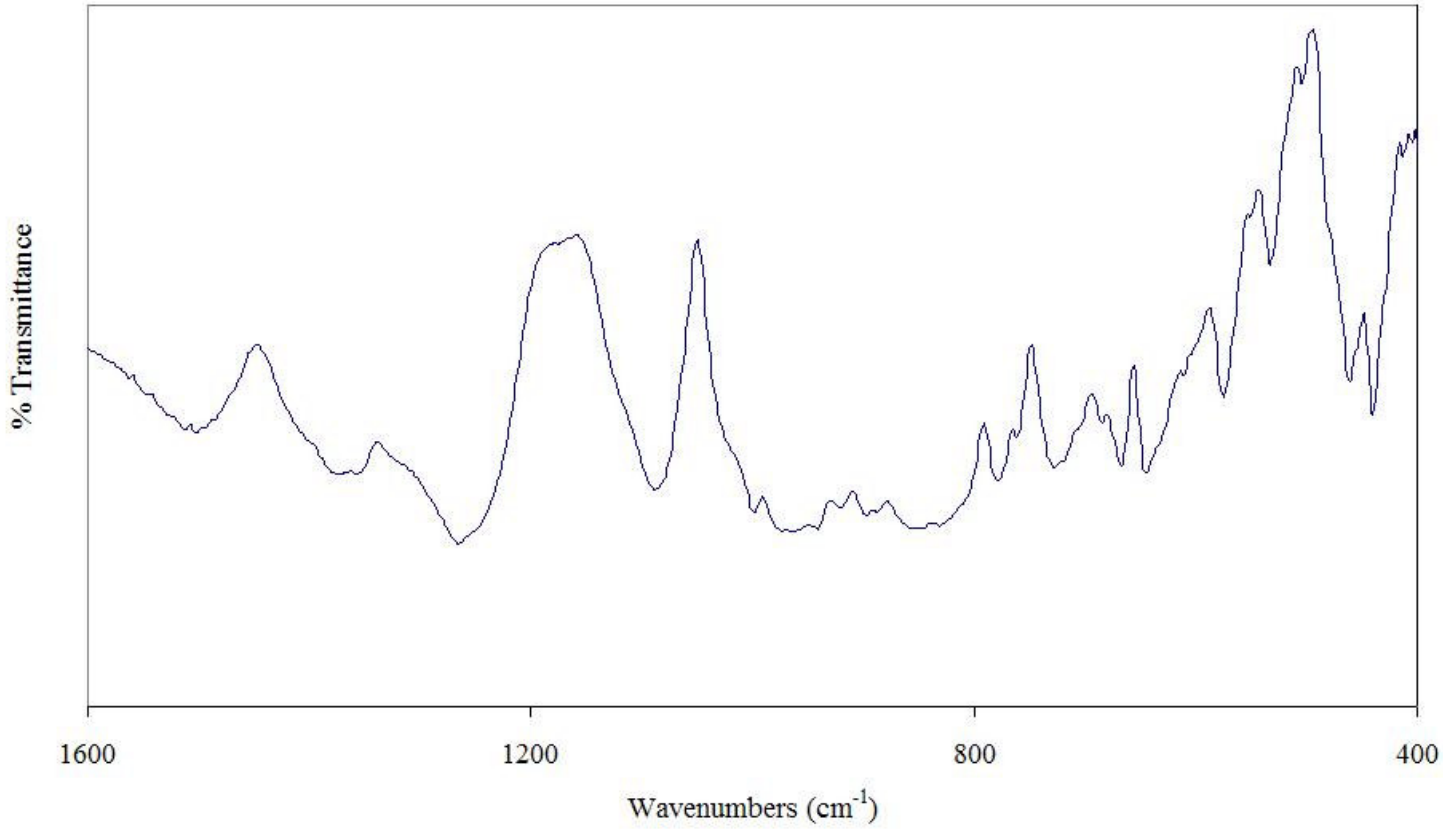

Figure C.14 *IR spectrum of LiB_3O_5 doped with 11% wt. La_2O_3 at 750℃ for 7 hours*

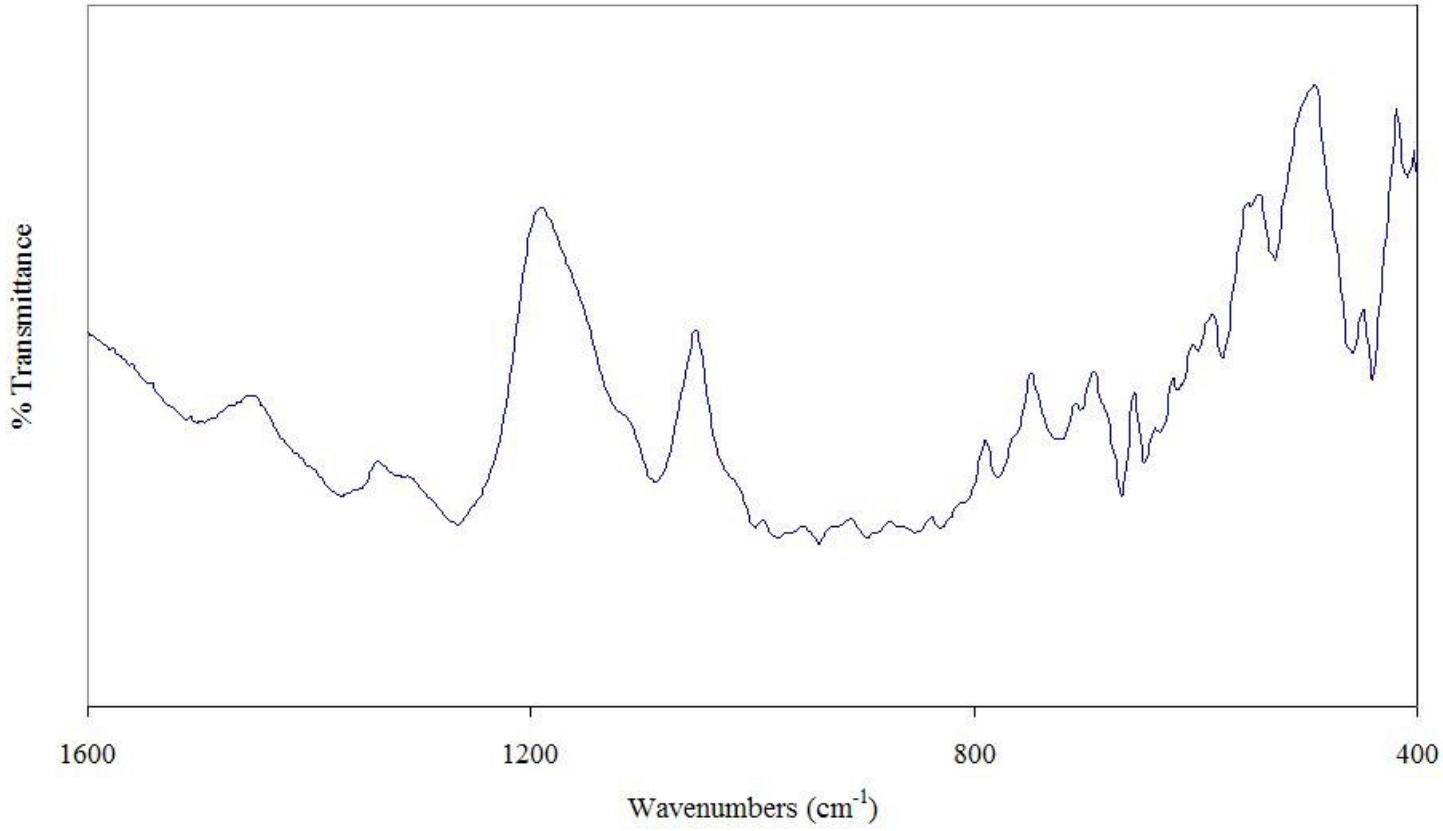

Figure C.15 *IR spectrum of LiB_3O_5 doped with 15% wt. La_2O_3 at 750℃ for 7 hours*

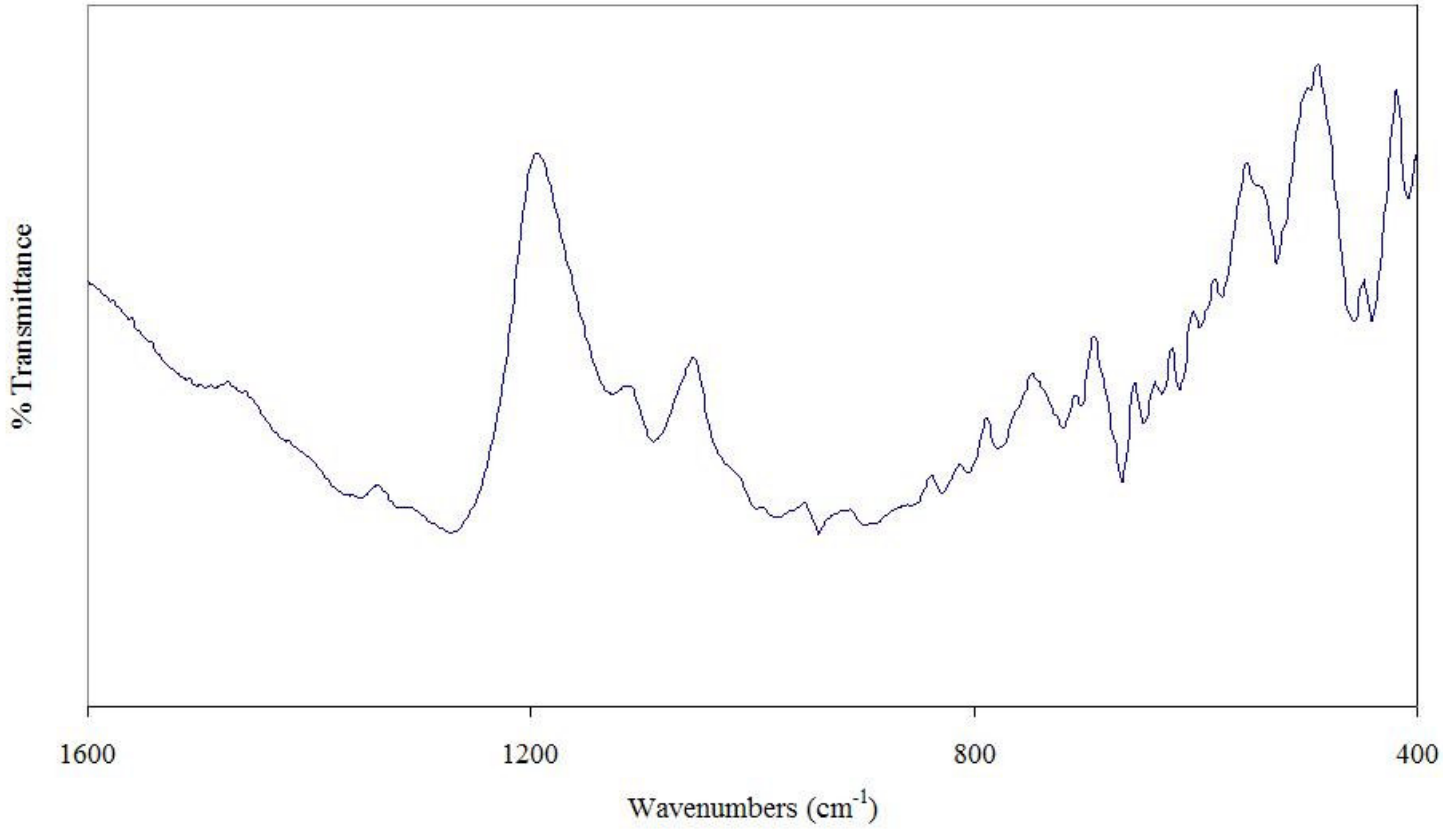

Figure C.16 *IR spectrum of LiB_3O_5 doped with 20% wt. La_2O_3 at 750℃ for 7 hours*

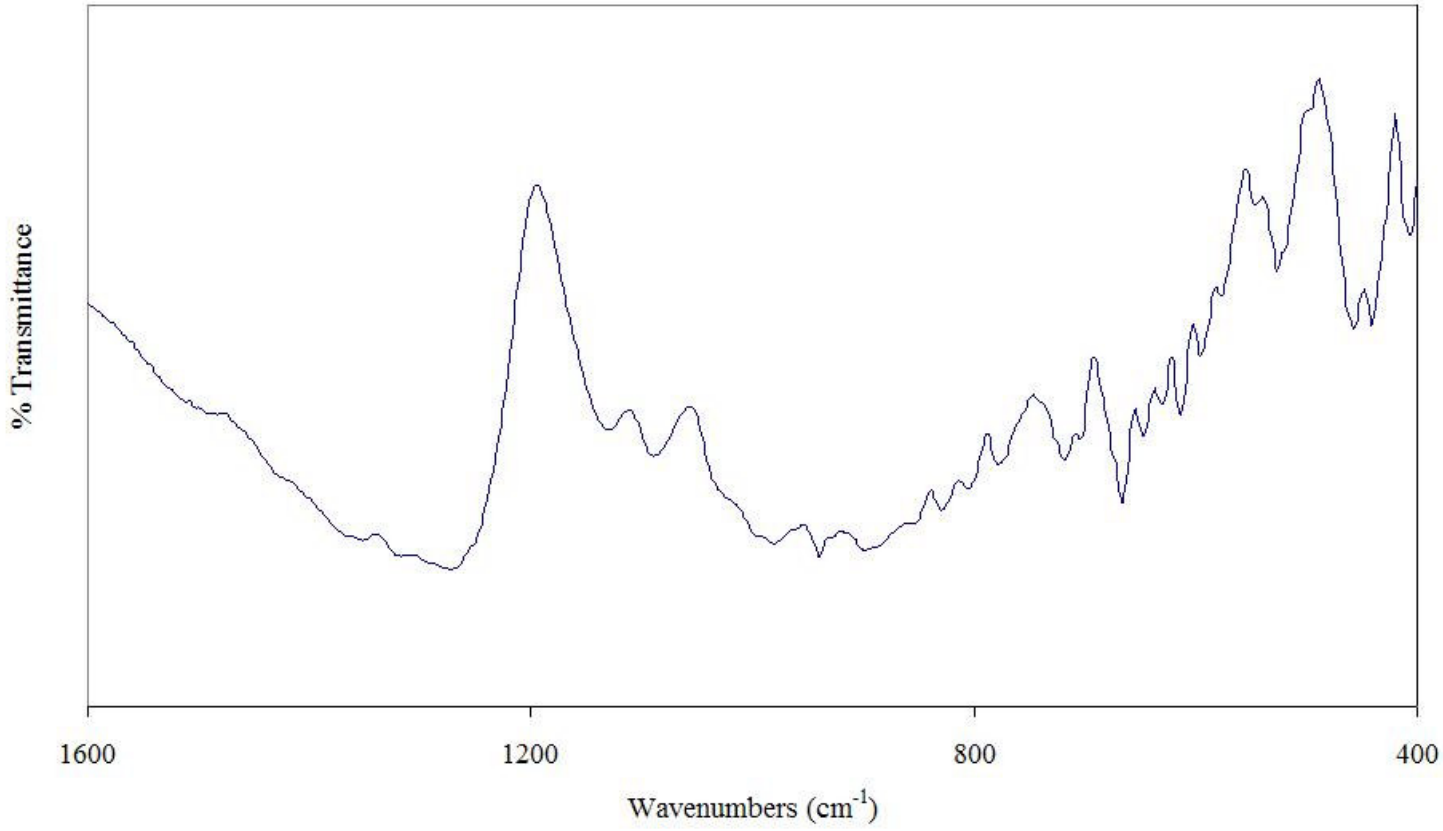

Figure C.17 *IR spectrum of LiB_3O_5 doped with 25% wt. La_2O_3 at 750℃ for 7 hours*

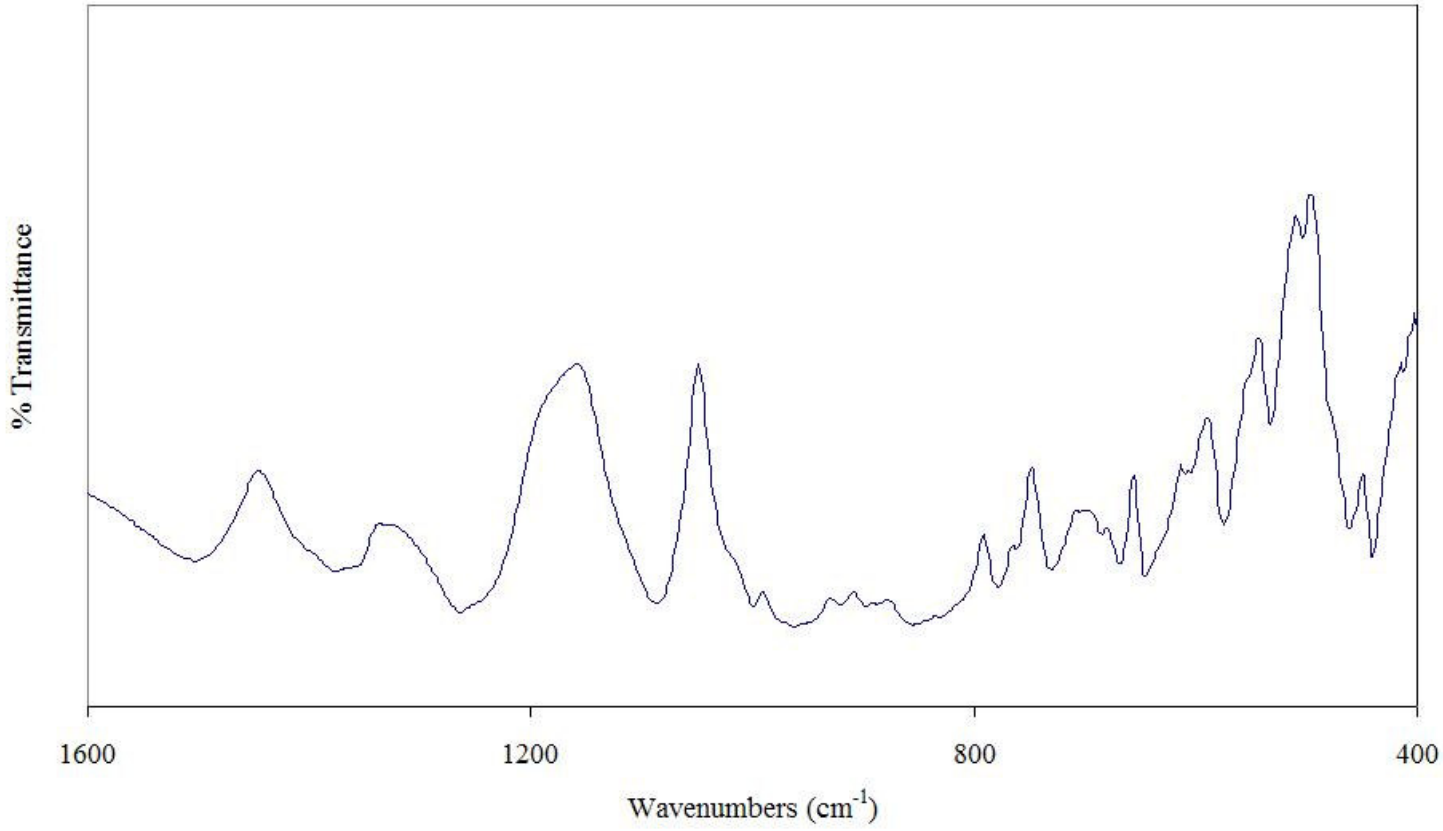

Figure C.18 *IR spectrum of LiB_3O_5 doped with 3% wt. Y_2O_3 at 750℃ for 7 hours*

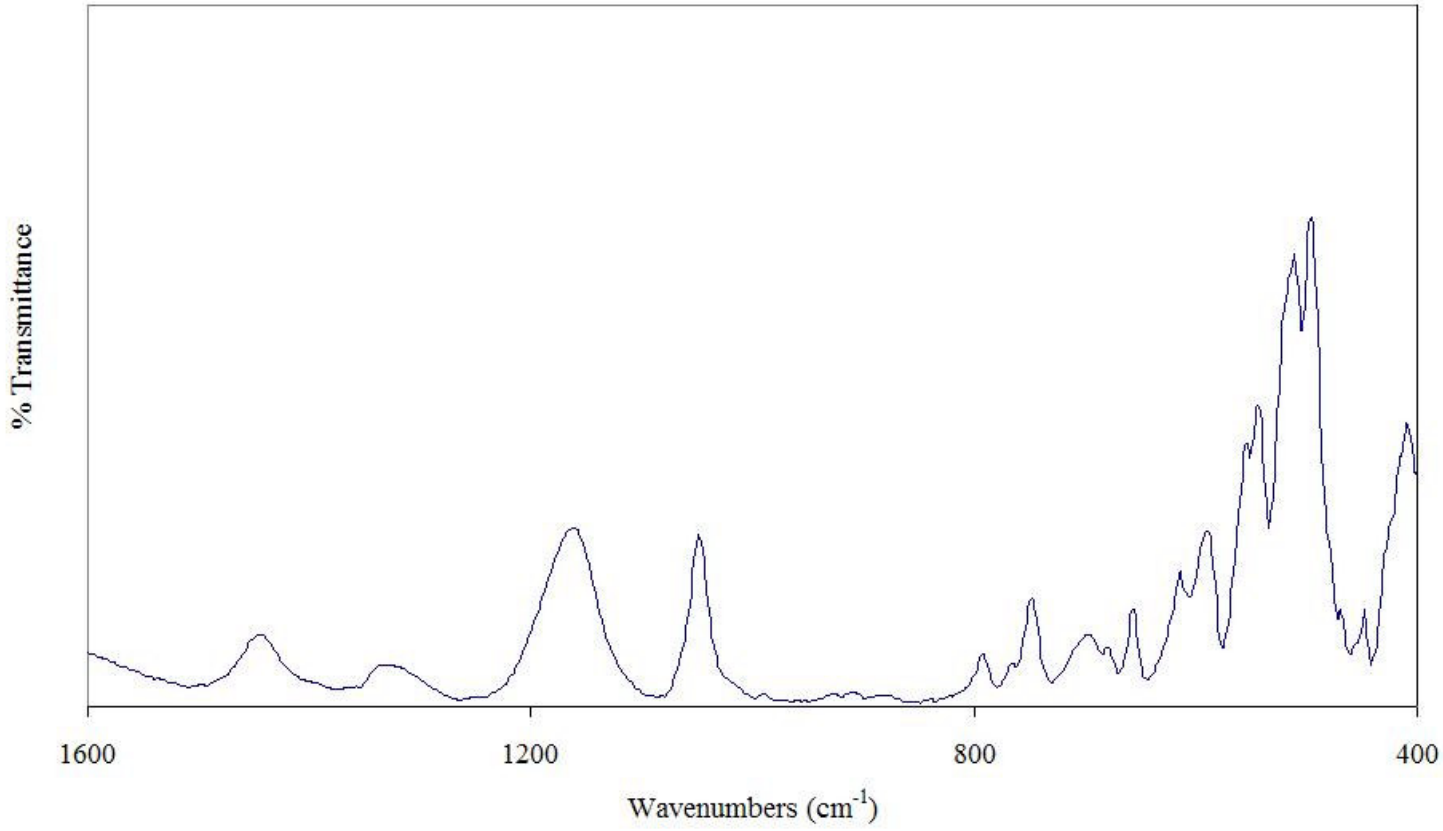

Figure C.19 *IR spectrum of LiB_3O_5 doped with 5% wt. Y_2O_3 at 750℃ for 7 hours*

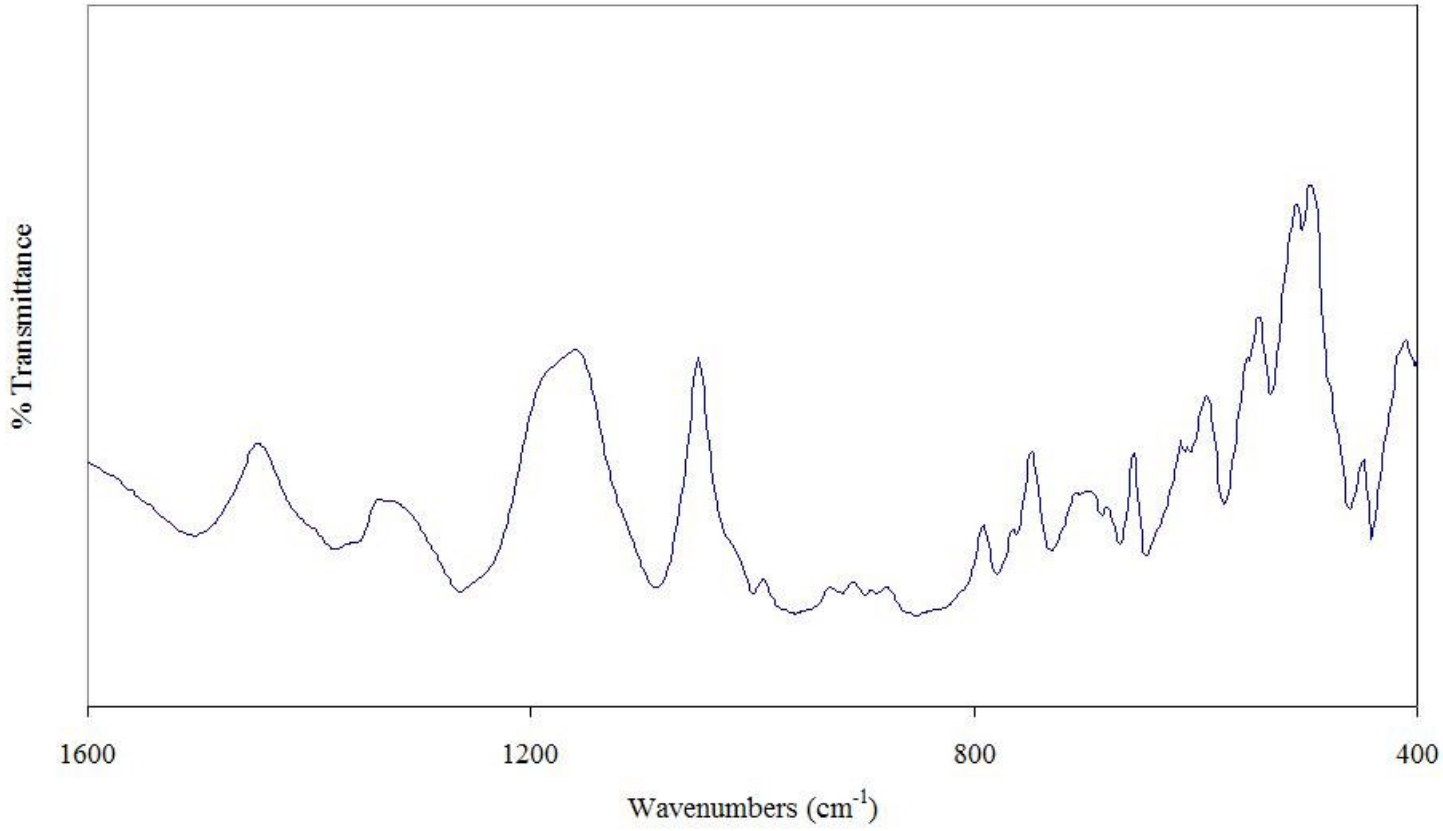

Figure C.20 *IR spectrum of LiB_3O_5 doped with 7% wt. Y_2O_3 at 750℃ for 7 hours*

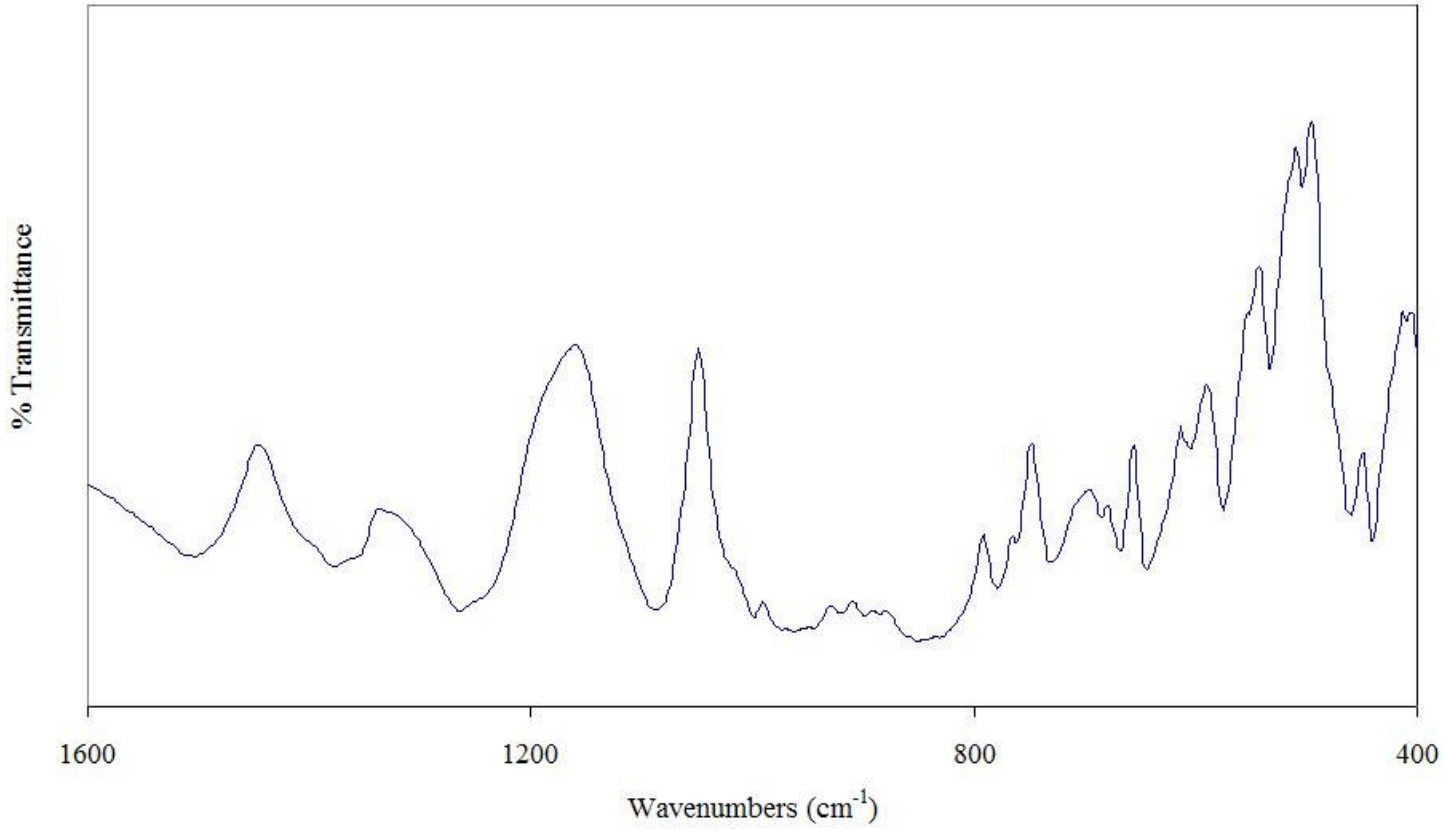

Figure C.21 *IR spectrum of LiB_3O_5 doped with 9% wt. Y_2O_3 at 750℃ for 7 hours*

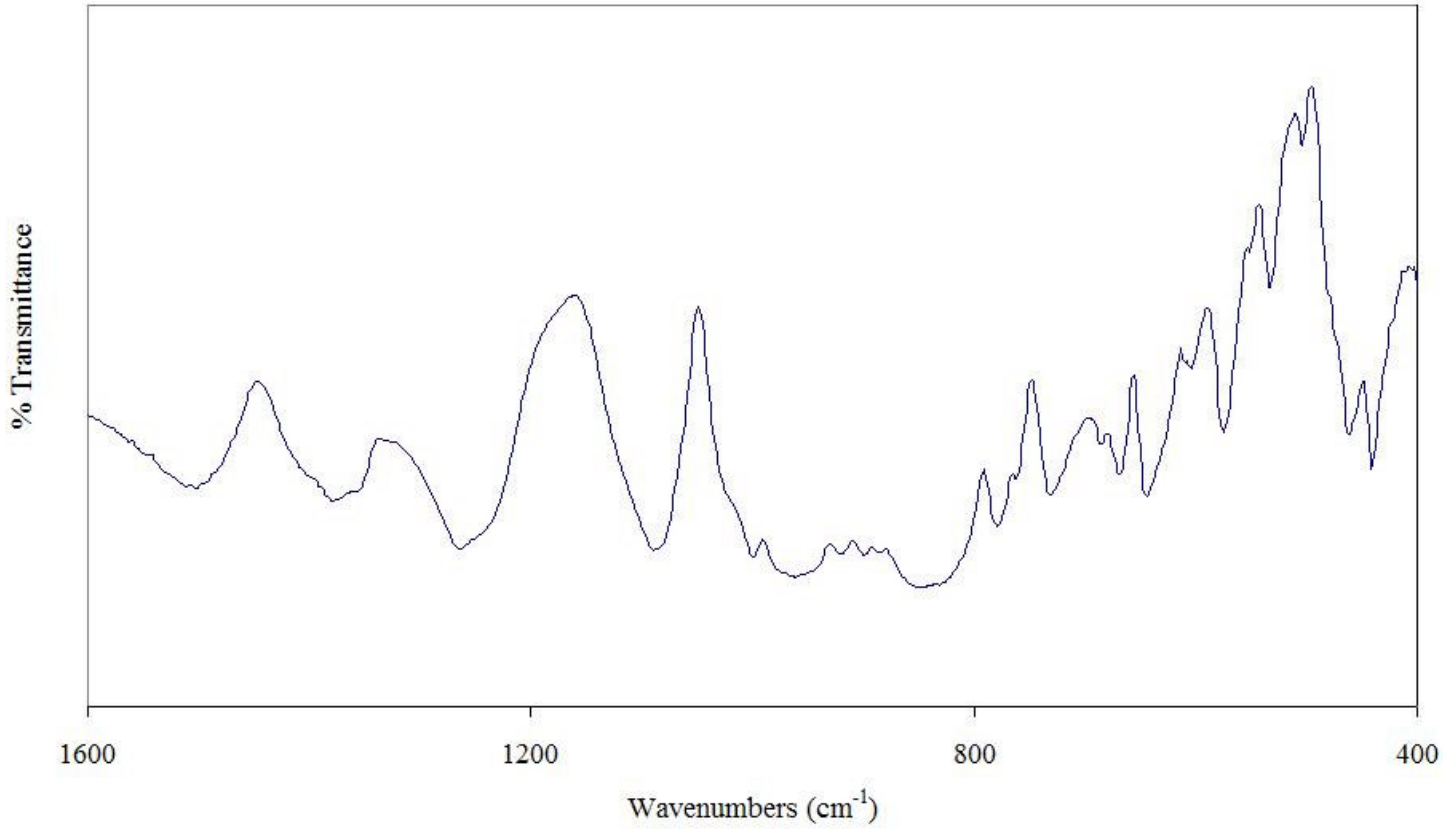

Figure C.22 *IR spectrum of LiB_3O_5 doped with 11% wt. Y_2O_3 at 750℃ for 7 hours*

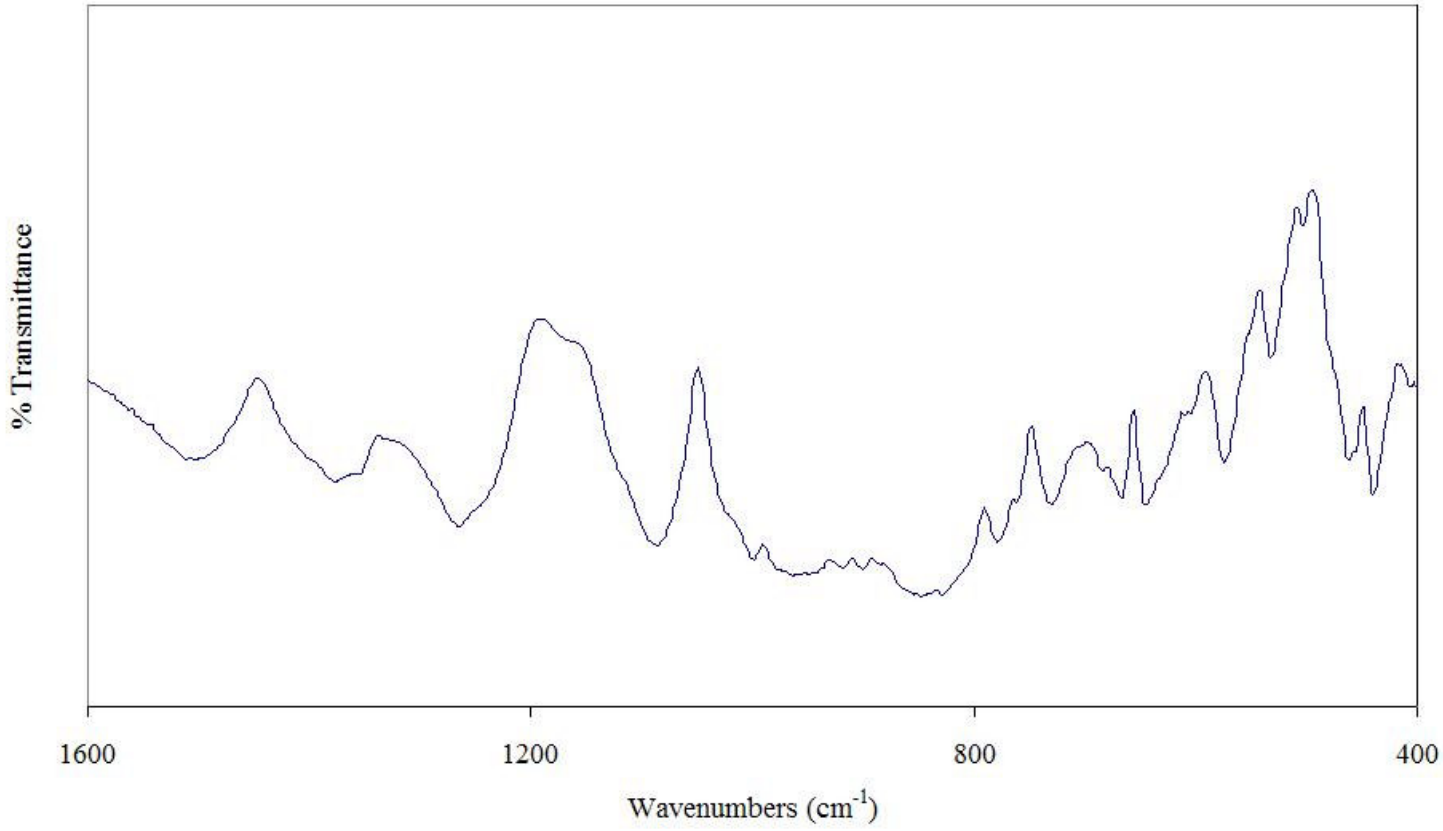

Figure C.23 *IR spectrum of LiB_3O_5 doped with 15% wt. Y_2O_3 at 750℃ for 7 hours*

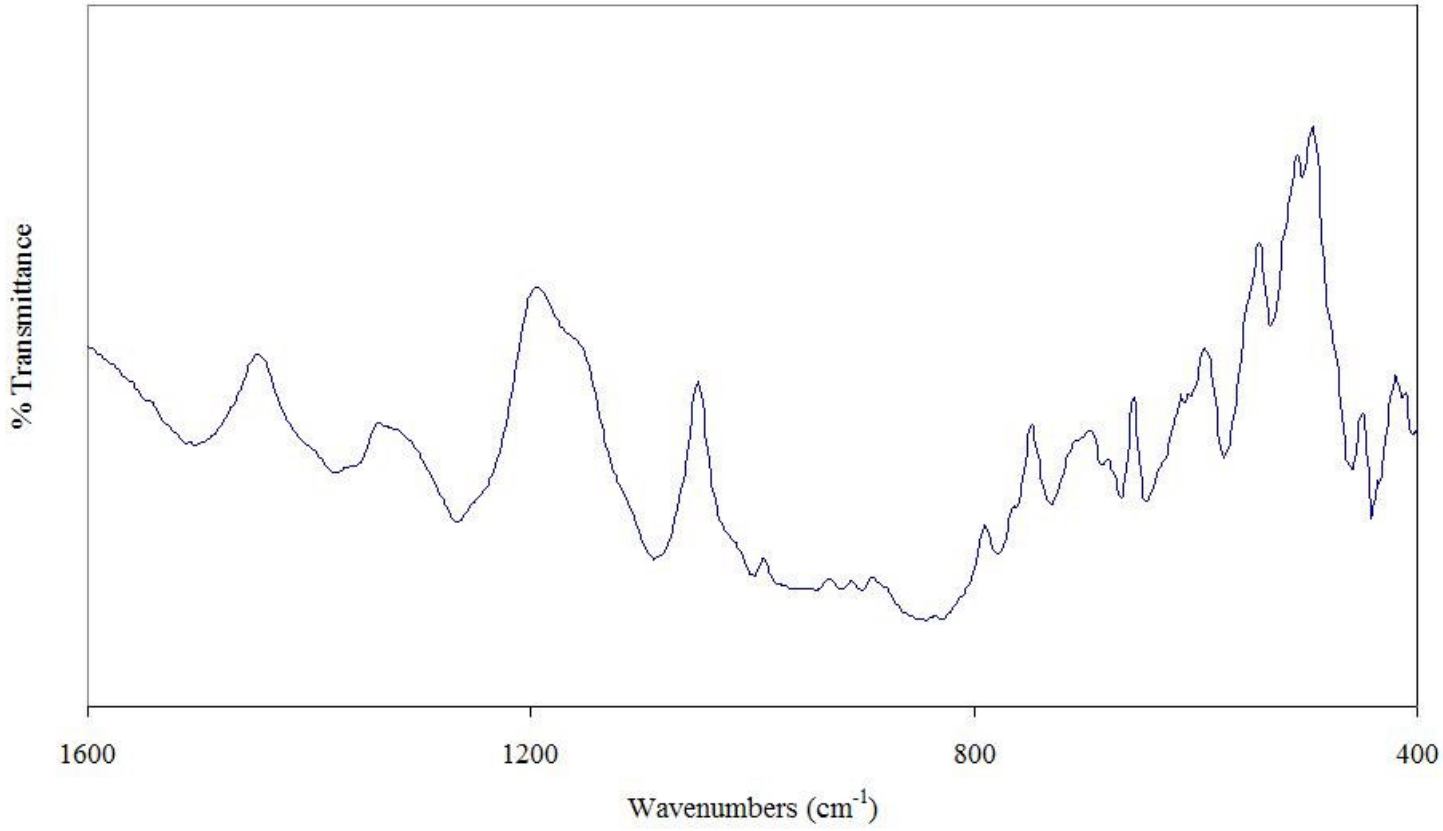

Figure C.24 *IR spectrum of LiB_3O_5 doped with 20% wt. Y_2O_3 at 750℃ for 7 hours*

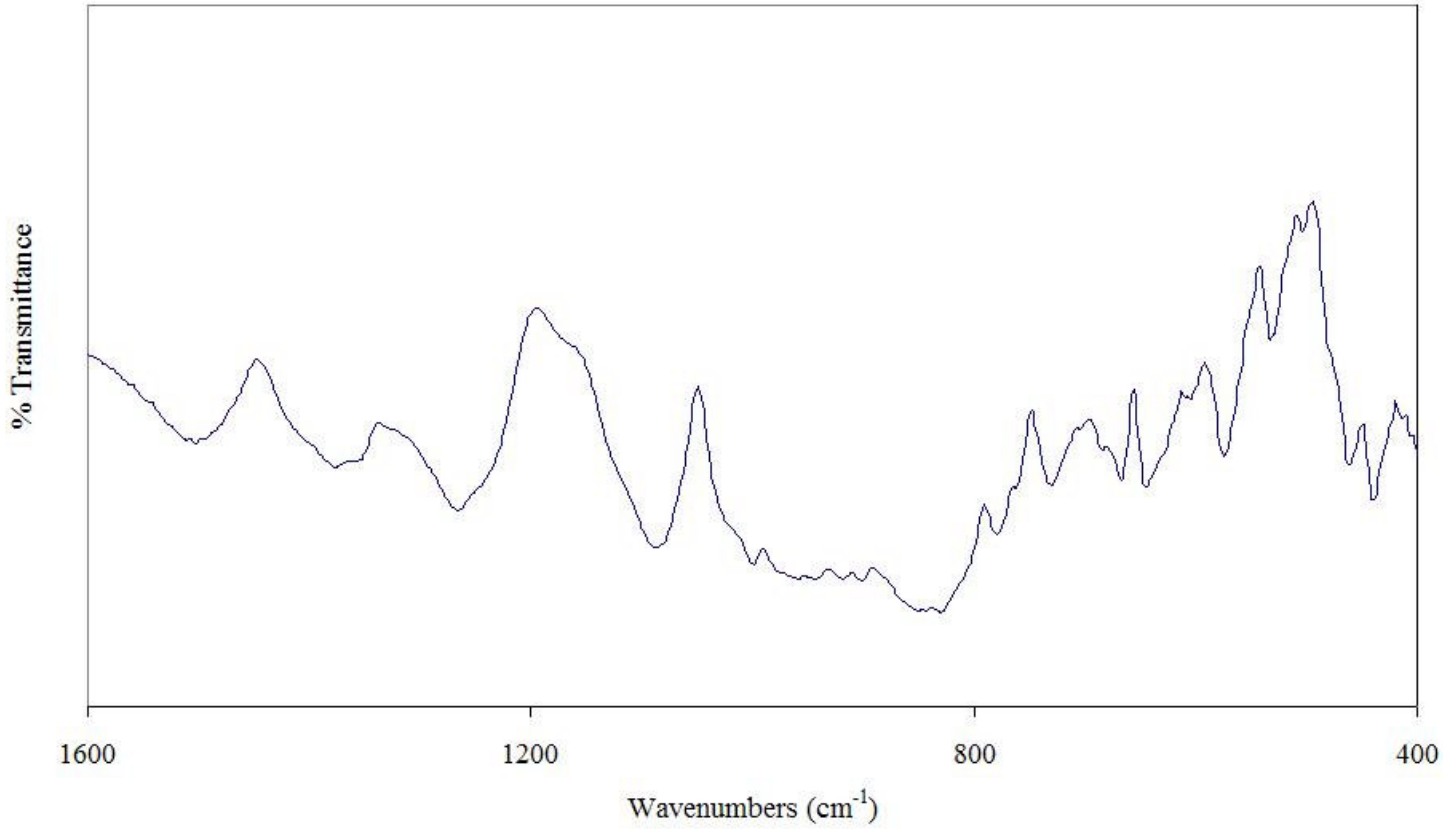

Figure C.25 *IR spectrum of LiB_3O_5 doped with 25% wt. Y_2O_3 at 750℃ for 7 hours*

APPENDIX C

DTA CURVES OF THE PRODUCED MATERIALS

The thermal behaviour of the produced new materials was illustrated in the following DTA curves. The curves of LBO and Gd_2O_3, La_2O_3 and Y_2O_3 doped LBO samples were given separately in this section.

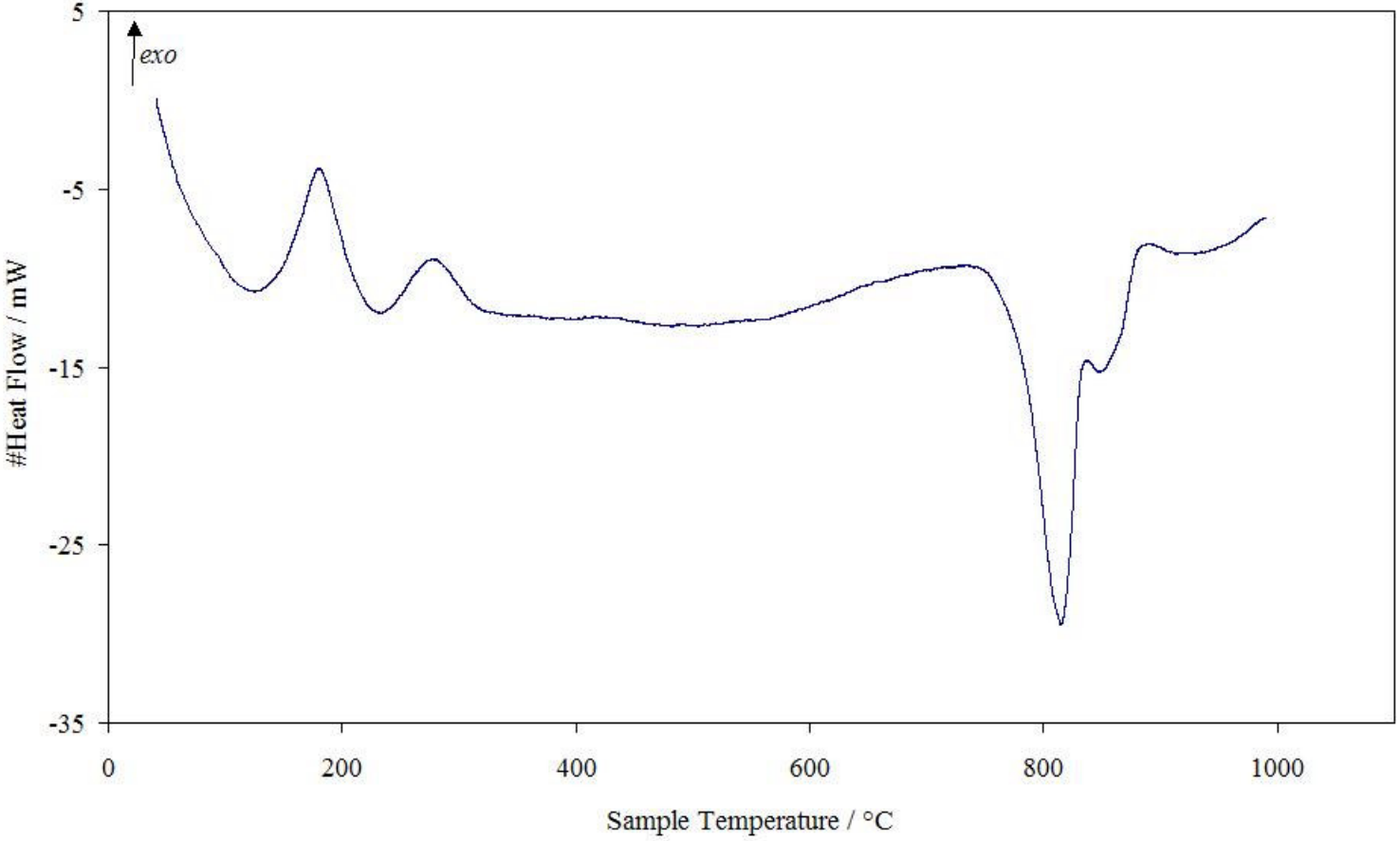

Figure D.1 *DTA curves of LiB_3O_5 obtained from the solid-state reaction of Li_2CO_3 and H_3BO_3 at 750℃ for 14 hours*

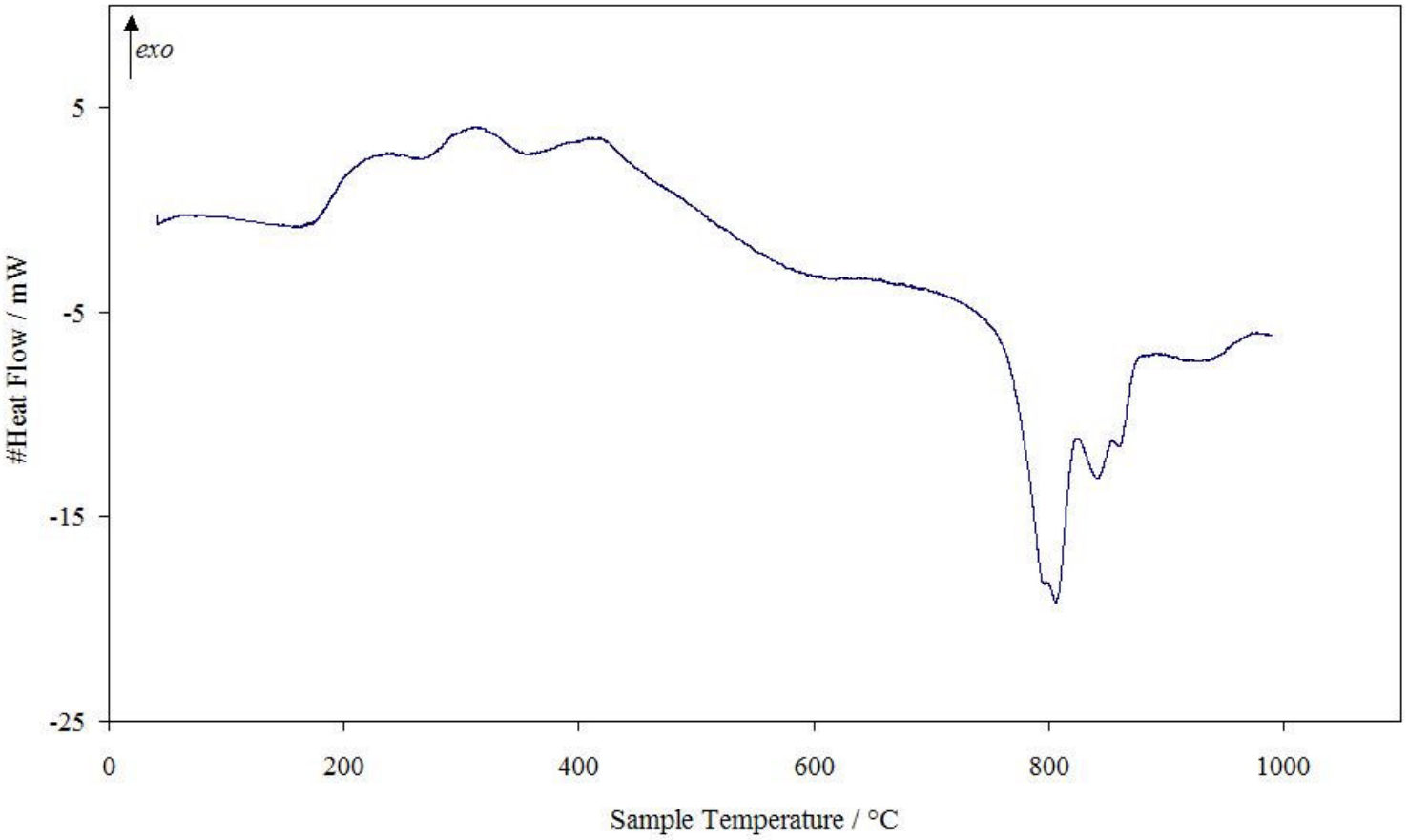

Figure D.2 *DTA curves of LiB_3O_5 doped with 5% wt. Gd_2O_3 at 750℃ for 7 hours*

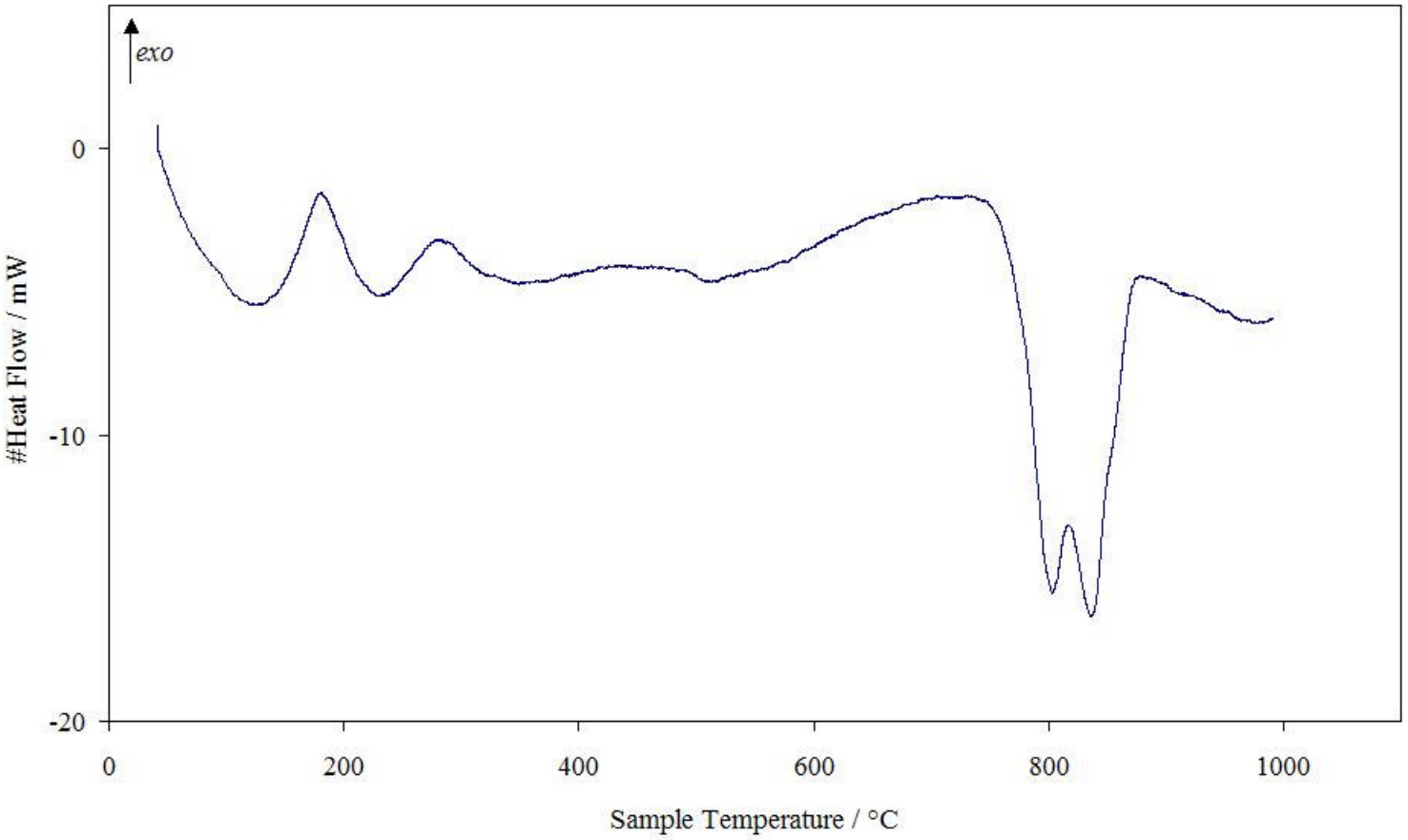

Figure D.3 *DTA curves of LiB_3O_5 doped with 11% wt. Gd_2O_3 at 750℃ for 7 hours*

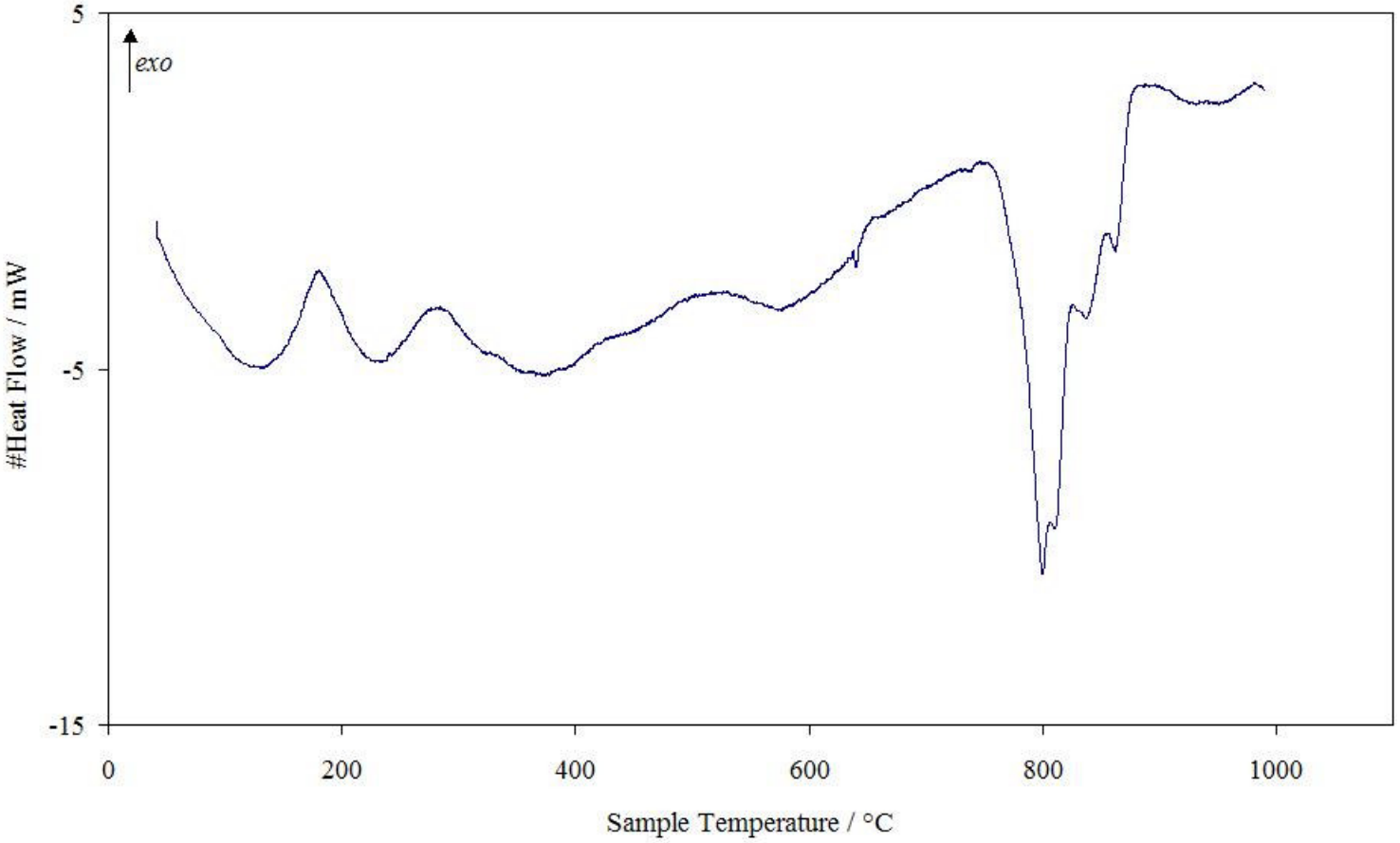

Figure D.4 *DTA curves of LiB_3O_5 doped with 5% wt. La_2O_3 at 750℃ for 7 hours*

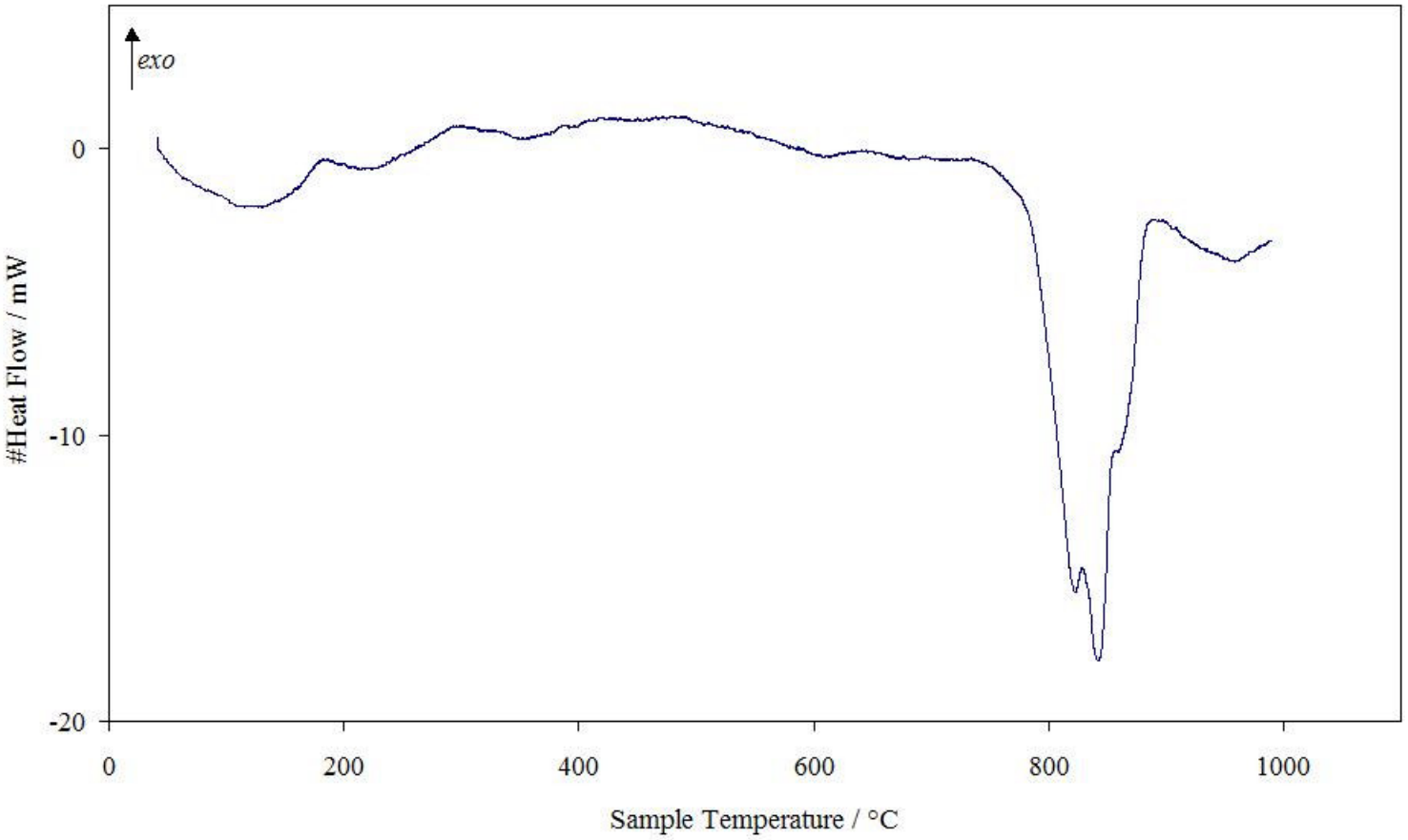

Figure D.5 *DTA curves of LiB_3O_5 doped with 11% wt. La_2O_3 at 750℃ for 7 hours*

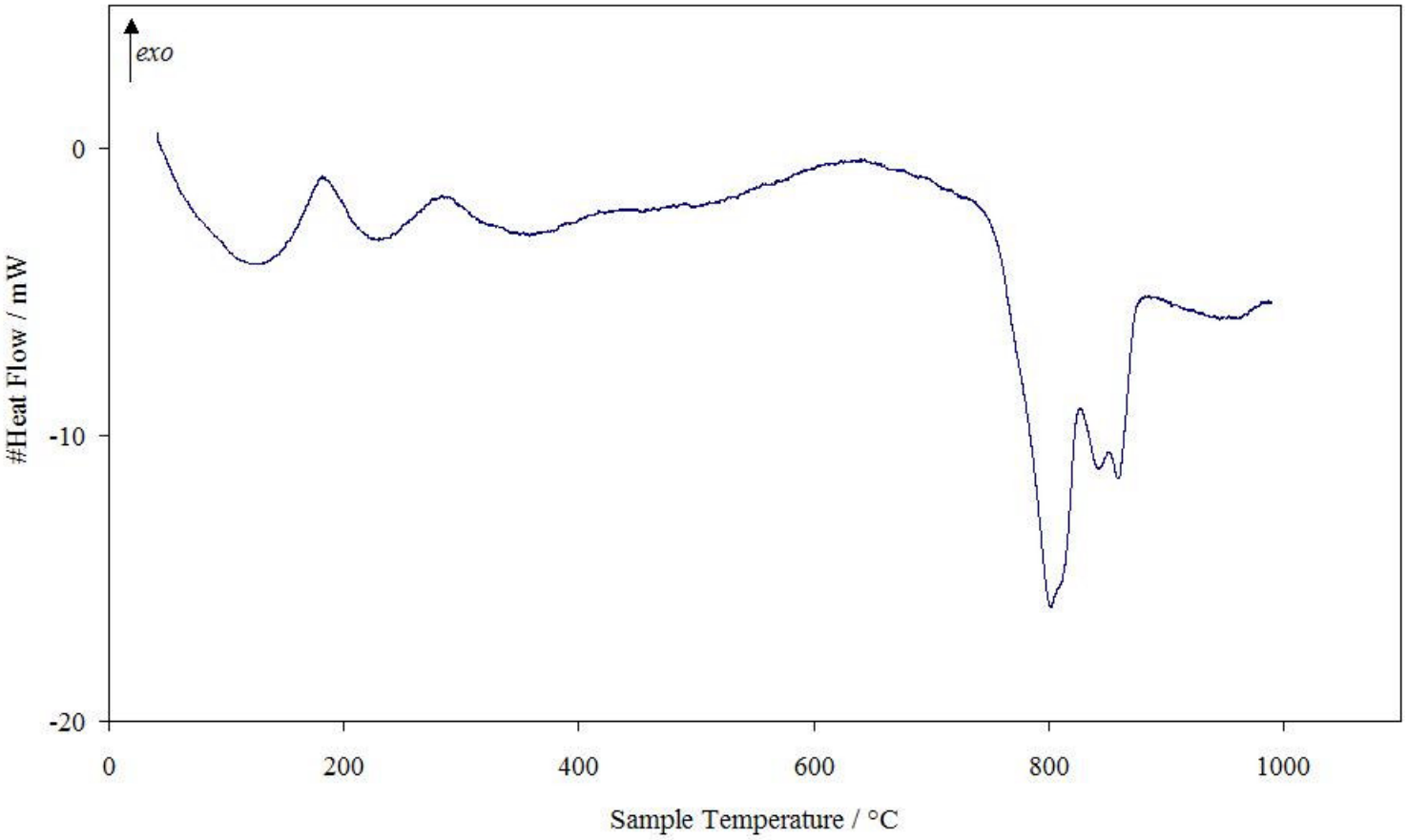

Figure D.6 *DTA curves of LiB_3O_5 doped with 5% wt. Y_2O_3 at 750℃ for 7 hours*

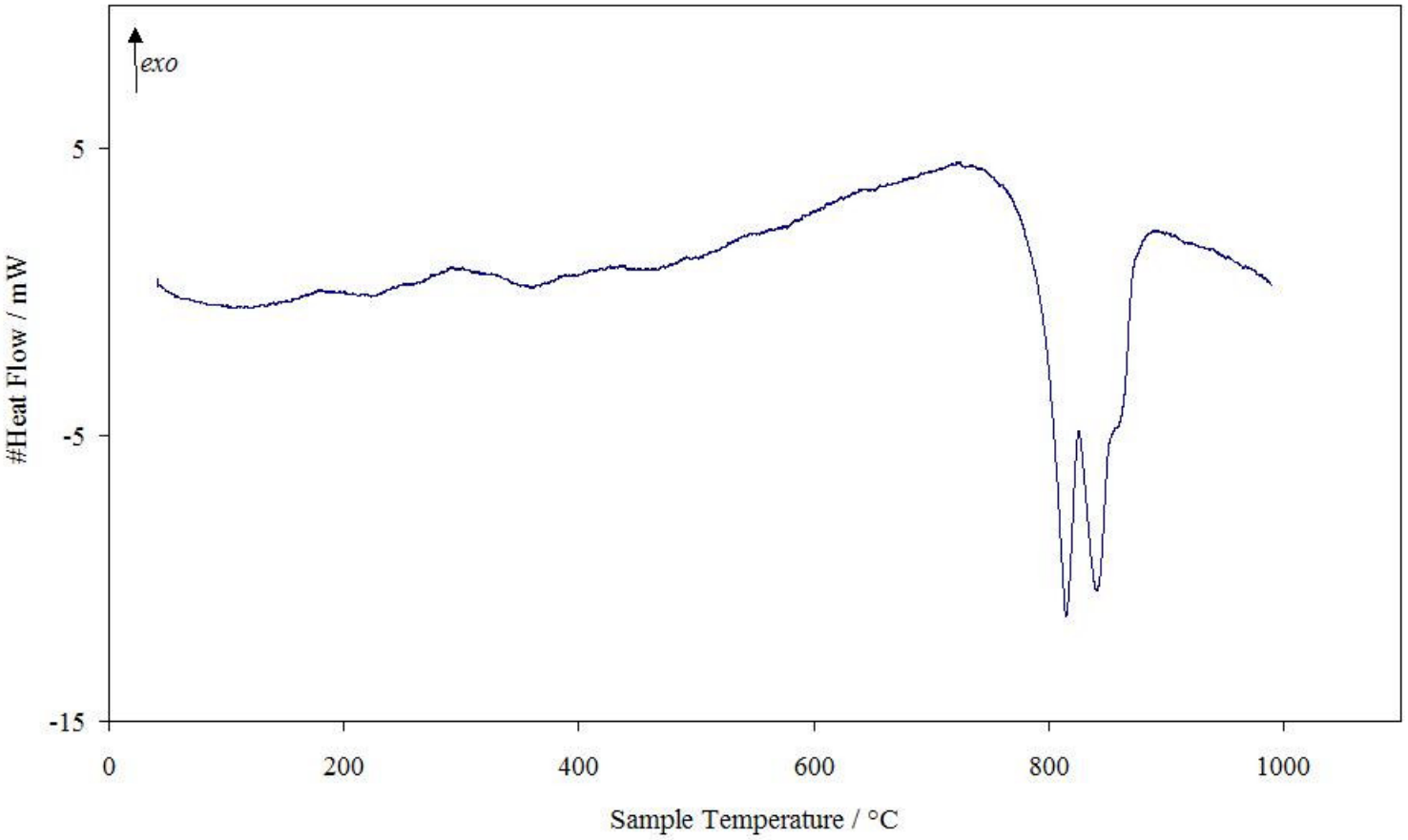

Figure D.7 *DTA curves of LiB_3O_5 doped with 11% wt. Y_2O_3 at 750℃ for 7 hours*

APPENDIX D

TL CURVES OF THE PRODUCED MATERIALS

The glow curves of the prepared samples are given separately in the following figures. In those figures, solid lines represent the samples of LBO and rare-earth doped LBO irradiated directly and the dotted lines represent the samples irradiated after 24 hours.

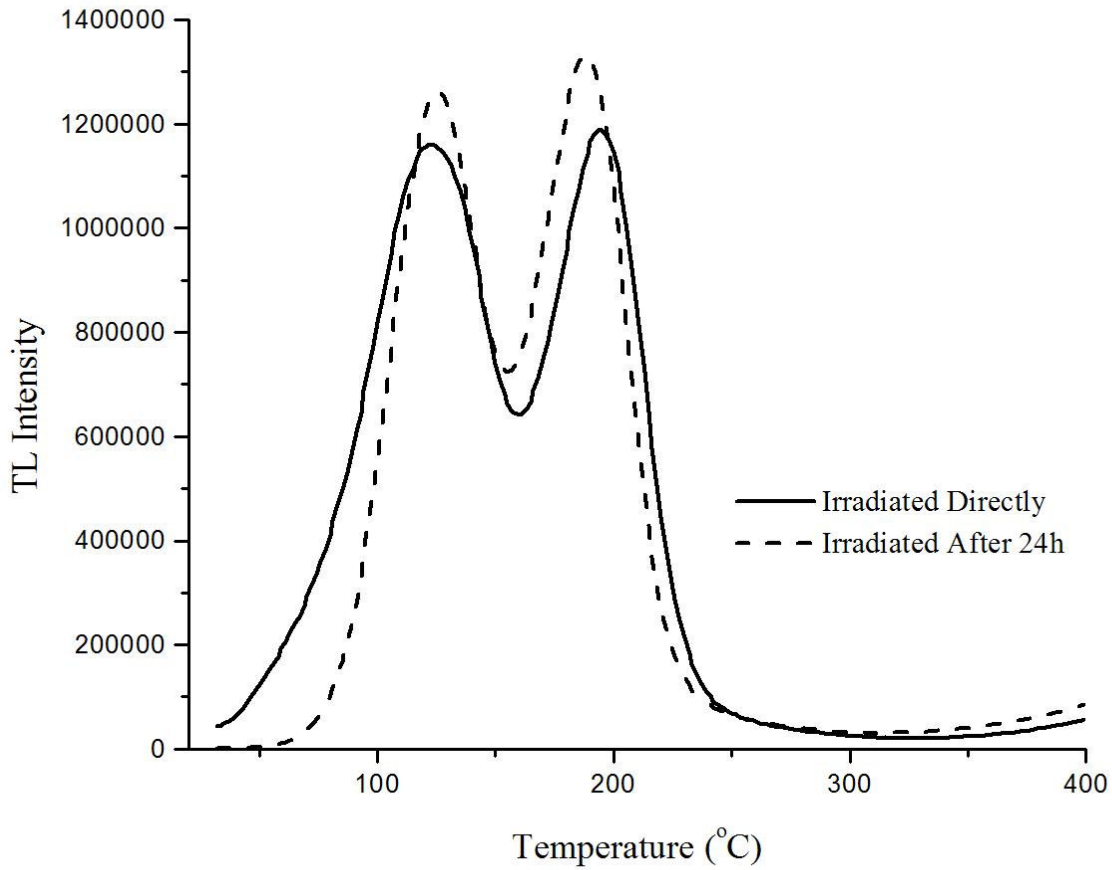

Figure E.1 *The glow curve of LiB_3O_5 from the solid-state reaction of Li_2CO_3 and H_3BO_3 at 750℃ for 14 hours*

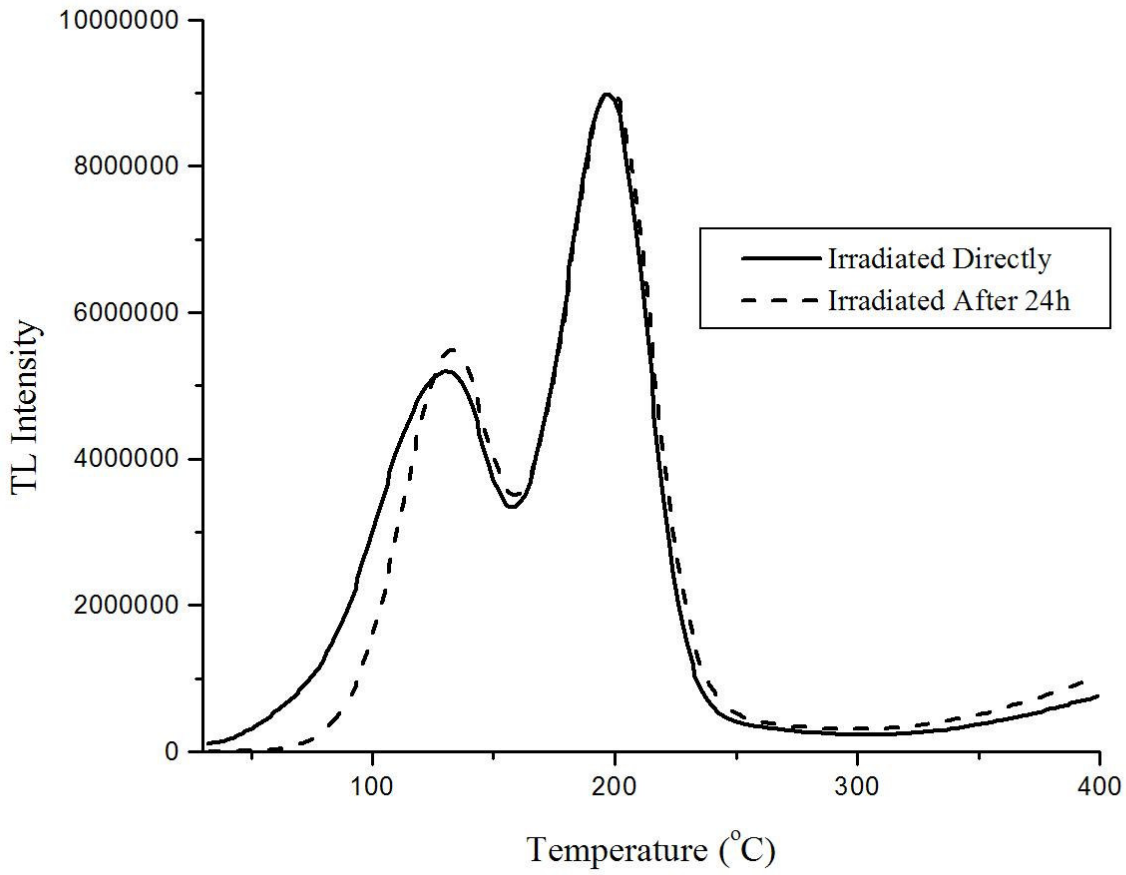

Figure E.2 *The glow curve of LiB_3O_5 doped with 5% wt. Gd_2O_3 at 750 ℃ for 7 hours*

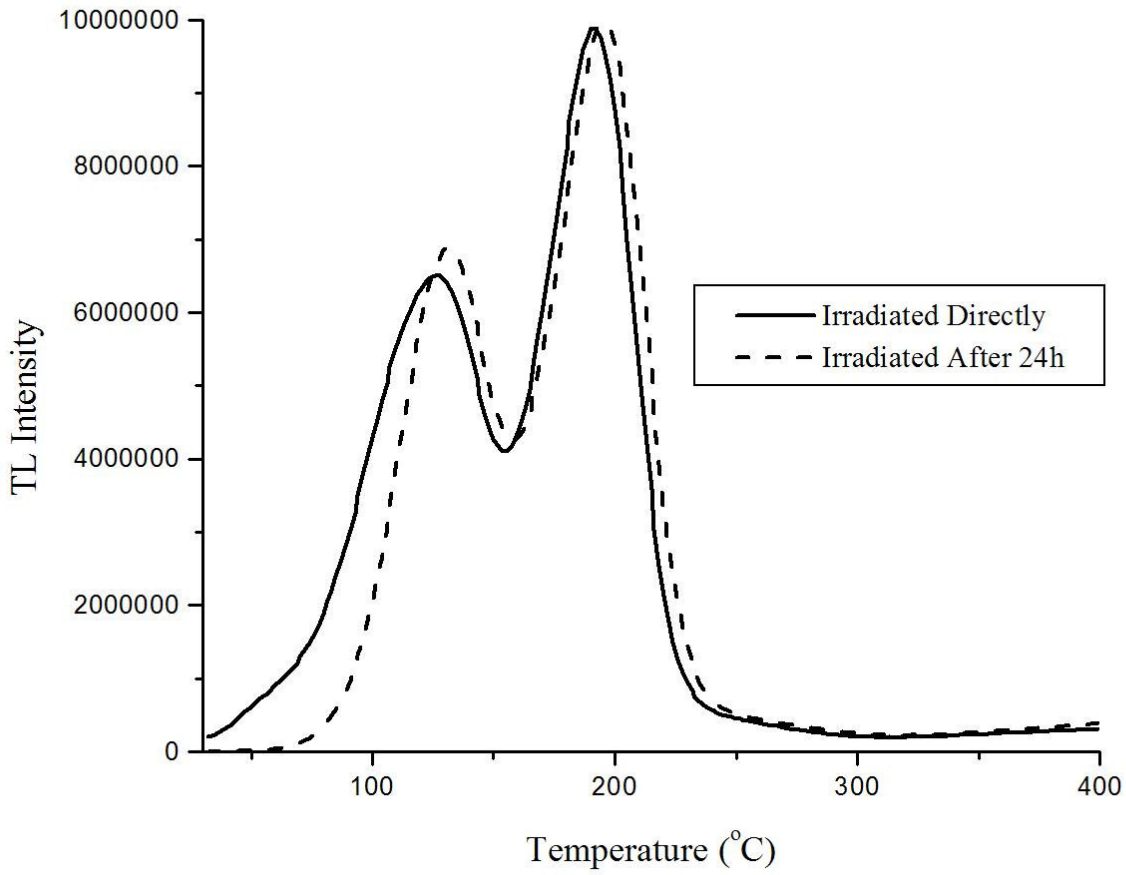

Figure E.3 *The glow curve of LiB_3O_5 doped with 7% wt. Gd_2O_3 at 750 ℃ for 7 hours*

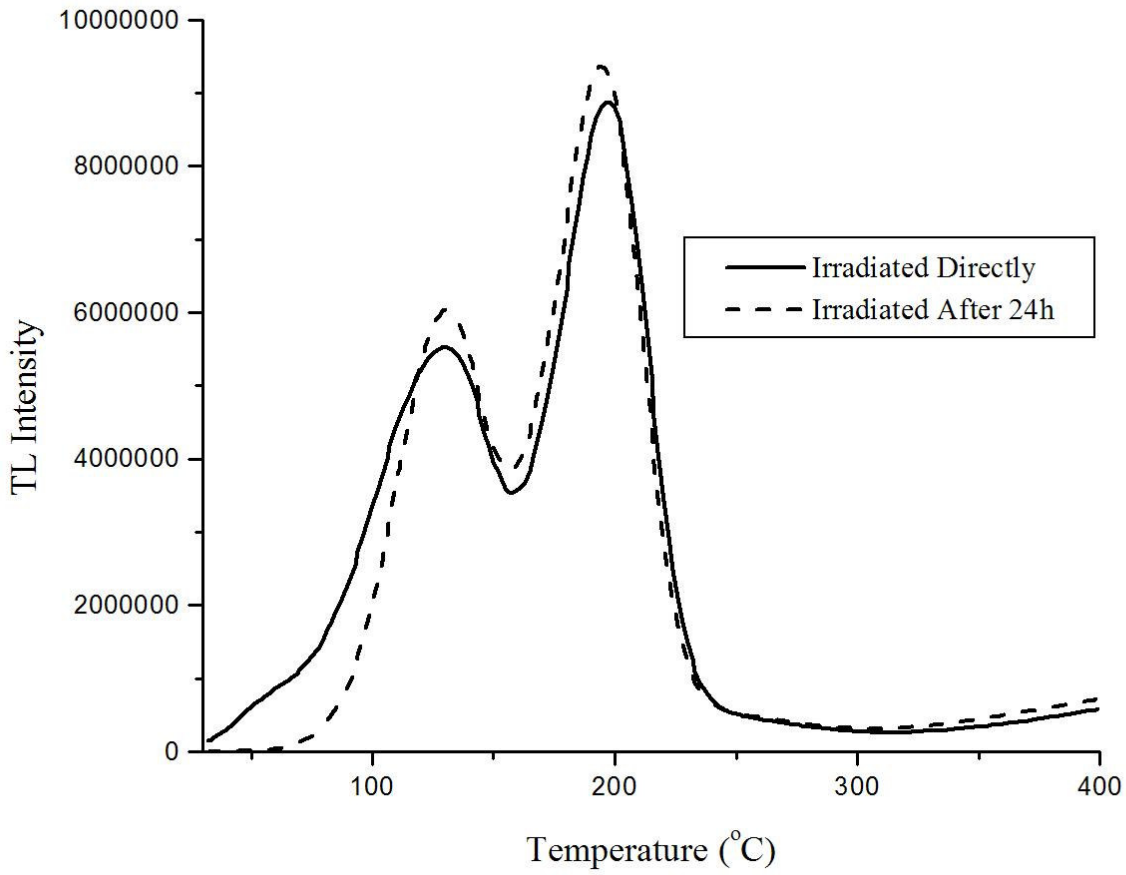

Figure E.4 *The glow curve of LiB_3O_5 doped with 11% wt. Gd_2O_3 at 750 ℃ for 7 hours*

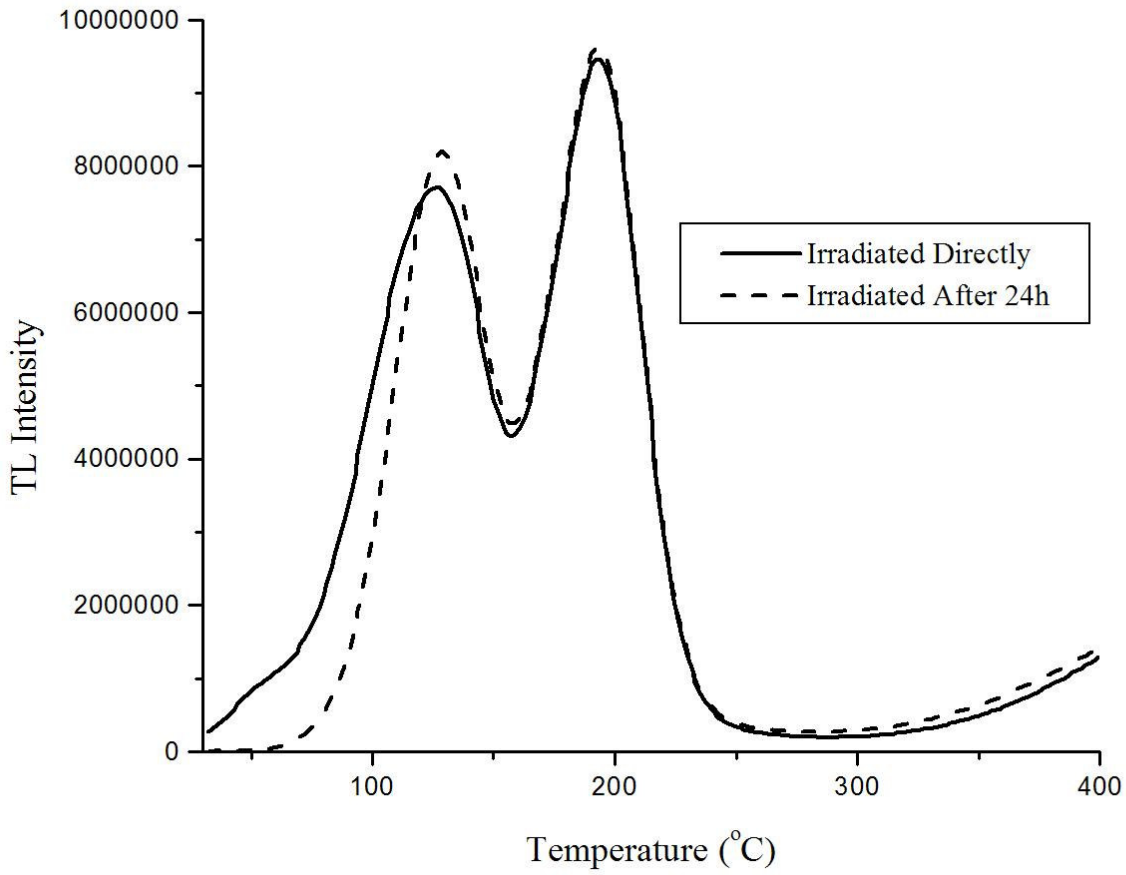

Figure E.5 *The glow curve of LiB_3O_5 doped with 5% wt. La_2O_3 at 750℃ for 7 hours*

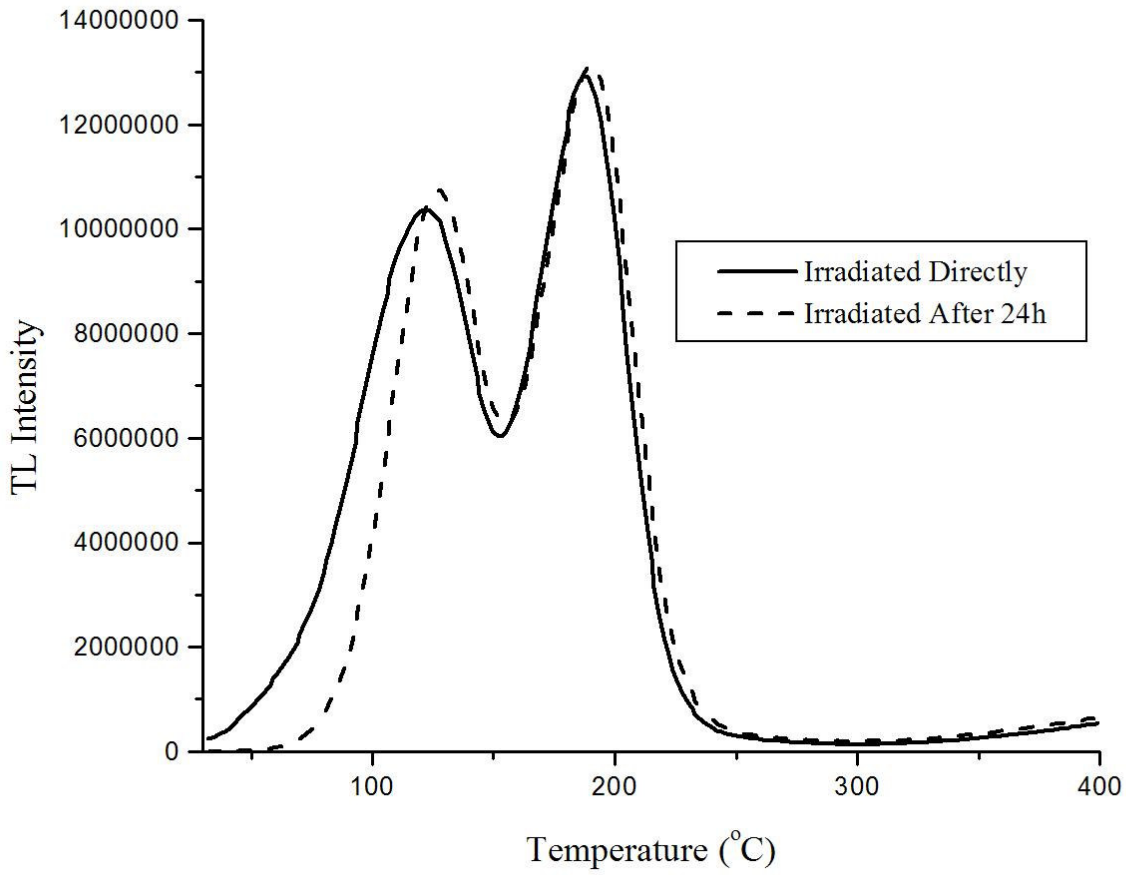

Figure E.6 *The glow curve of LiB_3O_5 doped with 7% wt. La_2O_3 at 750℃ for 7 hours*

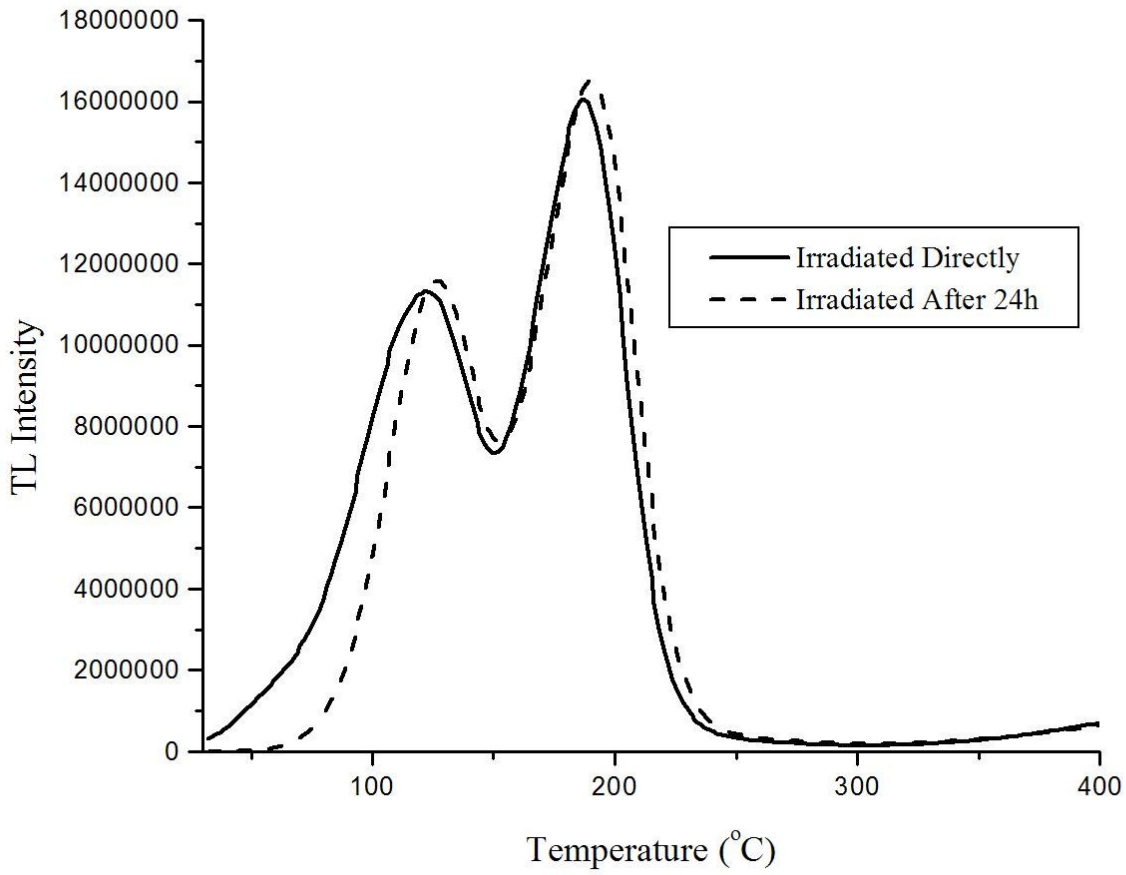

Figure E.7 *The glow curve of LiB_3O_5 doped with 11% wt. La_2O_3 at 750℃ for 7 hours*

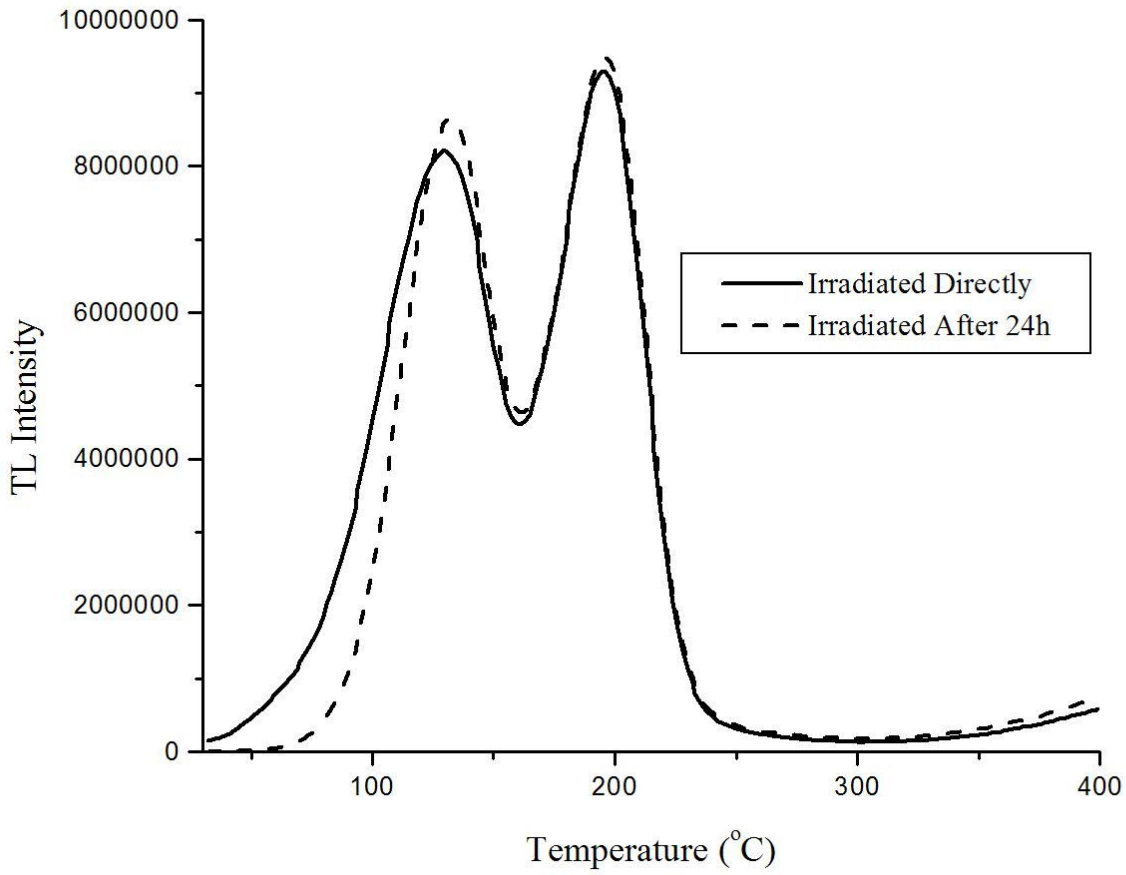

Figure E.8 *The glow curve of LiB_3O_5 doped with 5% wt. Y_2O_3 at 750℃ for 7 hours*

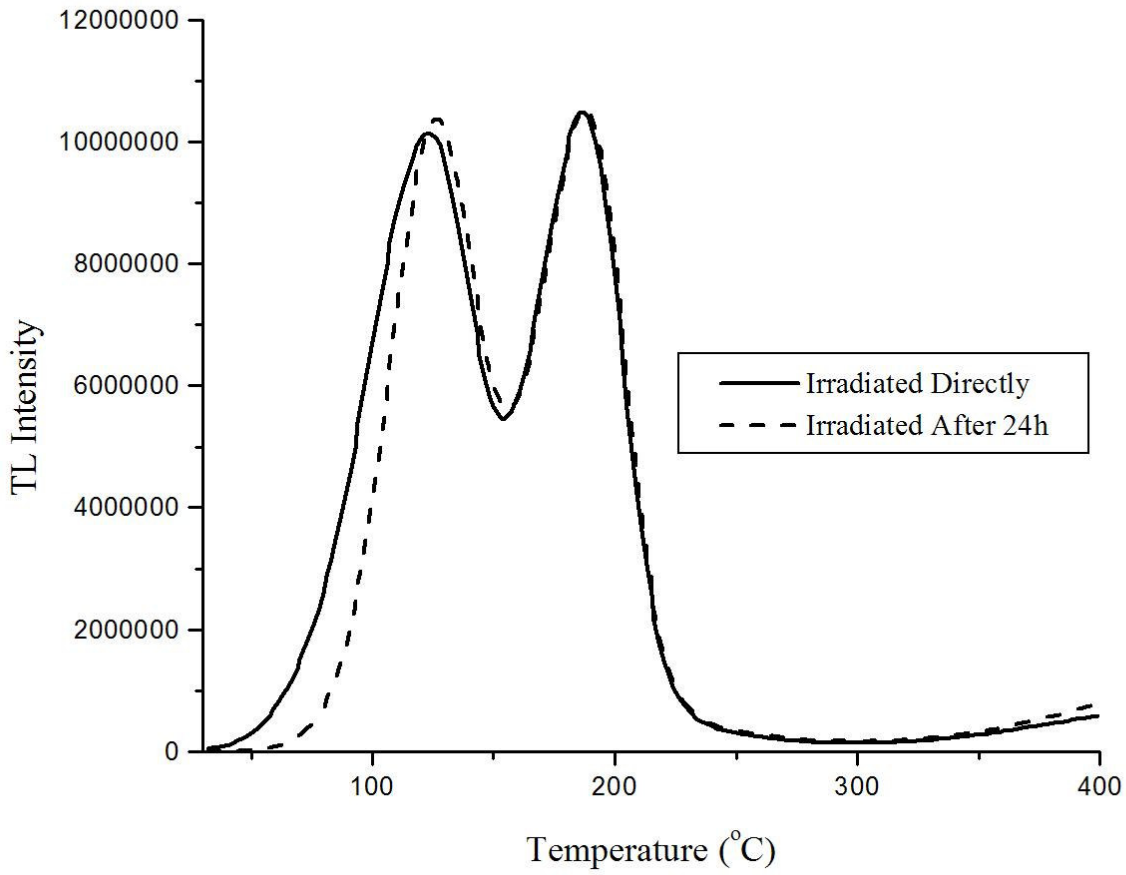

Figure E.9 *The glow curve of LiB_3O_5 doped with 7% wt. Y_2O_3 at 750℃ for 7 hours*

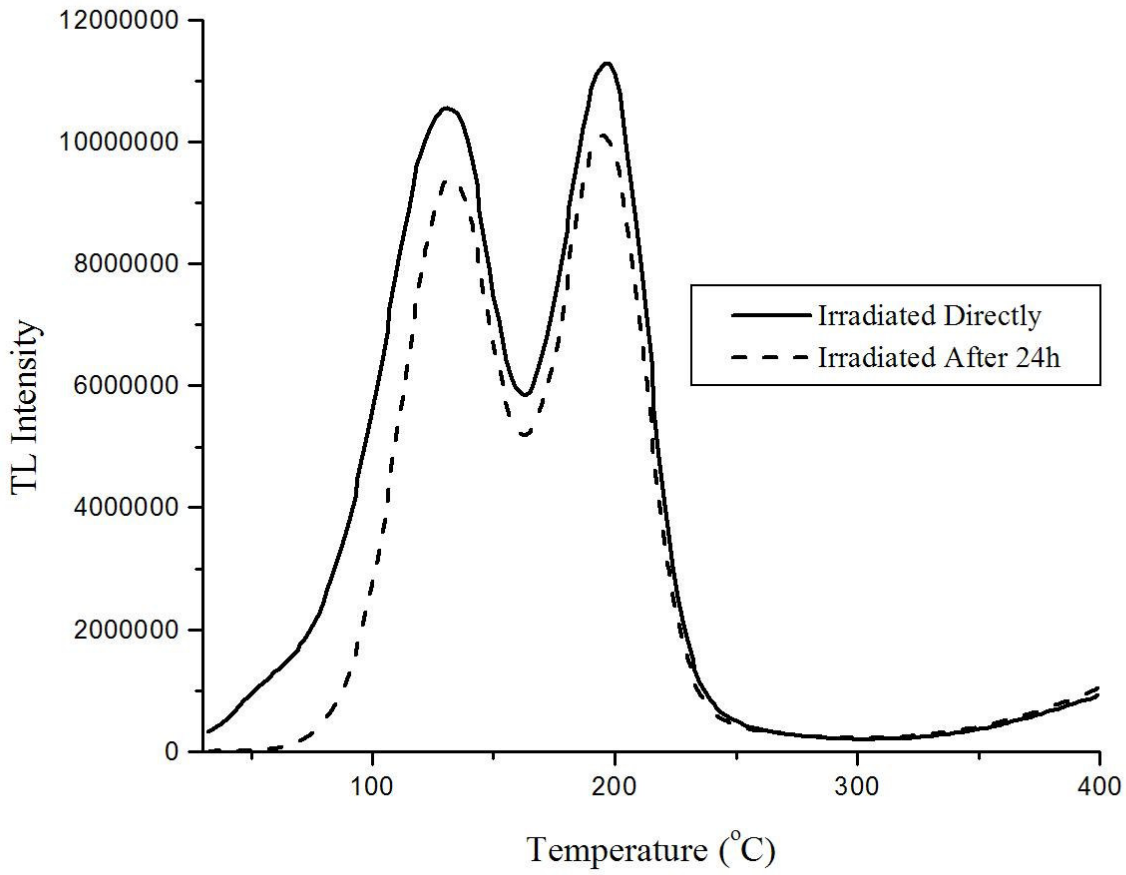

Figure E.10 *The glow curve of LiB_3O_5 doped with 11% wt. Y_2O_3 at 750℃ for 7 hours*